Particle fabrication and delivery systems for controlled release of bumped kinase inhibitors (BKIs) for malaria transmission blocking.

Christina S. Yacoob

A dissertation

submitted in partial fulfillment of the

requirements for the degree of

Doctor of Philosophy

University of Washington

2013

Reading Committee:

Hong Shen, Chair

David G. Castner

Wesley C. Van Voorhis

Program Authorized to Offer Degree:

Department of Chemical Engineering

University of Washington

ABSTRACT

Particle fabrication and delivery systems for controlled release of bumped kinase inhibitors (BKIs) for malaria transmission blocking.

Christina S. Yacoob

Chair of the Supervisory Committee:

Professor Hong Shen
Department of Chemical Engineering

The main goal of this research is to successfully fabricate particulate systems for sustained delivery of bumped kinase inhibitors (BKIs) for malaria transmission blocking. The report focuses on optimization of a nanoparticle-based BKI-delivery system and the effects between different fabrication methods and drug hydrophobicity. The first chapters consist of an overview of material/method choices and reviews on both sustained drug delivery systems and nanoparticle fabrication techniques. The middle chapters discuss fabrication and characterization of BKI-loaded particles via emulsification and fluidic nanoprecipitation (fNP). The last chapters compare these two fabrication methods and two BKI molecules for effects on particle characteristics, incorporation, and release.

Using the emulsification and fNP fabrication methods we produced BKI-loaded poly (DL-lactide-co-glycolide) (PLGA) particles. BKIs used included RM-1-132 and 1294 *(provided by the Van Voorhis and Maly groups, University of Washington)*. These BKIs are generally amphiphilic, with 1294 displaying a

slightly more hydrophobic tendency. The amphiphilic nature of the drug molecule creates a challenge for incorporation into delivery systems, which work optimally with strongly hydrophilic or hydrophobic molecules. Increasing the fabrication pH to a basic pH beyond the molecule's pKa neutralized the molecule and enhanced the incorporation into the PLGA particles. Additional optimization was performed to further increase incorporation. Particles were characterized for size, surface charge, and evaluated for total BKI content and release. Our best systems had ~100% incorporation, and >100ng/hr release (per 25mg particles) up to 4 days (~50ng/hr per 25mg particles up to 4 weeks).

Comparisons were made between particle size, fabrication methods and drug hydrophobicity to elucidate fundamentals of amphiphilic drug incorporation. The fNP-fabricated particles displayed >60% incorporation efficiency regardless of drug hydrophobicity, but also displayed higher polydispersity when initial loading or drug hydrophobicity increased. The emulsion system displayed a maximum loading for BKI-loaded particles, which shifted higher as drug hydrophobicity increased. Particle size remained mostly monodisperse except at the highest initial loading. We also examined parallel models to understand the differences between the two fabrication methods and drug molecules, as well as to predict *in vivo* behavior.

Overall, we have successful fabricated a BKI-loaded particulate delivery system which can extend the release on BKIs to help improve malaria transmission blocking and reduce the need for multiple drug administrations.

Future directions include increasing and extending the release, testing activity of the released BKI *in vivo,* and optimizing storage conditions for particles.

TABLE OF CONTENTS

LIST OF FIGURES

Figure 4.3. Scanning electron microscopy images of various system II particles *(ratios are DMSO : hydrophilic additive (v/v); top row = water as the hydrophilic additive; bottom row = glycerol as hydrophilic additive). Scale bar = 10um or 100um as indicated.*

Figure 4.4. Scanning electron microscopy images of various system III (core/shell)particles *(A = single emulsion PLGA/ter microparticles, B = double emulsion PLGA/ter microparticles, C = PLGA/Alg with 5ug/mg drug loading, D = PLGA/Alg with 10ug/mg drug loading). Scalle bar = 1um.*

Figure 4.5. Incorporation efficiency of system II (hydrophilic additives) particles based on DMSO: hydrophilic additive ratio (v/v) *(no PE = control sample with no hydrophilic additive).*

Figure 4.6. Figure 4.6. Release profiles of RM-1-132 from various systems per mg of particles. *(Ratios are amounts in uL of DMSO : water or DMSO : glycerol, if indicated by (G) in middle graph).*

Figure 4.7. Release profiles of RM-1-132 from various systems per mg of particles. *(Ratios are amounts in uL of DMSO : water; t =terpolymer coating, Alg = alginate core; ug/mg are initial loadings of ug RM-1-132 / mg PLGA polymer).*

Figure 4.8. Schematic and summarized results of the three systems employed for RM-1-132 drug incorporation. *(System 1 = solid dispersion / emulsion, System 2 = hydrophilic additives, System 3 = core/shell).*

Figure 4.9. Final loading and incorporation efficiency of select parameters from a parameter design matrix for pH effects on three steps in the fabrication process. (*Initial loading was set at 2ug RM-1-132/mg PLGA, Water pH: pH of internal aqueous phase of double emulsion NPs, Fabr. pH: fabrication pH of emulsification or fNP system, Rinse pH: pH of water used to triple rinse particles after fabrication).*

Figure 4.10. Partition coefficient for increasing concentrations of RM-1-132 at pH 6, 8, 10, and 12. *(A concentration of 1 ug/mL is equivalent to 20ug/mg initial loading during particle fabrication).*

Figure 4.11. Final loading and incorporation efficiency of single and double emulsion RM-1-132-loaded PLGA particles at 2ug/mg and 10ug/mg initial loadings. *(Fabrication pH = 12).*

Figure 4.12. Particle diameter based on SEM size measurements for RM-1-132-loaded PLGA particles at various initial loadings *(A = emulsion fabricated particles, B = fNP fabricated particles).*

Figure 4.13. Final loading and incorporation efficiency of RM-1-132-loaded PLGA particles from 2ug/mg to 50ug/mg initial loading.

LIST OF TABLES

CHAPTER 1. INTRODUCTION

Drug delivery systems originated for an assortment of reasons: to optimize effectiveness of marketed pharmaceuticals, to administer drugs with low solubility, and to replace expensive, inaccessible medicine.[1] Controlled release systems have great potential because they extend the time between dosing and are typically easier to administrate. These systems are prospective solutions for diseases like malaria, where health facilities are constantly running out of treatment supply and medication is so expensive that patients turn to cheaper and more dangerous formulations.[2] Additionally, delivery systems can navigate to targeted sites for release of localized treatment to assist in applications like cancer therapeutics. Even with all these advances, there are still challenges in the development of effective and pliable controlled release drug delivery systems.

The basic requirements for drug delivery systems include biocompatibility, effectiveness, and ease of administration. The dispensed drug should provide a prolonged therapeutic effect with minimized side effects and low toxicity. The sustained release therapy should be more advantageous than an intravenous injection or traditional administration that is currently in use. Harsh solvents, if used during the fabrication process, should be removed to diminish adverse effects. Administration should be cheap, non-repetitive, and in some cases self-treatment should be a possibility. If a particle system is employed, a consistent size and stability in storage is preferred to ensure reliability of the product.

Incorporation of all these demands into a delivery system is essential for successful drug delivery.

The goal of this research is to develop particulate-based delivery systems for delivery of bumped kinase inhibitors (BKIs). The first section of this report is a review into drug delivery and particle fabrication methods/characterization, with an emphasis on emulsification and fluidic nanoprecipitation (fNP). The next section utilizes these methods to create BKI-loaded poly (DL-lactide-co-glycolide) (PLGA) particles. The incorporation efficiency and drug release from these systems were examined. The particulate-based systems were also optimized for the highest incorporation by altering parameters like continuous phase pH and speed of the fNP system. The BKIs used included RM-1-132 and 1294, which are similar molecules except for one additional methyl group on the end of the 1294 molecule.[3] Effects on particle characteristics, incorporation, and release based on modification of fabrication system and drug molecule, as well as predictions into *in vivo* release behavior were further examined in the last section of this report.

This chapter provides an overview of the principal methods, materials, and processing parameters chosen to form the main systems in this report.

1.7. Method Selection

1.7.1. Emulsion

Emulsification is one of the most common physicochemical particle fabrication techniques. Either the drug and polymer are suspended in an organic

solution then dropwise added to an aqueous phase (single emulsion, oil in water, o/w), or an aqueous drug suspension is suspended into an organic polymer solution and then resuspended into the aqueous solution (double emulsion, water in oil in water, w/o/w). This differentiation of hydrophobic and hydrophilic liquids assists in the creation of the particles. This method was chosen to create a particulate system for drug delivery because of its quick and inexpensive set-up, and its frequent use of PLGA particle fabrication.[4] Although, disadvantages can include large size distribution and leakage of contents during the process.[5] [6] Further system description can be found in chapter 3 & 4.

1.7.2. **Fluidic Nanoprecipitation**

Another method chosen for fabrication of particles was fluidic nanoprecipitation (fNP). fNP is an adapted form of nanoprecipitation, which involves solubilization of a polymer and drug into a water-miscible solvent, which is then drop-wise added to an aqueous surfactant solution.[7] [8] fNP incorporates flow of the continuous aqueous phase to allow individual particle creation via rapid solvent diffusion.[9] fNP was chosen because of the system advantages including the elimination of harsh solvents, scalability of the process, use of polymer and not monomeric units, and low cost.[9] [10] Further system description can be found in chapter 3 and 4.

1.8. Materials Section

1.8.1. Polymers (PLGA)

Many biodegradable polymers or polymer precursors could have been utilized for particle fabrication. Preformed polymers were chosen to eliminate risk of harsh solvent residue leftover from polymerization reactions. Some biodegradable polymers most commonly used include poly(DL-lactide-co-glycolide) (PLGA), poly(cyanoacrylate) (PCA), and poly(caprolactone) (PCL). PCL had an excessively longer degradation rate, while PCA had too fast of a degradation rate.[11] PLGA was chosen because it has a controllable degradation rate based on the lactide:glycolide ratio selected.[12]

1.8.2. **Solvents (Acetone, Acetonitrile, Dichloromethane)**

Both fNP and emulsification require PLGA dissolution in a solvent. fNP prefers a water-miscible solvent, while emulsification requires an organic solvent. Typical PLGA solvents include dichloromethane, tetrahydrofuran, ethyl acetate, chloroform, and acetone.[13] Acetonitrile and dichloromethane was both selected for fNP fabrication due to chemical compatibility with the equipment (tubes, pumps) and its mid to high miscibility with water.[9] Dichloromethane was selected for the emulsification fabrication method because it has a mid-range solubility; it is more miscible in water than solvents like chloroform, but less miscible than solvents like acetone and ethyl acetate.[14]

1.8.3. **Surfactant (PVA)**

There are many surfactants available for fNP or emulsion stabilization. Nonionic surfactants consist of macromolecules with amphiphilic properties, while ionic surfactants utilize electrostatic interactions.[4] Some main nonionic

surfactants include ethoxylated alcohols, fatty acid esters, and polyalcohols.[15] Poly(vinyl alcohol) was chosen because of it high solubility in water and it is a commonly used surfactant for emulsified particles.

1.8.4. **Bumped Kinase Inhibitors (BKIs: RM-1-132, 1294)**

The two bumped kinase inhibitors used in this study include RM-1-132 and 1294. Both drug molecules were designed and synthesized by the Maly Group in the Department of Chemistry and the Van Voorhis group in the Department of Medicine (*both at the University of Washington)*. The structures of both molecules are below:

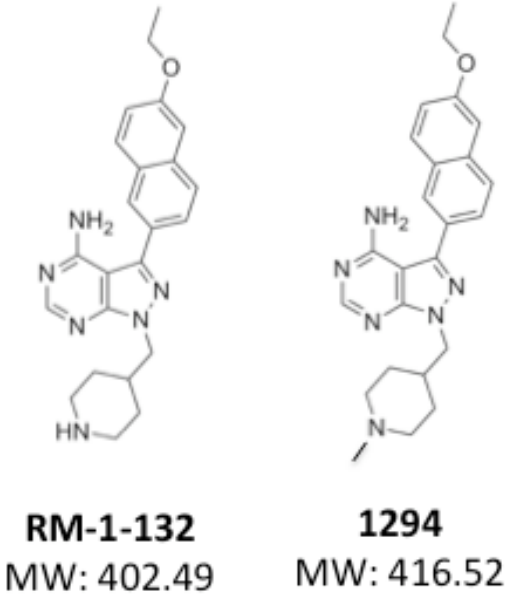

Figure 1.1. Schematic of bumped kinase inhibitors RM-1-132 and 1294 structure.

These molecules block the development of the malaria parasite from the gametocyte to gamete phase, specifically blocking the calcium dependent protein kinase 4 (CDPK4) whose knockout inhibits exflagellation in the male

gametocyte.[3, 16, 17, 18] This hinders growth of the malaria parasite inside of the mosquito, which reduces transmission of the parasite from mosquito to human. Effective malaria parasite transmission blocking has the potential to eradicate malaria.

1.9. **Processing Parameters**

Processing parameters were previously assessed prior to this study. For the fNP method, various dispersant flow rates, polymer input flow rates, type of pumps, and concentration of polymer was tested by J. Lee, C. Yang, and T. Gjersee *(H. Shen Lab, University of Washington)*. J. Lee optimized centrifugation parameters including volume of liquid, speed, and timing for the highest particle recovery. T. Gjersee optimized solvent ratio, needle direction, and location for the polymer input. All other parameters were based on the work of Xie, H.[9] For the emulsification methods, the procedure was adapted from K.K. Tran's protocol *(H. Shen Lab, University of Washington)*. Only sonication, vortexing time, and surfactant concentration was altered to create smaller dispersions as needed.

1.10. Thesis Objectives and Approach

Sustained drug delivery systems can ease administration by lowering frequency of doses required. The overall objective of this work was to develop a sustained drug delivery system for malaria transmission blockers. Extended delivery of these bumped kinase inhibitors (BKIs) can effectively block exflagellation of the malaria parasite leading to a reduction in disease

transmission, and hopefully the eradication of malaria.[3, 17, 19, 20] The first objective was to optimize a delivery system with the potential for administration. The second objective was to see how small differences in drug molecule or fabrication system could affect delivery system characteristics, incorporation of the drug molecule, and release. The third objective was to interpret the observed differences and predict *in vivo* behavior based on parallel models of the delivery systems.

Chapter 2 introduces various types of drug delivery systems highlighting advantages and disadvantages of each system and when each system is best applicable. The two main systems include implantable scaffolds and particulate injections, both commonly used in medication administration today. Chapter 2 presents the qualitative basis for selecting a particulate system for our drug delivery. Chapter 3 expands into nanoparticle fabrication techniques. Emulsification and fluidic nanoprecipitation (fNP) are methods used to create particulate systems. Emulsification is widely used, while fNP is still being optimized, but has a theoretical advantage for higher incorporation due to its faster “crash” nanoprecipitation.

Chapter 2 and 3 give insight into the experimental approach of the delivery system chosen. Chapter 4 discusses the fabrication of particulate systems in detail and the optimization steps for BKI incorporation. Fabrication pH played a key role in maximizing the incorporation. Increasing the continuous phase pH above the drug molecules’ pKa allowed higher incorporation of the drug molecule within the polymer matrix. Chapter 5 emphasizes the effects of a slight variable

added to the system. Adding one methyl group to the drug molecule or changing the fabrication system can have major effects on the particle characteristics, drug incorporation, and drug release. Chapter 6 investigates model systems to predict the drug delivery system's *in vivo* behavior and to further improve our particle systems. Lastly, Chapter 7 focuses on the main conclusions and future directions for osustained drug delivery systems for malaria transmission blockers.

Overall, this work describes the design and optimization of a sustained release system for delivery of BKIs for malaria transmission blocking. It also investigates into possible reasons why discrepancies were seen between different drug molecules and fabrication systems, and also predicts *in vivo* behavior.

1.11. Main Thesis Publications

Chapter 4 - 6: ***Yacoob C****, Ojo KK*, Maly DJ, Van Voorhis WC, Shen H. "Utilizing physicochemical parameters to optimize delivery systems for controlled release of amphiphilic bumped kinase inhibitors (BKI) for malaria transmission blocking" (in process).*

Yacoob C*, Park J, Yi MC, Sun BB, and Shen H. "The effect of length and terminal group of PEG-terminated self-assembled monolayers on dendritic cell maturation and function" (submitted, under review, 2013).*

***Yacoob C**, Hayes ET, Sangvanich T, Tran K, Shen H. "Mechano-regulation of the T cell activation" (in process).*

***Yacoob C**, Gjersee T, Lee J, Yang CP, Shen H. " Drug distribution within particles via fluidic nanoprecipitation (fNP) optimization" (in process)*

Other Publications:

1. *Sun B, Yi M, **Yacoob C,** Nguyen H, and Shen H. (2012) Effect of surface chemistry on gene transfer efficiency mediated by surface-induced DNA-doped nanocomposites. Acta Biomaterialia **8:**1109-1116.*
2. ***Yacoob C**, Liu W, and Adanur S. (2010) Properties and Flammability of Electrospun PVA and PVA/Laponite ® Membranes. Journal of the Industrial Textile **40:**33-48.*

1.12. References

1. Rosen H, Abribat T. The rise and rise of drug delivery. *Nature Reviews Drug Discovery* 2005, **4**(5)**:** 381-385.

2. Health CotEoADBoG. *Saving Lives, Buying Time: Economics of Malaria Drugs in an Age of Resistance*. The National Academies Press: Washington D.C., 2004.

3. Ojo KK, Pfander C, Mueller NR, Burstroem C, Larson ET, Bryan CM*, et al.* Transmission of malaria to mosquitoes blocked by bumped kinase inhibitors. *Journal of Clinical Investigation* 2012, **122**(6)**:** 2301-2305.

4. Astete CE. Synthesis of poly(DL-lactide-co-glycolide) nanoparticles with entrapped magnetite. Master of Science thesis, Louisiana State University, Louisiana State University, 2005.

5. Hans ML, Lowman AM. Biodegradable nanoparticles for drug delivery and targeting. *Current Opinion in Solid State & Materials Science* 2002, **6**(4)**:** 319-327.

6. Torche AM, Jouan H, Le Corre P, Albina E, Primault R, Jestin A*, et al.* Ex vivo and in situ PLGA microspheres uptake by pig ileal Peyer's patch segment. *International Journal of Pharmaceutics* 2000, **201**(1)**:** 15-27.

7. Leroueil-Le Verger M, Fluckiger L, Kim YI, Hoffman M, Maincent P. Preparation and characterization of nanoparticles containing an antihypertensive agent. *European Journal of Pharmaceutics and Biopharmaceutics* 1998, **46**(2)**:** 137-143.

8. Fessi H, Puisieux F, Devissaguet JP, Ammoury N, Benita S. NANOCAPSULE FORMATION BY INTERFACIAL POLYMER DEPOSITION FOLLOWING SOLVENT DISPLACEMENT. *International Journal of Pharmaceutics* 1989, **55**(1)**:** R1-R4.

9. Xie H, Smith JW. Fabrication of PLGA nanoparticles with a fluidic nanoprecipitation system. *Journal of Nanobiotechnology* 2010, **8**(18)**:** 1-7.

10. Schubert S, Delaney JT, Schubert US. Nanoprecipitation and nanoformulation of polymers: from history to powerful possibilities beyond poly(lactic acid). *Soft Matter* 2011, **7**(5)**:** 1581-1588.

11. Nair LS, Laurencin CT. Biodegradable polymers as biomaterials. *Progress in Polymer Science* 2007, **32**(8-9)**:** 762-798.

12. Anderson JM, Shive MS. Biodegradation and biocompatibility of PLA and PLGA microspheres. *Advanced Drug Delivery Reviews* 1997, **28**(1)**:** 5-24.

13. Polymers D-LA. Chemical & Physical properties. 2012 [cited 2012 January 12]Available from: http://www.absorbables.com/properties.htm

14. Yeo Y, Park KN. Control of encapsulation efficiency and initial burst in polymeric microparticle systems. *Archives of Pharmacal Research* 2004, **27**(1)**:** 1-12.

15. Salager J-L. Surfactants: types and uses. In: Andes UdL, editor. 2 ed. Merida, Venezuela: Laboratory of Formulation, Interface Rheology, and Processes; 2002. p. 50.

16. Ojo KK, Larson ET, Keyloun KR, Castaneda LJ, DeRocher AE, Inampudi KK*, et al.* Toxoplasma gondii calcium-dependent protein kinase 1 is a target for selective kinase inhibitors. *Nature Structural & Molecular Biology* 2010, **17**(5)**:** 602-U102.

17. Johnson SM, Murphy RC, Geiger JA, DeRocher AE, Zhang ZS, Ojo KK*, et al.* Development of Toxoplasma gondii Calcium-Dependent Protein Kinase 1 (TgCDPK1) Inhibitors with Potent Anti-Toxoplasma Activity. *Journal of Medicinal Chemistry* 2012, **55**(5)**:** 2416-2426.

18. Murphy RC, Ojo KK, Billker O, Van Voorhis W, Maly DJ. BUMPED KINASE INHIBITORS BLOCK MALARIA TRANSMISSION TO MOSQUITOES. Journal of Investigative Medicine: Western Regional Meeting Infectious Diseases Concurrent Session; 2012 January 27, 2012; Carmel, CA: Journal of Investigative Medicine; 2012. p. 169-170.

19. Ojo KK, Van Voorhis W, *al. e*. *Submitted, Under Review*. *JCI* 2012.

20. Murphy RC, Ojo KK, Billker O, Van Voorhis W, Maly DJ. BUMPED KINASE INHIBITORS BLOCK MALARIA TRANSMISSION TO MOSQUITOES. *Journal of Investigative Medicine* 2012, **60**(1)**:** 169-170.

CHAPTER 2. DRUG DELIVERY SYSTEMS: A REVIEW

2.1 Introduction

Drug delivery systems are engineered-materials that dispense a constant supply of drugs to a patient for a desired dosage period. These systems can consist of particulate injections, implantable scaffolds, transdermal patches, ingestible tablets, or adaptations of these techniques.[1] [2] [3] [4] The first challenge is obtaining constant drug release necessary for therapeutic effects, which needs to remain at a level underneath the maximum toxic concentration (MTC) and above the minimum effective concentration (MEC).[5] Another challenge is system pliability to drug properties, i.e. hydrophobicity or size, which can alter overall drug retention or *in vivo* release kinetics.[6] Thus, engineering a system that is easy to fabricate and administer to patients with a sustained release over a desired time period and capability of incorporating any type of drug, or combination of therapeutics, regardless of properties is an idyllic system still being uncovered today.

2.2 Drug Delivery Systems

2.2.1 Sustained Release and Pharmacokinetics

Pharmacokinetics and pharmacodynamics are the mathematical assessments of drug release into the system and its subsequent effects in the body.[7] The required drug concentration in the blood needs to be below the MTC, also called the maximum tolerated dose (MTD), to ensure that toxic repercussions do not occur.[8] The drug concentration also needs to be above the

MEC, or minimum therapeutic dose (MTD), with the quantity of the inputted drug into the patient at a sufficient amount for absorption, distribution, and clearance from the body.[7 8] An example of a sustained dosage over four weeks is shown in Figure 2.1.

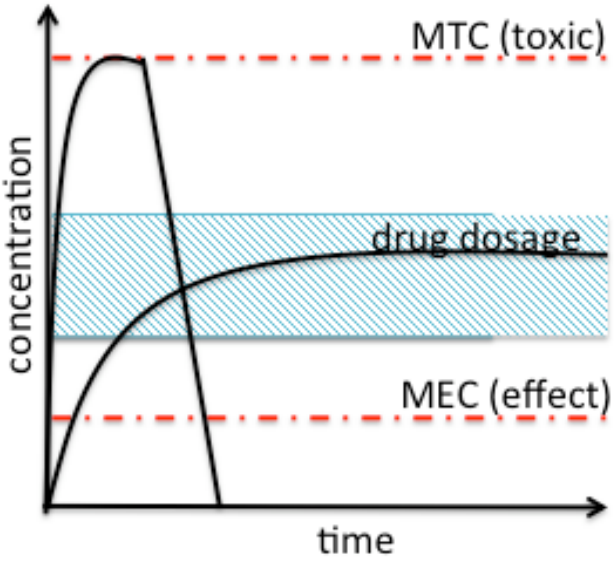

Figure 2.1. Drug concentration for a bolus injection versus a controlled release system over time. Bolus injection causes sharp rise and fall of drug concentration as compared to the controlled release from a delivery system, i.e. drug-loaded microspheres, which provided a constant sustained amount of drug. Dotted lines on the graph indicate the maximum toxic concentration (MTC) and the minimum effective concentration (MEC).

Drug dosage can therefore be plotted as profiles with desired drug plasma concentration, C_p, versus time to examine drug release from delivery systems and/or drug elimination from the body.[5 7] These plots can be categorized into kinetic profiles with instantaneous release, zero-order release, or first-order release (Figure 2.2).[5 9] Instantaneous release is typically a bolus injection where

the patient receives a large amount of drug in a short period of time, and is not fully investigated here.

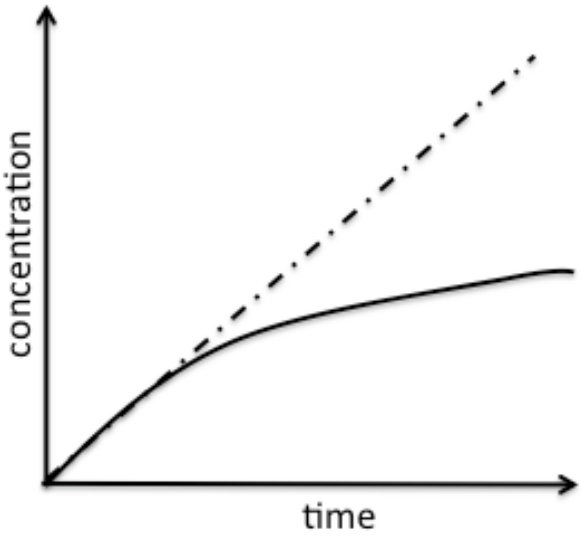

Figure 2.2. Graph of zero-order *(dotted line)* and first-order *(solid line)* kinetics.

Zero-order releases the drug at a constant rate represented by the following equation:

$$\frac{dA}{dt} = k_0$$

where A = drug mass, t = time, k_0 = zero-order kinetic rate constant.[5]

First-order releases the drug at a rate determined by the amount of drug at absorption sites, or by alternative factors, represented by the following equation:

$$\frac{dC_p}{dt} = k_a C_{abs}$$

where C_p = drug plasma concentration, t = time, k_a = absorption rate constant, and C_{abs} = concentration of drug at the site of absorption.[5]

The ideal system is a zero-order or first order release system that can remain above the MEC and below the MTC for a desired period of time. This would facilitate a predictable, reliable treatment without the necessity for repeated and frequent dosages.

2.2.2 Types of Sustained Release Systems

2.2.2.1 Implantable Scaffolds

Systematic administration of drugs have some limitations, including trafficking through complex biology to the intended administration site and dispensing an effective enough amount without adverse effects on the body.[8] One of the solutions to these predicaments is implantable scaffolds. These are polymeric materials embedded directly at a tissue site that permit the slow release of drug near a target, i.e. tumor, for a prolonged period of time.[8] Furthermore, the drug can be protected from degradation until release into the treatment site.

Typically, these implantable materials are fabricated from non-degradable polymers or biodegradable polymers. Non-degradable materials include silicone, silicone-nylon, and poly(ethylene-co-vinyl acetate) (EVAc).[10] [11] These devices can either be refillable polymer tubes or homogenously dispersed drug/polymer matrices, where drug release is controlled by diffusion through the polymeric shell/matrix.[8] Some biodegradable matrices include poly(lactide-co-glycolide)

(PLGA), poly(carboxyphenoxy-propane/sebacic acid) anhydride (PCPP-SA), and polymetacrylic methyl acid (PMMA).[12 13 14] In addition to diffusion, these systems release drugs by polymer degradation from hydrolysis and erosion, which are parameters that can be manipulated during fabrication or with material choice.[15] Some of these release mechanisms are exemplified in Figure 2.3.

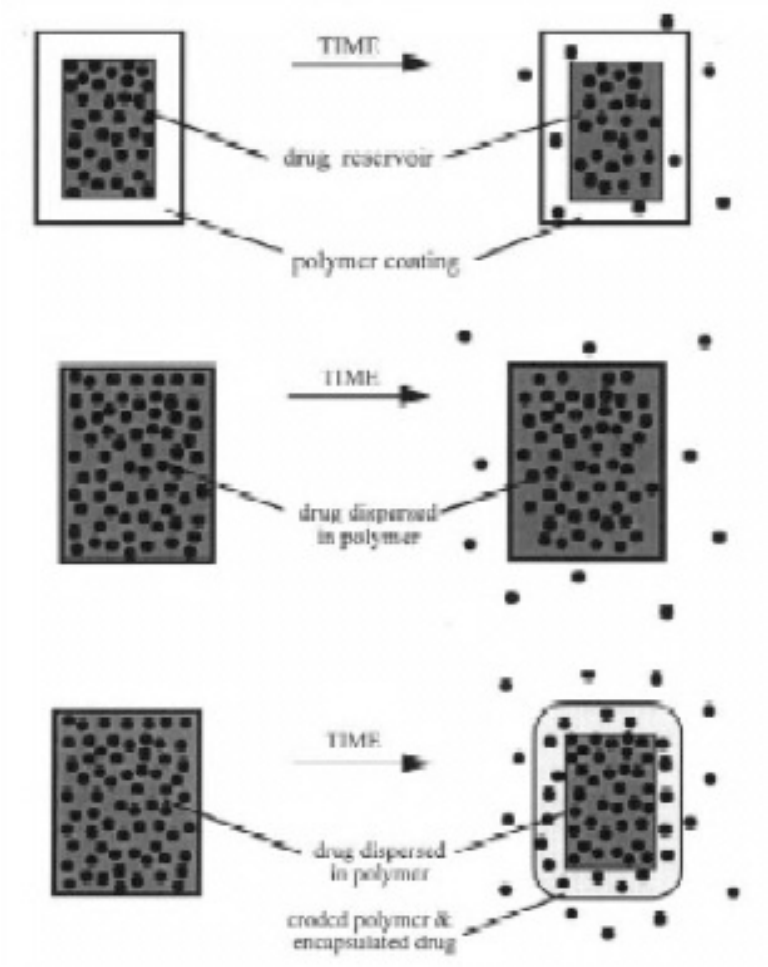

Figure 2.3. Schematics of diffusion controlled reservoir system *(top),* diffusion-controlled matrix system *(middle),* and dual diffusion/erosion-controlled biodegradable polymeric system *(bottom)*. Permission obtained from Ref. Fung [8]

2.2.2.2 Particulate Injections

Recently, micro and nanoparticulate systems have also shown great promise as drug delivery systems by overcoming delivery barriers of traditional pharmaceutics.[16] An injectable particulate system can be administered intramuscularly or systematically while protecting the integrity of the drug. Particle surface characteristics can be modified to passively or actively transport particles to target-specific locations where treatment is needed.[1] Additionally, release rates can be modulated to control amount and duration of a sustained therapeutic delivery.[6] However, some limitations include aggregation in storage and reliability from particle to particle and batch to batch.[1]

Particle fabrication methods include emulsification, spray-drying, supercritical antisolvent process (SAS), molding, and polymerization.[4 17 18 19 20] Types of particulate systems produced include particles where drugs are uniformly dispersed throughout a matrix system, and capsules where a drug depot is surrounded by a polymeric membrane.[1] For particles, fabrication parameters play a crucial role in amount of drug incorporated as shown in Figure 2.4. Drug release from the particles is similar to the implantable systems, where release is controlled by diffusion and polymer degradation/erosion. Although, for capsules, the drug release is controlled by material choice for the shell, where an impermeable layer regulates release through porosity and channels, and a permeable layer via rate of diffusion through the polymer.[2 6]

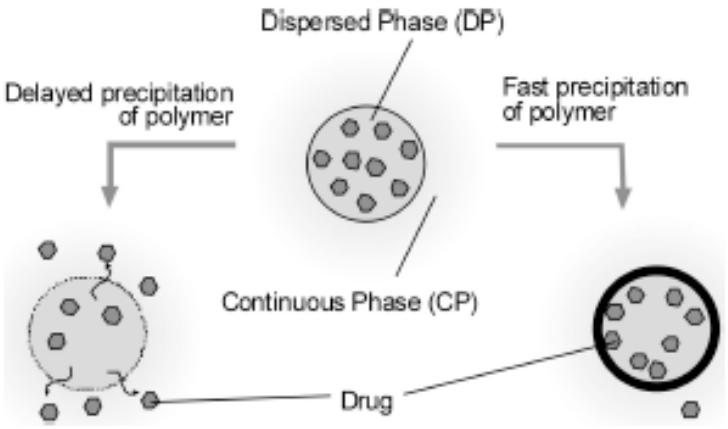

Fig. 1. Schematic description of the rationale for encapsulation efficiency.

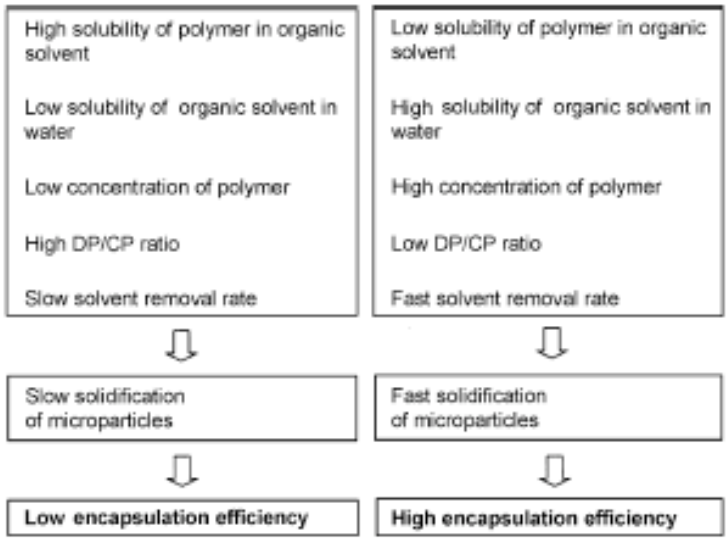

Figure 2.4. Schematic of particulate fabrication parameters influencing drug incorporation. Permission obtained from Ref. Yeo [6]

2.2.2.3 Alternative Systems

Alternative drug delivery systems are also under current investigation to improve ease of delivery, availability to patients, and increase duration of therapeutic benefit. Some sustained-release alternative systems include cell-mimicking particles, microneedle arrays, and *in situ* forming polymers.[3 21 22] Red

blood cell (RBC)-mimicking particles were created to match the sophistication of the body's biology including flexible shape and ability to carry oxygen, in addition to the usual nanoparticles functions of encapsulating drugs and/or imaging agents.[3] These RBC-mimicking particles demonstrate the advantages of impersonating the complex biology of the body to improve circulation time, increase targeting effectiveness, extend sustained drug release, and reduce side effects due to factors like immune system recognition of non-self particles.[3]

Dissolving microneedle patches have been utilized as a simpler and safer injection/implantation technique to eliminate the need for hypodermic needles or trained medical staff.[21] [23] These patches are applied directly to the skin, then removed leaving the microneedles behind which can slowly release drug as they are dissolved, typically occurring within five days.[24] [25]

Another novel system, *in situ* forming implants, congeal to form a solid structure after injection into the body.[22] The solidification usually occurs due to solution cooling to body temperature, but may also form via polymer precipitation, heating, or swelling.[22] [26] Some disadvantages of this technique include the loss of drug while solution is gelling.

2.2.3 Drug Molecule Characteristics

Usually the delivery system is designed around drug properties, i.e. hydrophobicity, size, or need for protection. For hydrophobic drugs systems oil-base injections, drug suspensions, or particulate systems are utilized. Oil based injections are drugs mixed into an oil-based solvent and systematically injected

into the blood stream. The disadvantage is that clearance from the body is based on the half-life of the drug, which although slightly extended from the increased lipophilicity can still not be prolonged enough.[27] Injectable drug suspensions are similar except that the drug is suspended in an aqueous solution. Disadvantages include formation of drug crystals, which can promote a rapid onset as opposed to a sustained release over time.[28] Additionally, single emulsion into an organic solvent for hydrophobic drug entrapment has been successfully used for schizophrenia or cancer treatment therapy with system adaptability of release from hours to months.[22]

For hydrophilic drugs, *in situ* forming gel matrices have been utilized. For example injection of lanreotide acetate will self-assemble into crystalline rods when exposed to at least 10% water.[26] Disadvantages could include pre-release of drug before entire gel is formed. Another system is the double emulsion of aqueous phase into an organic phase (water in oil in water, or w/o/w) for hydrophilic drug incorporation into microparticles. A disadvantage is that the w/o/w process elicits problems like low drug retention during fabrication and tendency for burst release.[29]

Researchers are now looking for systems which have adaptability for drugs with varying properties either for single or co-delivery.[30] For single delivery, advantages include minimum redesign of the entire system when the drug is altered, especially if it is for the same therapeutic application. In addition, these systems would be good for amphiphilic drugs, which are not easily classified into strictly hydrophobic or hydrophilic carriers.[16] For co-delivery, advantages include

synergistic effects, suppressed drug resistance due to a “cocktail” delivery, and drug dosage tuning within a particle.[30]

2.3 Characterization

2.3.1 Size and Size Distribution

Implantable materials are usually fabricated in molds, where the size is pre-determined prior to casting. Particulate systems size and size distribution is classified by a combination of methods, with the most popular being dynamic light scattering (DLS) and microscopy, including optical, scanning electron microscopy (SEM), and transmission electron microscopy (TEM).[31] Zeta potential can also be measured to ensure particle stability when in suspension. Measurements can be taken for peak mean sizes, polydispersity or size distribution, and electrical charge using the same equipment and sample.

2.3.2 Morphology

Optical, SEM and TEM imaging are utilized to visually determine scaffold topography, particle surface morphology, as well as structural changes for *in situ* gels.[26] Morphology is important to ensure that the delivery system is correctly formed, as well as to determine any structural problems, i.e. porosity increase or membrane coating cracking or unevenness. TEM can also show variances in regards to material composition if the there are known differences in electron density.[32]

2.3.3 Total Drug Yield

Total drug yield usually involves a complete dissolution of the material and recovery of contents. The drug can either have a fluorescent label or radiolabel to help quantify the amount incorporated into the system.[17] Moreover, the activity of the drug can be tested to quantify incorporation or as proof that drug integrity and function was sustained throughout fabrication processes. Additionally, if the drug in conjugated to the peptide carrier or polymer used in scaffold or particulate matrices, the unconjugated excess drug may be assayed to determine total incorporation.[33]

2.3.4 Release Kinetics

For release studies, or *in vitro* studies, drug delivery systems are usually held in an aqueous or body fluid-mimicking environment at 37C, possibly with agitation, with supernatant removals at specified timepoints. Drug release can be analyzed from the collected samples by the techniques listed above or by other methods including high-performance liquid chromatography (HPLC).[30]

2.3.5 *In vivo* testing

In vivo experimentation encompasses the administration of the drug delivery systems through their specified routes, i.e. intramuscular injection or subcutaneous implantation, to animals or humans.[34] Animals can be challenged by a virus or disease, or already have a pre-existing condition for which this drug delivery system is applicable. Plasma samples at specific intervals and recording

of disease advancement/recession are collected and assayed to determine system efficacy.

2.4 Conclusions

There are a multitude of systems available for sustained drug release. The main goal is to ensure that the drug is delivered continuously for a prolonged period of time while staying below toxic levels but above minimum effective levels. The release for the delivery system also needs to be kinetically favorable, which is generally zero-order because this provides a constant release.

The two main delivery systems include implantable scaffolds and particulate delivery systems. These are easy to fabricate and administer, while also having manipulative properties to yield determined drug release profiles. Implantable scaffolds are either reservoirs of drug or diffusion-based systems for at-the-site administration. Particles allow systematic or intramuscular injection of protected drug that transport to specific sites where diffusion-based drug administration can occur. Novel systems including microneedle arrays and cell-mimicking particles, which permit self-administration and even longer circulation times *in vivo*.

Advances still need to be made on overall drug incorporation especially with drugs with different properties. Co-delivery has been considered especially for cancer therapeutics to avoid drug-resistance of single drug administration. Versatility of the delivery system is very important, as drug-specific systems may

not be feasible in scale-up production or for flexibility in types of drug incorporated.

2.5 References

1. Mohanraj V, Chen Y. Nanoparticles - a review. *Tropical Journal of Pharmaceutical Research* 2006, **5**(1)**:** 561-573.

2. Freese A, Sabel BA, Saltzman WM, During MJ, Langer R. Controlled release of dopamine from a polymeric brain implant - *in vitro* characterization. *Experimental Neurology* 1989, **103**(3)**:** 234-238.

3. Doshi N, Zahr AS, Bhaskar S, Lahann J, Mitragotri S. Red blood cell-mimicking synthetic biomaterial particles. *Proceedings of the National Academy of Sciences of the United States of America* 2009, **106**(51)**:** 21495-21499.

4. Wen Y, Gallego MR, Nielsen LF, Jorgensen L, Everland H, Moller EH*, et al.* Biodegradable nanocomposite microparticles as drug delivering injectable cell scaffolds. *Journal of Controlled Release* 2011, **156:** 11-20.

5. Uchizono JA. *Application of pharmacokinetics and pharmacodynmics in the design of controlled delivery systems*. McGraw-Hill: New York, 2006.

6. Yeo Y, Park KN. Control of encapsulation efficiency and initial burst in polymeric microparticle systems. *Archives of Pharmacal Research* 2004, **27**(1)**:** 1-12.

7. Dhillon S, Gill K. *Basic pharmacokinetics*. Pharmaceutical Press: Grayslake, IL, 2006.

8. Fung LK, Saltzman WM. Polymeric implants for cancer chemotherapy. *Advanced Drug Delivery Reviews* 1997, **26**(2-3)**:** 209-230.

9. Corporation WB. Excerpt from "Introduction to enzymes". *Manual of Clinical Enzyme Measurements* 1972**:** 17.

10. Ueno N, Refojo MF, Liu LHS. CONTROLLED RELEASE RATE OF A LIPOPHILIC DRUG (BCNU) FROM A REFILLABLE SILICONE-RUBBER DEVICE. *Journal of Biomedical Materials Research* 1982, **16**(5)**:** 669-677.

11. Shen H, Goldberg E, Saltzman WM. Gene expression and mucosal immune responses after vaginal DNA immunization in mice using a controlled delivery matrix. *Journal of Controlled Release* 2003, **86**(2-3)**:** 339-348.

12. Craig PH, Williams JA, Davis KW, Magoun AD, Levy AJ, Bogdansky S*, et al.* BIOLOGIC COMPARISON OF POLYGLACTIN-910 AND POLYGLYCOLIC ACID SYNTHETIC ABSORBABLE SUTURES. *Surgery Gynecology & Obstetrics* 1975, **141**(1)**:** 1-10.

13. Brem H, Piantadosi S, Burger PC, Walker M, Selker R, Vick NA*, et al.* PLACEBO-CONTROLLED TRIAL OF SAFETY AND EFFICACY OF INTRAOPERATIVE CONTROLLED DELIVERY BY BIODEGRADABLE POLYMERS OF CHEMOTHERAPY FOR RECURRENT GLIOMAS. *Lancet* 1995, **345**(8956)**:** 1008-1012.

14. Kubo O, Tajika Y, Muragaki Y, Nitta M, Kagawa M, Yoshida M*, et al.* TREATMENT OF MALIGNANT BRAIN-TUMOR WITH SLOWLY RELEASING ANTICANCER DRUG-POLYMER COMPOSITES. *Radiation Physics and Chemistry* 1992, **39**(6)**:** 521-525.

15. von Burkersroda F, Schedl L, Gopferich A. Why degradable polymers undergo surface erosion or bulk erosion. *Biomaterials* 2002, **23**(21)**:** 4221-4231.

16. Zhang X-X, Eden HS, Chen X. Peptides in cancer nanomedicine: drug carriers, targeting ligands and protease substrates. *Journal of Controlled Release* 2011**:** 14.

17. De Temmerman M-L, Rejman J, Vandenbroucke RE, De Koker S, Libert C, Grooten J*, et al.* Polyelectrolyte LbL microcapsule versus PLGA microspheres for immunization with protein antigen. *Journal of Controlled Release* 2011**:** 8.

18. Yeo SD, Kiran E. Formation of polymer particles with supercritical fluids: A review. *Journal of Supercritical Fluids* 2005, **34**(3)**:** 287-308.

19. Rosenberg RT, Siegel SJ, Dan N. Release of highly hydrophilic drugs from poly(epsilon-caprolactone) matrices. *Journal of Applied Polymer Science* 2008, **107**(5)**:** 3149-3156.

20. Crownover E, Duvall CL, Convertine A, Hoffman AS, Stayton PS. RAFT-synthesized graft copolymers that enhance pH-dependent membrane destabilization and protein circulation times. *Journal of Controlled Release* 2011, **155**(2)**:** 167-174.

21. Sullivan SP, Koutsonanos DG, Martin MD, Lee JW, Zarnitsyn V, Choi SO*, et al.* Dissolving polymer microneedle patches for influenza vaccination. *Nature Medicine* 2010, **16**(8)**:** 915-U116.

22. Rhee Y-S, Park C-W, DeLuca PP, Mansour HM. Sustained-Release Injectable Drug Delivery. *PharmTech* 2010.

23. Lee JW, Park JH, Prausnitz MR. Dissolving microneedles for transdermal drug delivery. *Biomaterials* 2008, **29**(13)**:** 2113-2124.

24. Martin CJ, Allender CJ, Brain KR, Hodson D, Birchall JC. Biodegradable sugar glass microneedles for macromolecular drug delivery. *Journal of Pharmacy and Pharmacology* 2010, **62**(6)**:** 799-799.

25. Park JH, Allen MG, Prausnitz MR. Polymer microneedles for controlled-release drug delivery. *Pharmaceutical Research* 2006, **23**(5)**:** 1008-1019.

26. Valery C, Artzner F, Robert B, Gulick T, Keller G, Grabielle-Madelmont C*, et al.* Self-association process of a peptide in solution: From beta-sheet filaments to large embedded nanotubes. *Biophysical Journal* 2004, **86**(4)**:** 2484-2501.

27. Ruiz P, Strain E. *Lowinson and Ruiz's Substance Abuse*, 5th edn. Lippincott Williams & Wlikins: Philadelphia, 2011.

28. Rosen H, Abribat T. The rise and rise of drug delivery. *Nature Reviews Drug Discovery* 2005, **4**(5)**:** 381-385.

29. Domb A, Kumar N, Ezra A. Biodegradable polymers in clinical use and clinical development. 1st ed: John Wiley & Sons; 2011. p. 752.

30. Zhang LF, Radovic-Moreno AF, Alexis F, Gu FX, Basto PA, Bagalkot V*, et al.* Co-delivery of hydrophobic and hydrophilic drugs from nanoparticle-aptamer bioconjugates. *Chemmedchem* 2007, **2**(9)**:** 1268-1271.

31. Instruments M. Dynamic Light Scattering (DLS). Laboratory Products 2011 [cited 2011 Dec 29]Company]. Available from: http://www.malvern.com/labeng/technology/dynamic_light_scattering/dynamic_light_scattering.htm

32. Woehrle GH, Hutchison JE, Ozkar S, Finke RG. Analysis of nanoparticle Transmission Electron Microscopy data using a public-domain image-processing program, Image. *Turkish Journal of Chemistry* 2006, **30**(1)**:** 1-13.

33. Anglin EJ, Cheng LY, Freeman WR, Sailor MJ. Porous silicon in drug delivery devices and materials. *Advanced Drug Delivery Reviews* 2008, **60**(11)**:** 1266-1277.

34. Burns R, McRae G, Sanders L. A ONE YEAR CONTROLLED RELEASE IMPLANT FOR THE LUTEINIZING-HORMONE-RELEASING HORMONE SUPERAGONIST RS-49947 .2. CLINICAL-PERFORMANCE RESULTS. *Journal of Controlled Release* 1990, **14**(3)**:** 233-241.

CHAPTER 3. NANOPARTICLE FABRICATION: A REVIEW

3.1 Introduction

Nanoparticulate systems are colloidal suspensions of 10nm – 1000nm sized polymeric spheres. For pharmaceutical applications, nanoparticles are advantageous because they are easy to deliver intravenously, have high bioavailability, and can be utilized to target specific cells for drug delivery or gene therapy.[1] Therefore, formulation of nanoparticles with the appropriate size, minimized size distribution, consistent morphology, and controlled properties is a challenge in order to guarantee both an effective and reliable treatment.[2]

3.2 Current Nanoparticle Fabrication Methods

Current nanoparticle fabrication systems include physical methods, i.e. milling and spray drying, chemical synthesis methods like polymerization, and physicochemical methods including emulsification and nanoprecipitation.[3] [4] [5] [6] Milling involves granulating particles down to a particular size with either high velocity vibratory ball mills or with grinding motion using planetary ball mills.[7] Spray drying techniques encompass drying liquid substances rapidly while in aerosol form into a solid powder, usually by spraying the liquefied polymer into a stream of heated air.[2] [3] Step-growth polymerization comprises of a reaction-controlled assembly of monomeric units into a micro/nanostructure.[8]

Emulsification, one of the physicochemical techniques, utilizes the hydrophobic and hydrophilic incompatibility of polymers, drugs, and solvents to

create nanoparticles. A polymer is dissolved in an organic phase that is partially miscible in water and is drop-wise suspended into a surfactant/water mixture under agitation. The polymer hardens and forms into particles as the organic solvent diffuses into the water. The advantages of this method are that it is easy to set up and requires low energy since only agitation is required.[4] The disadvantages are that internalized contents may leak out during the solvent evaporation step and particle size is difficult to control.[5 9] Additionally, this emulsification method can be adapted to a double emulsion technique to incorporate hydrophilic drugs by suspending droplets of an aqueous drug mixture in the polymer/organic phase before emulsification into the surfactant/water mixture.[10]

Another prevalent method is nanoprecipitation, which can eliminate the use of harsh solvents, i.e. chlorinated organics used in emulsification. The polymer and drug are solubilized in a semi-polar water-miscible solvent, i.e. acetone or propylene carbonate, then added to an aqueous surfactant solution.[11 12] The acetone can be eliminated by dialysis, evaporation via reduced pressure, or by stirring for a prolonged time period.[5 11 13] This technique has recently been adapted by Xie, et. al. to a fluidic system where the polymer mixture is added to a flowing stream of stabilizer/water (Figure 3.1).[6] Both macro-scale and micro-fluidic devices have utilized this interfacial polymerization technique to create and collect these nanoparticles as they are formed.[14 15 16] Lorber et al. review various types of fluidic nanoprecipitation systems including a T-junction, co-flow, and cross-flow devices.[17] The advantages of these systems include

instantaneous particle formation by rapid solvent diffusion, use of benign solvents, use of polymers not monomeric units which may leave residue, influence over particle properties, i.e. size by controlling concentration and velocity of channels, and low energy requirements.[6] [16] The disadvantages include the possible loss of the particle load to the fast-moving continuous phase and some increased difficulties with solvent removal.[16]

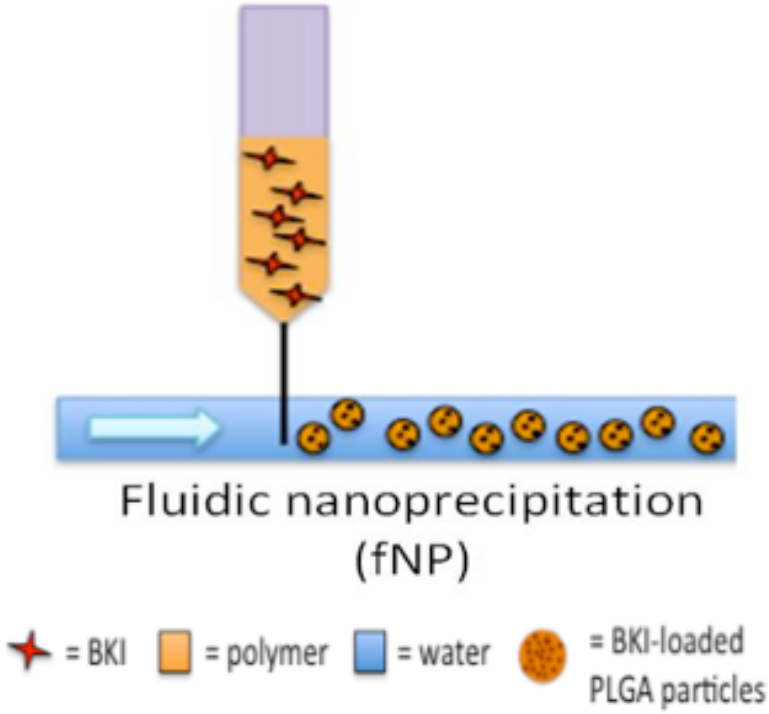

Figure 3.1. Schematic of fluidic nanoprecipitation system.

3.2.1 Emulsification and Process Parameters

Process parameters of the emulsification process can affect particle properties. Concentration of surfactant in the continuous phase, type of surfactant, as well as duration and power of homogenization/ultrasonication can

alter particle size.[18] Controlling the water miscibility of the solvents used will also affect the diffusion into the continuous phase; a faster diffusion will elicit a smaller particle size.[19]

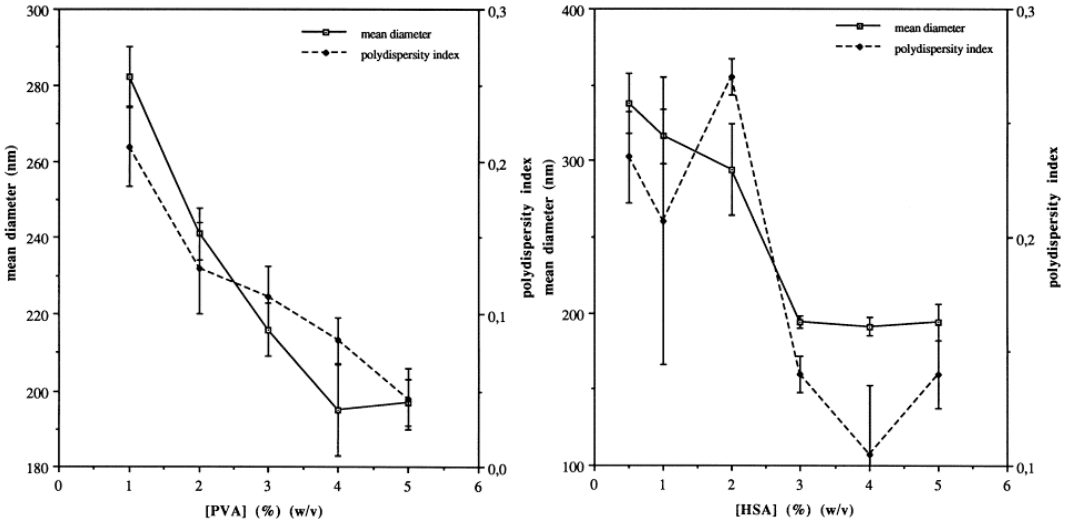

Figure 3.3. Controlling PLGA nanoparticle size by surfactant concentration in an emulsification system (A: PVA, B: HAS). Reproduced from Ref. Zambaux et al. [18]

Emulsion fabricated particles are being used for current medications, the most well known is Tocosol Paclitaxel. Paclitaxel, an inhibitor of cell division, passively targets tumors after release from a deposition of these emulsion-fabricated particles.[20] Other medications utilize emulsion-fabricated particles for delivery of antibodies and drugs, with a strong focus on cancer treatments like curcumin whose hydrophobic tendency allows higher incorporation into the o/w emulsion-fabricated particle system.[21]

3.2.2 Fluidic Nanoprecipitation and Process Parameters

Many of the process parameters of the fluidic nanoprecipitation (fNP) system can be more easily manipulated to result in various particle properties, unlike alternative methods of particle fabrication, i.e. emulsification or spray drying. The data obtained by Xie et al. shows that increasing the dispersant flow enables quicker solvent removal from the particle and can reduce particle size (Figure 3.4).[6] Additionally, lowering the polymer concentration likewise facilitates smaller particle size, but can also cause issues with decreased overall loading (Figure 3.4).[6 22] Furthermore, Xie et al. and Jeyanthi et al. both revealed that additives in the dispersant phase, i.e. methanol, can facilitate water diffusion from the particle into the dispersant to cause a decrease in particle size (Figure 3.5, Figure 3.6).[6 22 23] These defined parameters are easy to manipulate in an inexpensive fNP system and can help yield uniform particles with the desired size and properties.

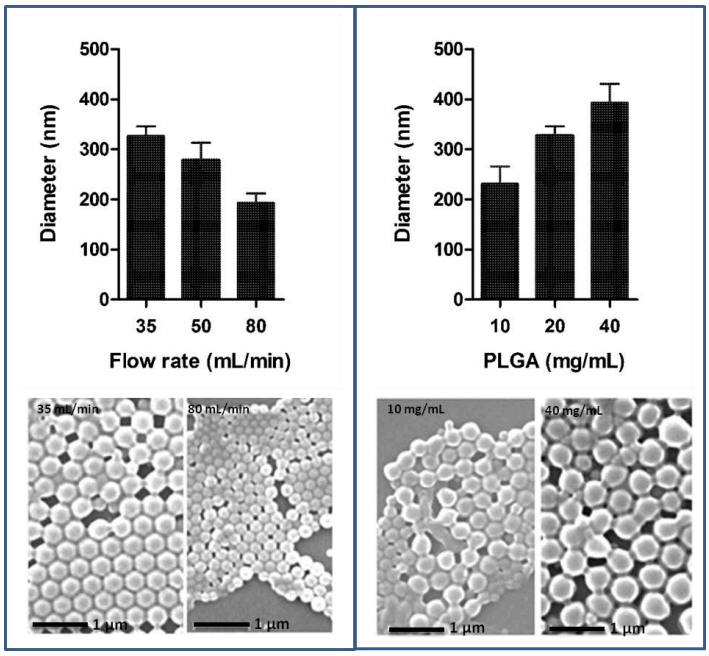

Figure 3.4. Controlling PLGA nanoparticle size by dispersant flow rate and PLGA concentration in a fluidic nanoprecipitation system. Permission obtained from Ref. Xie et al. [6]

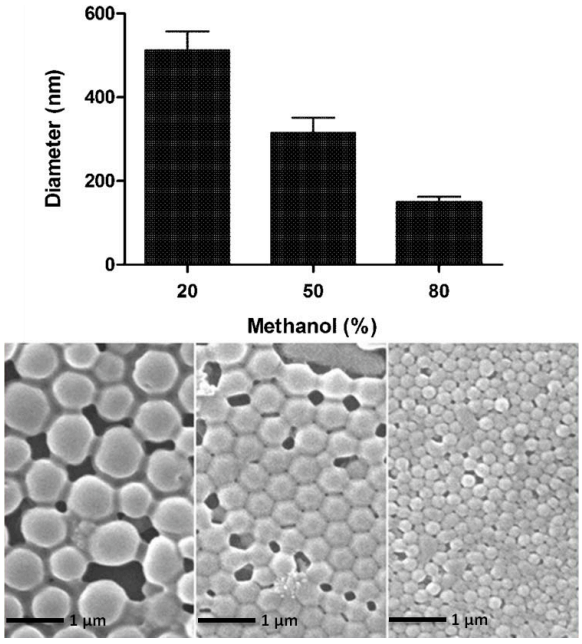

Figure 3.5. Controlling PLGA nanoparticle size by concentration of methanol added into the dispersant phase in a fluidic nanoprecipitation system. Permission obtained from Ref. Xie et al. [6]

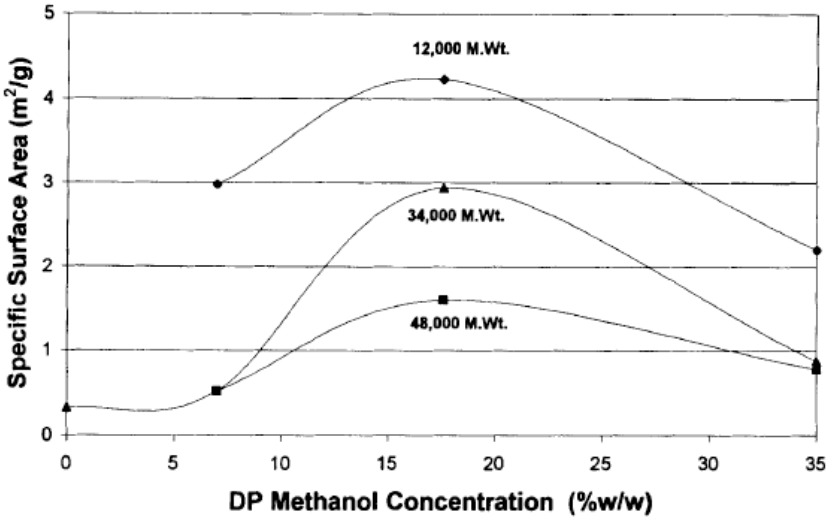

Figure 3.6. Effect of methanol concentration on particle surface area for three PLGA molecular weights. Permission obtained from Ref. Jeyanthi et al. [23]

Fluidic nanoprecipitation (fNP) fabricated particles can be utilized for a variety of applications including drug delivery systems and imaging tools.[6] Schubert et al. described how nanoprecipitation is appealing for amphiphilic block polymers because assembly can be calculated and controlled.[16] These amphiphilic carriers can be employed as hydrophobic drug carriers, protein delivery systems, cosmetic applications, and pesticidals.[16] Fluidic nanoprecipitation has also been exploited for controlled combination drug therapeutics because its low variability from particle to particle facilitates the administration of drugs with different solubility, charge, and molecular weight.[24] Nisisako et al. fabricated bichromal particles made of black or white pigment-colored monomers using a Y-junction flow.[25] These particles can be utilized for electrical displays like electronic reusable paper.

Essentially, the tunability of the fNP process, i.e. flow rates, precursor composition, and dispersant composition allows control over the nanoparticle fabrication process and resultant particles. Manipulating these properties can yield desired particle size, structure, and drug loading. Moreover, the rapid solvent mixing to form and harden the particles generates more homogeneous nanoparticles, making administration of treatments and reliance of applications more dependable.[15]

3.3 Characterization

3.3.1 Size and Size Distribution

Size and size distribution is typically analyzed by a combination of methods including dynamic light scattering (DLS) and imaging via microscopy. DLS, also referred to as photon correlation spectroscopy (PCS) or quasi-elastic light scattering (QELS), is non-invasive and requires an expendable amount of sample.[26] Zeta potential was also measured to determine particle composition and stability of the nanoparticle suspension. Typically the suspension is well-mixed by either vortexing or sonication to reduce aggregation. Measurements are taken for z-average size based on the hydrodynamic radius, peak mean sizes, polydispersity or size distribution, and electrical charge using the same equipment and sample.

3.3.2 Morphology

The methods generally used to visually characterize nanoparticle morphology are optical microscopy, scanning electron microscopy (SEM) and

transmission electron microscopy (TEM).[4] Morphology is important to ensure accurate and precise particle formation. Optical microscopy allows a real-time view of the sample highlighting internal and surface morphology.[27] SEM allows higher resolution than light microscopy to analyze fine details and topography of surfaces. TEM is useful since electrons will absorb differentially based on the thickness and type of material, so that composition data can be obtained as well.[28]

3.3.3 Additional Properties

Additional nanoparticle characterization methods include Fourier transform infrared spectroscopy (FTIR), atomic force microscopy (AFM), nuclear magnetic resonance (NMR), ultraviolet-visible spectroscopy (UV-Vis), and x-ray diffraction (XRD).[4] FTIR provides information on surface modifications of the particles due to adsorbed proteins or conjugation of specific components.[29] Ignjatovic et al. used FTIR to confirm the structure and phase organization of PLGA coated calcium phosphate particles.[30] AFM is another method to analyze size and morphology of particles, and use of specific AFM tips can provide additional surface chemistry information. Mohamed et al. used AFM to directly measure particle-particle interaction to understand *in vitro* effects of aerosol particles.[1]

NMR can be utilized to identify specific structures in the nanoparticle.[4] Taniguchi et al. used NMR to ensure core/shell formation of P(St-CPEM)-*g*-PDMAEMA nanoparticles.[31] UV-Vis can be utilized to measure amount of incorporated material or the polymer itself. Choi et al. utilized UV-Vis to measure

the amounts of BMP-2 incorporated inside PLGA/Alginate microcapsules.[32] Lastly, XRD is another method to measure incorporated material. Gou et al. used XRD to compare free curcumin versus curcumin-loaded mPEG-PCL micelles.[33]

3.4 Conclusions

There are many methods to fabricate nanoparticles, each with their own advantages and disadvantages. Systems should be chosen based on the desired particle properties and effects. Emulsification and nanoprecipitation are both popular methods employed for PLGA nanoparticle fabrication due to the ease of production and control over size. Fluidic nanoprecipitation adds extra advantages including increasing the control over particle properties with easily manipulative process parameters and by the possible elimination of some harsh chemicals.

Different characterization techniques permit comprehensive evaluation of nanoparticulate systems. DLS and imaging can be employed to quantify size, size distribution, and charge analysis. Optical microscopy, TEM, SEM, and AFM allow examination of the surface morphology and composition to highlight successful particle structure or defects. UV-Vis and XRD can be utilized to determine amount of incorporated materials.

Uniform and consistent nanoparticulate systems are the focus of current research. These investigations will help create reliable and effective drug delivery systems, imaging tools, and improved therapeutics. Several questions

will be addressed in this report, such as the uniformity of nanoparticles fabricated with the emulsification versus the fluidic nanoprecipitation system, incorporation efficiency of small molecules, and system parameter effects on particle characteristics and incorporation. With all things considered, we can hopefully optimize incorporation and release of BKI-loaded particles.

3.5 References

1. Mohamed F, van der Walle CF. Engineering biodegradable polyester particles with specific drug targeting and drug release properties. *Journal of Pharmaceutical Sciences* 2008, **97**(1)**:** 71-87.

2. Li XA, Anton N, Arpagaus C, Belleteix F, Vandanune TF. Nanoparticles by spray drying using innovative new technology: The Buchi Nano Spray Dryer B-90. *Journal of Controlled Release* 2010, **147**(2)**:** 304-310.

3. De Temmerman M-L, Rejman J, Vandenbroucke RE, De Koker S, Libert C, Grooten J*, et al.* Polyelectrolyte LbL microcapsule versus PLGA microspheres for immunization with protein antigen. *Journal of Controlled Release* 2011**:** 8.

4. Astete CE. Synthesis of poly(DL-lactide-co-glycolide) nanoparticles with entrapped magnetite. Master of Science thesis, Louisiana State University, Louisiana State University, 2005.

5. Hans ML, Lowman AM. Biodegradable nanoparticles for drug delivery and targeting. *Current Opinion in Solid State & Materials Science* 2002, **6**(4)**:** 319-327.

6. Xie H, Smith JW. Fabrication of PLGA nanoparticles with a fluidic nanoprecipitation system. *Journal of Nanobiotechnology* 2010, **8**(18)**:** 1-7.

7. Singh R, Lillard JW. Nanoparticle-based targeted drug delivery. *Experimental and Molecular Pathology* 2009, **86**(3)**:** 215-223.

8. Liu K, Nie ZH, Zhao NN, Li W, Rubinstein M, Kumacheva E. Step-Growth Polymerization of Inorganic Nanoparticles. *Science* 2010, **329**(5988)**:** 197-200.

9. Torche AM, Jouan H, Le Corre P, Albina E, Primault R, Jestin A*, et al.* Ex vivo and in situ PLGA microspheres uptake by pig ileal Peyer's patch segment. *International Journal of Pharmaceutics* 2000, **201**(1)**:** 15-27.

10. Lemoine D, Preat V. Polymeric nanoparticles as delivery system for influenza virus glycoproteins. *Journal of Controlled Release* 1998, **54**(1)**:** 15-27.

11. Leroueil-Le Verger M, Fluckiger L, Kim YI, Hoffman M, Maincent P. Preparation and characterization of nanoparticles containing an antihypertensive agent. *European Journal of Pharmaceutics and Biopharmaceutics* 1998, **46**(2)**:** 137-143.

12. Fessi H, Puisieux F, Devissaguet JP, Ammoury N, Benita S. NANOCAPSULE FORMATION BY INTERFACIAL POLYMER DEPOSITION FOLLOWING SOLVENT DISPLACEMENT. *International Journal of Pharmaceutics* 1989, **55**(1)**:** R1-R4.

13. Cheng J, Teply BA, Sherifi I, Sung J, Luther G, Gu FX*, et al.* Formulation of functionalized PLGA-PEG nanoparticles for in vivo targeted drug delivery. *Biomaterials* 2007, **28**(5)**:** 869-876.

14. Quevedo E, Steinbacher J, McQuade DT. Interfacial polymerization within a simplified microfluidic device: Capturing capsules. *Journal of the American Chemical Society* 2005, **127**(30)**:** 10498-10499.

15. Karnik R, Gu F, Basto P, Cannizzaro C, Dean L, Kyei-Manu W*, et al.* Microfluidic platform for controlled synthesis of polymeric nanoparticles. *Nano Letters* 2008, **8**(9)**:** 2906-2912.

16. Schubert S, Delaney JT, Schubert US. Nanoprecipitation and nanoformulation of polymers: from history to powerful possibilities beyond poly(lactic acid). *Soft Matter* 2011, **7**(5)**:** 1581-1588.

17. Lorber N, Sarrazin F, Guillot P, Panizza P, Colin A, Pavageau B*, et al.* Some recent advances in the design and the use of miniaturized droplet-

based continuous process: Applications in chemistry and high-pressure microflows. *Lab on a Chip* 2011, **11**(5)**:** 779-787.

18. Zambaux M, Bonneaux F, Gref R, Manicent P, Dellacherie E, Alonso M*, et al.* Influence of experimental parameters on the characteristics of poly(lactic acid) nanoparticles prepared by double emulsion method. *Journal of Controlled Release* 1998, **50:** 31-40.

19. Mohanraj V, Chen Y. Nanoparticles - a review. *Tropical Journal of Pharmaceutical Research* 2006, **5**(1)**:** 561-573.

20. Institute NC. Tocosol Paclitaxel. *NCI Drug Dictionary*: National Institutes of Health.

21. Anuchapreeda S, Fukumori Y, Okonogi S, Ichikawa H. Preparation of lipid nanoemulsions incorporation curcumin for cancer therapy. *Journal of Nanotechnology* 2012, **2012:** 11.

22. Yeo Y, Park KN. Control of encapsulation efficiency and initial burst in polymeric microparticle systems. *Archives of Pharmacal Research* 2004, **27**(1)**:** 1-12.

23. Jeyanthi R, Mehta RC, Thanoo BC, DeLuca PP. Effect of processing parameters on the properties of peptide-containing PLGA microspheres. *Journal of Microencapsulation* 1997, **14**(2)**:** 163-174.

24. Kolishetti N, Dhar S, Valencia PM, Lin LQ, Karnik R, Lippard SJ*, et al.* Engineering of self-assembled nanoparticle platform for precisely controlled combination drug therapy. *Proceedings of the National Academy of Sciences of the United States of America* 2010, **107**(42)**:** 17939-17944.

25. Nisisako T, Torii T, Higuchi T. Novel microreactors for functional polymer beads. *Chemical Engineering Journal* 2004, **101**(1-3)**:** 23-29.

26. Ltd MI. Dynamic Light Scattering (DLS). Laboratory Products 2011 [cited 2011 Dec 29]Company]. Available from: http://www.malvern.com/labeng/technology/dynamic_light_scattering/dynamic_light_scattering.htm

27. Slouf M. Polymer Morphology. Institute of Macromolecular Chemistry; 2011.

28. Woehrle GH, Hutchison JE, Ozkar S, Finke RG. Analysis of nanoparticle Transmission Electron Microscopy data using a public-domain image-processing program, Image. *Turkish Journal of Chemistry* 2006, **30**(1)**:** 1-13.

29. A. DB. Controlling Nonviral Gener Delivery through the Cell-Biomaterial Interface. Masters of Science thesis, University of Nebraska at Lincoln, Digital Commons @ University of Nebraska - Lincoln, 2010.

30. Ignjatovic NL, Liu CZ, Czernuszka JT, Uskokovi DP. Micro- and nano-injectable composite biomaterials containing calcium phosphate coated with poly(DL-lactide-co-glycolide). *Acta Biomaterialia* 2007, **3**(6)**:** 927-935.

31. Taniguchi T, Inada T, Kashiwakura T, Murakami F, Kohri M, Nakahira T. Preparation of polymer core-shell particles supporting gold nanoparticles. *Colloids and Surfaces a-Physicochemical and Engineering Aspects* 2011, **377**(1-3)**:** 63-69.

32. Choi DH, Park CH, Kim IH, Chun HJ, Park K, Han DK. Fabrication of core-shell microcapsules using PLGA and alginate for dual growth factor delivery system. *Journal of Controlled Release* 2010, **147**(2)**:** 193-201.

33. Gou M, Men K, Shi H, Xiang M, Zhang J, Song J*, et al.* Curcumin-loaded biodegradable polymeric micelles for colon cancer therapy in vitro and in vivo. *Nanoscale* 2011, **3**(4)**:** 1558-1567.

CHAPTER 4. FABRICATION AMD OPTIMIZATION OF NANO/MICROPARTICULATE BKI-DELIVERY SYSTEMS

4.1 Introduction

The last chapters described the multitude of engineered therapeutics that can be utilized for drug delivery including implantable devices/scaffolds and particulate systems.[1] Biocompatible polymeric or gel matrices can be situated into the body at exact sites to permit both localized and sustained release.[2] Micro/nanoparticles can be administered intravenously with additional factors including targeting agents, imaging tools, and a drug depot for extended systematic release.[3] These two categories can also be combined into injectable particles that release peptides at a constant rate and also form a scaffold *in situ* to promote cell adhesion and growth.[4] In addition, novel therapeutics like dissolvable microneedle arrays and red blood cell-mimicking particles are also under investigation for use as drug delivery systems.[5] [6]

Particulate delivery systems are attaining significant research interest due to several pharmacokinetic advantages. Particles can protect deliverables while in circulation, targeting moieties can be added to restrict drug release to certain tissue sites, and particles can be modified to administer drug with a pre-determined release profile.[7] Although, one factor that needs to be addressed is lowering the impact of drug properties, i.e. hydrophobicity or size, which may cause differences with drug incorporation into particles and reliability of the

overall system. Ideally, a particulate delivery system that can easily and effectively incorporate drugs with varying properties is highly desirable.

This chapter will focus on the fabrication of a particulate delivery system for a two types of bumped kinase inhibitors, BKIs, used for malaria transmission blocking. Non-particulate systems were also examined and tested, but particulate-based systems displayed the optimal properties for a sustained release system. The particulate system is fabricated via emulsion and fluidic nanoprecipitation (fNP) methods with changes in system parameters including polymer concentration, polymer type, fabrication pH, initial drug loading, and amounts of solvents used. These fabrication systems were chosen because the particles are easy to fabricate and the process can be scaled up.[7] PLGA was chosen as the base polymer because of its biodegradability and prior use in drug delivery.[8 9] A tri-block polymer, BMA-PAA-DMAEMA, was also tested in certain systems to create a shell around the PLGA particles. The BMA segment is hydrophobic permitting it to co-block with the PLGA, while the DMAEMA can generate a hydrophilic shield around the particle to accelerate solvent diffusion improving drug incorporation.[10 11 12] Alginate was also investigated as a inner core drug depot and was chosen due to its adaptable gel properties.[13] The double emulsion particles or the core/shell structure with either the BMA-PAA-DMAEMA shell or the alginate core should increase drug loading and perhaps control drug release. Overall, a matrix of particle formulations was tested to uncover the system with maximum BKI incorporation and optimal release profile.

4.2 Objectives

The aim of this research is to fabricate a particulate drug delivery system for extended release of amphiphilic BKIs. Nanoparticulate delivery systems are advantageous because they are easy to fabricate and administer. The two BKIs used included a slightly hydrophilic malaria inhibitor, RM-1-132, and a slightly hydrophobic malaria inhibitor, 1294 *(RM-1-132 and 1294 were provided by Dr. W. C. Van Voorhis from the Department of Medicine, University of Washington and Dr. D. J. Maly from the Department of Chemistry, University of Washington)*.[14] Various particulate systems were tested including solid dispersion/emulsions, emulsions with hydrophilic additives, and core/shell particles. The nanoparticles size, size distribution, and zeta potential were characterized with dynamic light scattering (DLS) and scanning electron microscopy (SEM). Total drug incorporation and release kinetics were calculated from inhibition assays *(IC50 assays created by K.K. Ojo, Department of Medicine, University of Washington)*.

4.3 Materials and Methods

4.3.1 Materials

Poly(DL-lactide-co-glycolide) (PLGA) resomer (50:50 ester-terminated with IV 0.55 – 0.75) was purchased from Lactel Absorbable Polymers (Cupertino, CA). RM-1-132 and 1294 BKIs were provided by Dr. W. C. Van Voorhis's group (Department of Medicine, University of Washington). Rhodamine-conjugated butyl metacrylate (BMA) - propylacrylic acid (PAA) - dimethylaminoethyl methacrylate (DMAEMA) (BMA-PAA-DMAEMA) terpolymer was generously

donated from Dr. P. Stayton's group (Bioengineering Department, University of Washington). Pronova Ultarpure LVM Alginate was purchased from NovaMatrix,(FMC BioPolymer, Philadelphia, PA). Poly(vinyl alcohol) (PVA) and calcium chloride ($CaCl_2$) was purchased from Sigma-Aldrich (St. Louis, MO). Dichloromethane (DCM) and dimethyl sulfoxide (DMSO) was purchased from EMD (EMD Chemicals, Inc., Gibbstown, NJ).

4.3.2 Particle Preparation

PLGA solutions were prepared by dissolving 50mg/mL PLGA in dichloromethane (DCM). Particles were created using either an emulsion method adapted from Dr. K. Tran (Chemical Engineering Department, University of Washington) which is described in more detail below, or a fluidic nanoprecipitation (fNP) method based on Xie, 2010.[15] PVA solutions were at pH=6.4 unless noted otherwise.

4.3.2.1.1 Solid Dispersion and Emulsions

RM-1-132 or 1294 was dissolved directly in the 1mL of the 50mg/mL PLGA/DCM solution or dissolved in DMSO, then mixed with the PLGA/DCM solution. Solutions were vortexed with the Vortex Genie 2 (Scientific Industries, Bohemia, NY) at a medium-high speed, then sonicated in a water bath approximately 5 times at 5 minutes each. For the emulsion system, this dispersion was sonicated for 10 seconds twice at output 7 with Model 3000 Ultrasonic Homogenizer (Biologics, Inc., Cary, NC). 2 mL of 5% PVA was added drop-wise while vortexing and sonicated. The solution was poured into 2 mL of

5% PVA while vortexing and lightly sonicated. Solution was then poured into 2mL of 1% PVA in a beaker and magnetically stirred for 3 – 4 hours. For the fNP system, the initial solution of approximately 1mL of PLGA/BKI was injected into a flowing stream of dispersant, collected into a beaker immediately, and magnetically stirred for 3 – 4 hours. Specifically, a stainless steel needle (BD-305127 25 ½ G) was inserted approximately halfway into 12" length of Vincon tubing (ID 1/8", OD 1/4") that was used to flow the dispersant phase. The PLGA/BKI solution was fed through the needle at 5mL/min using a 3 mL syringe controlled by a syringe pump (KD Scientific, Holliston, MA). The dispersant channel was 1% PVA adjusted to certain pH flowing at 60mL/min controlled by a Mini-pump with variable flow (Fisher Scientific).

Solutions were collected and centrifuged twice at 12,000 rpm for 10 minutes using a Sorvall Legend RT centrifuge (DJB Labcare Ltd. Buckinghamshire, England), and twice at 10,000rpm for 10 minutes using an Eppendorf Centrifuge 5415D (Eppendorf, San Diego, CA) with resuspensions in MilliQ water. Final resuspension was in 200 - 800uL MilliQ water depending on particle concentration. Samples were stored at 4C if not used for testing immediately. For the total drug incorporated (burst) experiments samples were lyophilized overnight using a Freezone 4.5 Freeze Dry System (Labconco Corporation, Kansas City, MO), then used for testing.

4.3.2.1.2 Hydrophilic Additives

RM-1-132 was dissolved in DMSO or a mixture of DMSO/water. RM-1-132 solution was added to 1mL of the PLGA/DCM solution while vortexing at a medium-high speed. This dispersion was sonicated for 10 seconds twice at output 7. An appropriate amount of water or glycerol was also added to select samples while vortexing. Mixtures were sonicated four times for 20 seconds at output 7. For the emulsion system, 2 mL of 5% PVA was added drop-wise while vortexing and samples was sonicated. The solution was poured into 2 mL of 5% PVA while vortexing and sample was sonicated. Solution was then poured into 2mL of 1% PVA in a beaker and magnetically stirred for 3 – 4 hours. For the fNP system, initial solutions of PLGA/BKI were injected into a flowing stream of dispersant, collected into a beaker immediately, and stirred for 3 – 4 hours. The particles were then recovered as described above.

4.3.2.1.3 Core/Shell Particles

PLGA/BMA-PAA-DMAEMA (PLGA/terpolymer) and PLGA/Alginate particles were also fabricated to examine the effects of an amphiphilic polymer coating and a gel core on increasing the RM-1-132 incorporation. For the PLGA/BMA-PAA-DMAEMA nanoparticles, BMA-PAA-DMAEMA was added to the already dissolved PLGA/DCM mixture at a 1:1 w/w ratio. Particles were created via emulsification or fNP as described above. For PLGA/Alginate nanoparticles, small amount of concentrated stock of RM-1-132/DMSO was mixed into an aqueous alginate gelling solution. 100uL of this solution was drop-

wise added into the PLGA/DCM solution while vortexing. Particles were then created via emulsification or fNP as described above. 50uL of 18mM $CaCl_2$ was added drop-wise to the mixture before adding to the final 2mL of 1% PVA. After approximately five minutes of stirring, 50uL of 2% (w/v) $CaCl_2$ was also added. Particles were recovered as described previously.

4.3.3 Particle Characterization

4.3.3.1 Size, Morphology, and Zeta Potential

10 uL of particles were resuspended into approximately 1 mL of 10mM KNO_3 solution. Particle size, polydispersity, and zeta potential were measured using a Zetasizer Nano-ZS (Malvern, Worcestershire, United Kingdom). Scanning electron microscope (SEM) was used to examine the morphology of the particles. 1uL of fresh (System I – III) or previously stored particles were dried overnight on a silicon wafer, then sputter-coated with gold using a SPI Sputter Coater (Structure Probe, Inc., West Chester, PA). Images were taken with a JEOL7000F SEM with a beam voltage of 5 – 10 kV (Electron Microscopy Center, University of Washington, Seattle, WA). If size measurements from the DLS readings were out of the DLS range (>5um) then size was also measured from the SEM images taken. Particle diameter was measured 2 – 3 times per particle and approximately 60 – 500 particles per sample. All particle sizes measured were reported on a box chart to allow representation of all populations of particle sizes.

4.3.3.2 Total Drug Incorporated (IC50 Assay)

Lyophilized particles were completely dissolved in established amounts of DMSO to produce between 1 – 5 mM of estimated drug content. Samples were centrifuged to separate any remaining polymer out. Samples were tested for inhibition via a *Plasmodium falciparum* calcium-dependent protein kinase (Pfal-CDPK) specific kinase-Glo assay (IC50 inhibition assay) developed by Dr. K.K Ojo and colleagues of Dr. W Van Voorhis's Lab (Department of Medicine, University of Washington, Seattle, WA).

Both the total drug incorporated and the time-release samples were tested via the IC50 assay. Data was analyzed using Prism software into a half maximal inhibitory concentration (IC50) graph with pure RM-1-132 or 1294 as a positive control. Values for total amount of BKI in particles were calculated using the following equation (*where I = amount of drug in particles (ug)*, C_s *= starting concentration (estimated, (mM))*, *D = dilution factor, usually 1000x*, $IC50_{RM1}$ *= soluble drug concentration for 50% inhibition (uM)*, $IC50_{NP}$ *= drug in nanoparticle concentration for 50% inhibition (uM)*, *V = volume used to dilute particles (L)*, *MW = molecular weight of drug (ug/umol)*):

$$I = C_s \times D \times \frac{IC50_{RM1}}{IC50_{NP}} \times V \times MW$$

4.3.3.3 Drug Release

After fabrication, approximately 1 – 10mg of particles were resuspended in 100uL of sterile PBS (pH 7.4) and incubated in a 37C water bath. At each timepoint, samples were centrifuged for 10 minutes at 10,000 rpm. For system I - III experiments, 10uL of the supernatant was removed and replaced with 10uL fresh PBS. For experiments after system III, the entire supernatant was removed, and particles were fully resuspended in 100 uL of fresh PBS. Samples were returned to the 37C water bath. Timepoints were between 0 – 12hrs on day 0, every day until day 7, and either weekly or bi-weekly after that. Amount of drug released, cumulative drug release, and percent release were calculated based on the IC50s of the time-released samples. Minimum reliability of inhibition, or the minimum effective concentration (MEC) was set at 20% or 0.2ng of RM-1-132 or 1294 for most samples. Values for total amount of BKI released from particles were calculated using the following equation (*where R = amount of drug released from particles (ug),* I_{NP} *= percent inhibition of drug from nanoparticles,* I_{RM1} *= percent inhibition of drug from nanoparticles):*

$$R = I_{NP} \times \frac{IC50_{RM1}}{I_{RM1}} \times D \times V \times MW$$

Cumulative release, cumulative percent release, and release rates per mg of particles were calculated based on these IC50-based values.

4.3.3.4 Partition Coefficient

Partition coefficient was analyzed utilizing an adapted shake-flask method from the Office Journal of the European Communities, 2002.[24] Briefly, BKI-1 or 1294 (from 200ug – 5mg) were dissolved in mixtures of DCM and water (140uL DCM and 860uL water) at pH = 6, 8, 10, and 12 (pH raised with 1 - 5 mM NaOH). Solutions were vortexed and allowed to separate for approximately 1 – 2 hours. Samples were taken from the organic layer and the aqueous layer and processed via an IC50 inhibition assay for total inhibitor content. Log P was calculated from these results.

4.4 Results and Discussion

4.4.1 Determining a Particle System for Sustained BKI Release

Poly(DL-lactide-co-glycilide) (PLGA) was used to fabricate nanoparticles containing RM-1-132, a slightly hydrophilic malaria inhibitor.[14] RM-1-132 and the emulsification fabrication method was used for most of the initial systems; 1294 and fNP fabrication was used later when systems' were optimized to conserve the amount of drug being used.[7] Three systems were initially created to incorporate the maximum amount of RM-1-132. The first system involved solid dispersion or emulsion particles where the drug and polymer were dissolved in the same or miscible solvents. The second system involved emulsion particles where a hydrophilic additive was emulsified into a drug/polymer/organic phase. A hydrophilic additive was utilized because this would permit faster solvent extraction into the continuous phase leading to higher encapsulation efficiency.[12]

The last system involved either addition of an amphiphilic polymer coating or a drug-containing gel core surrounded by a polymer shell to control drug release.[12] Schematics of what the particle system may look like are shown in the following figure (Figure 4.1).

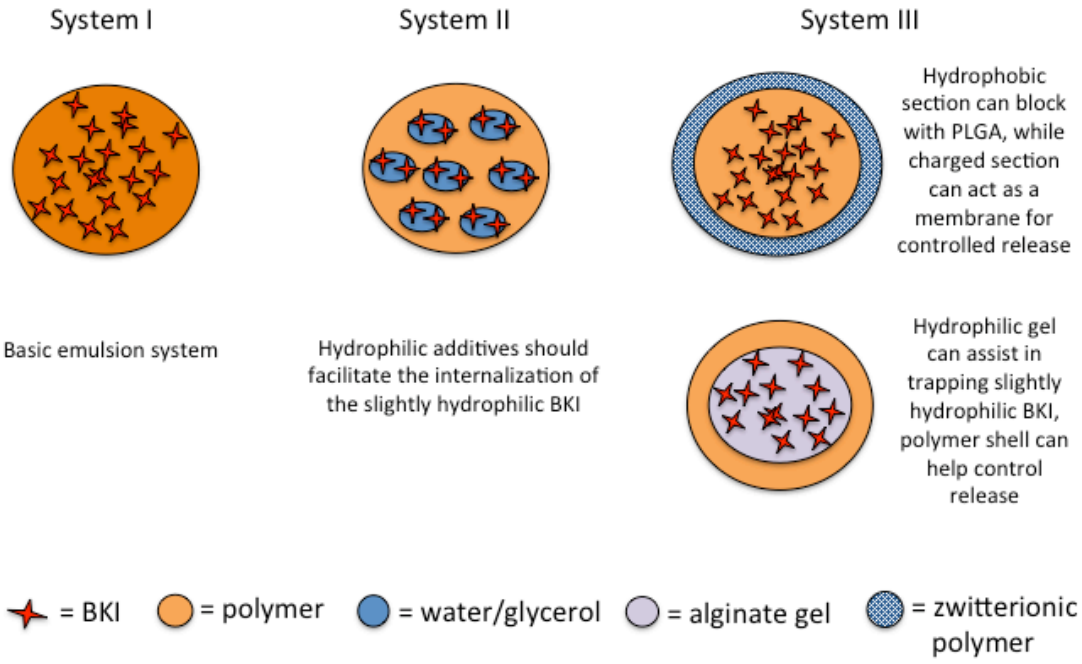

Figure 4.1. Schematic of the three systems employed for RM-1-132 drug incorporation. *(System 1 = solid dispersion / emulsion, System 2 = hydrophilic additives, System 3 = core/shell).*

4.4.1.1 System I: Solid Dispersion and Emulsions

Size, size distribution, and zeta potential were analyzed for the particles using dynamic light scattering (DLS) (Table 4.1). The first section of the table are unloaded nanoparticles, the second section are particles where RM-1-132 was dissolved in DMSO then mixed with PLGA/DCM (solid dispersion / single emulsion), and the third section are particles where RM-1-132 was dissolved in a

DMSO:water mixture and then mixed into PLGA/DCM (double emulsion). Overall, the diameter of the particles was approximately 300 – 500nm with a broad range of polydispersities from 0.1 to 1. Particle diameter was slightly elevated when RM-1-132 was dissolved in a DMSO:water mixture before addition to the system. Zeta potentials were slightly negative, consistent with the neutral to negative charge on PLGA.

System I: Single emulsion particles

PLGA (mg/mL)	DMSO (uL)	water (uL)	RM-1-132 (ug drug/ mg polymer)	Peak 1 Mean (nm)	PDI	Zeta Potential (mV)	
50	10	90	none	370	0.53	-0.2	
10	10	90	none	390	0.35	-0.5	A
10	150	none	none	320	0.12	-1.1	
10	500	none	none	340	0.58	-1.2	
50	none	none	10	348	1	-0.2	
10	20	none	100	390	0.56	-0.7	B
10	150	none	50	270	0.08	1.1	
10	500	none	50	320	0.24	-1.3	
50	2	98	10	486	0.76	-0.2	
10	10	90	100	390	0.67	-0.6	C
10	10	90	100	470	0.49	-0.61	
50	10	90	10	445	0.75	-0.6	
50	10	90	20	400	0.68	-0.5	D

Table 4.1. Size and zeta potential data for various formulations of system I (solid dispersion and emulsion particles). *PDI is the polydispersity index based on the width of the assumed Gaussian distribution, with 0 indicating a narrow monodisperse population.*

Morphology of the particles was also investigated using scanning electron microscopy (SEM) (Figure 4.2). The images are representative of the previous particle set and are marked with corresponding letters on Table 4.1. There was not a huge difference between the unloaded PLGA particles (sample A) and the

RM-1-132-loaded DMSO:water particles (sample C & D). There was a decreased amount of particles and more inconsistencies with size for just DMSO RM-1-132-loaded particles (sample B) compared with the other samples. This may be due to lack of water in the system and the larger initial drug loading possibly causing the RM-1-132 drug to aggregate upon exposure to the hydrophobic solvent. Size of the particles was mostly consistent with DLS values, although some discrepancies were apparent with the high PDI.

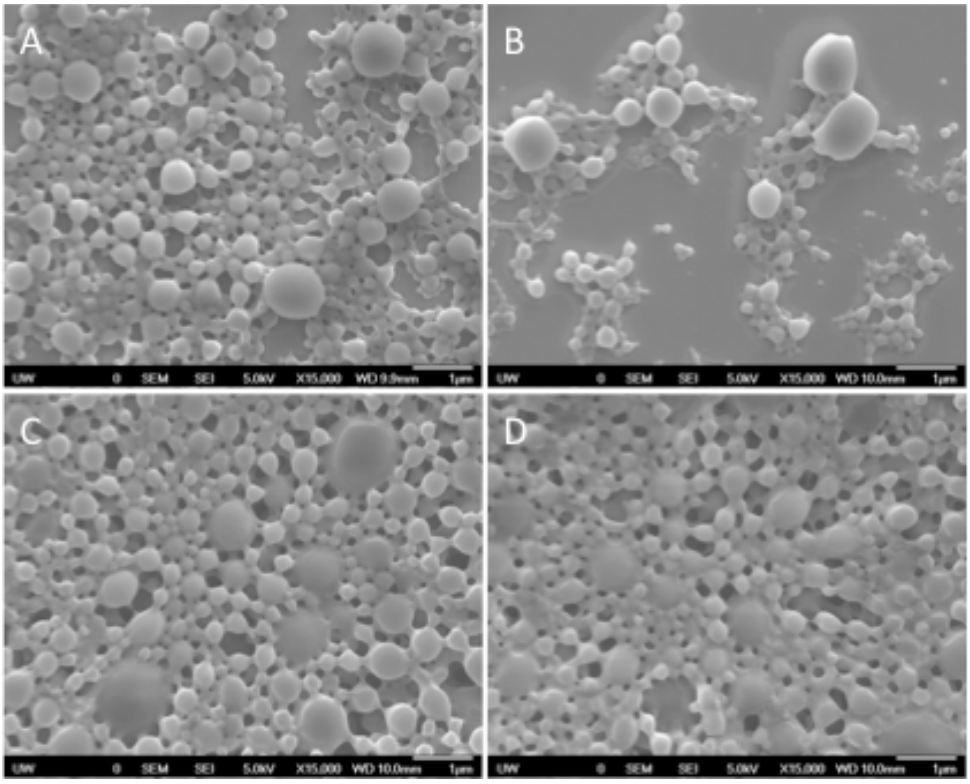

Figure 4.2. Scanning electron microscopy images of various system I particles *(A = unloaded particles with a 10:90 DMSO:water (v/v, units = uL) ratio; B = DMSO/RM-1-132 particles with a 20:0 DMSO:water ratio; C = DMSO:water/RM-1-132 particles with a 10:90 DMSO:water ratio; D = DMSO:water/RM-1-132 particles with 5x higher PLGA concentration and a 10:90 DMSO: water ratio; more details can be found on Table 4.1.) Scale bar = 1um.*

4.4.1.2 System II: Hydrophilic Additives

For this system, either water or glycerol was emulsified into the RM-1-132/DMSO-PLGA/DCM mixture. Addition of a hydrophilic solvent should facilitate organic solvent removal and increase drug incorporation.[12] For system II, particle size was analyzed from SEM images because of the high size distribution observed from the DLS results (Table 4.2). The particle diameter ranged from 20 nm to 300 um. Additionally, the particle structure became more porous as the ratio of DMSO:hydrophilic additive (v/v) increased from 5:5 to 5:45 (Figure 5.3). This indicates a limit of the amount of hydrophilic additive that can be included into the system. Employing glycerol as the hydrophilic additive augmented porosity at a faster rate as compared to water, and may not be the optimal choice for a system. In addition particle size in the micron range may not be optimal for injection.

System II: Double emulsion particles

PLGA (mg/mL)	DMSO (uL)	water (W)/ glycerol (G) (uL)	RM-1-132 (ug drug/ mg polymer)	Average Size
50	5	5 (W)	10	30 - 60um
50	5	20 (W)	10	20 - 300um
50	5	45 (W)	10	20nm - 20um
50	5	5 (G)	10	20 - 90um
50	5	20 (G)	10	100nm - 30um
50	5	45 (G)	10	50 - 200um
50	5	none	10	200nm - 30um

Table 4.2. Size analysis of various formulations of system II (hydrophilic additives) based on scanning electron microscopy (SEM) images.

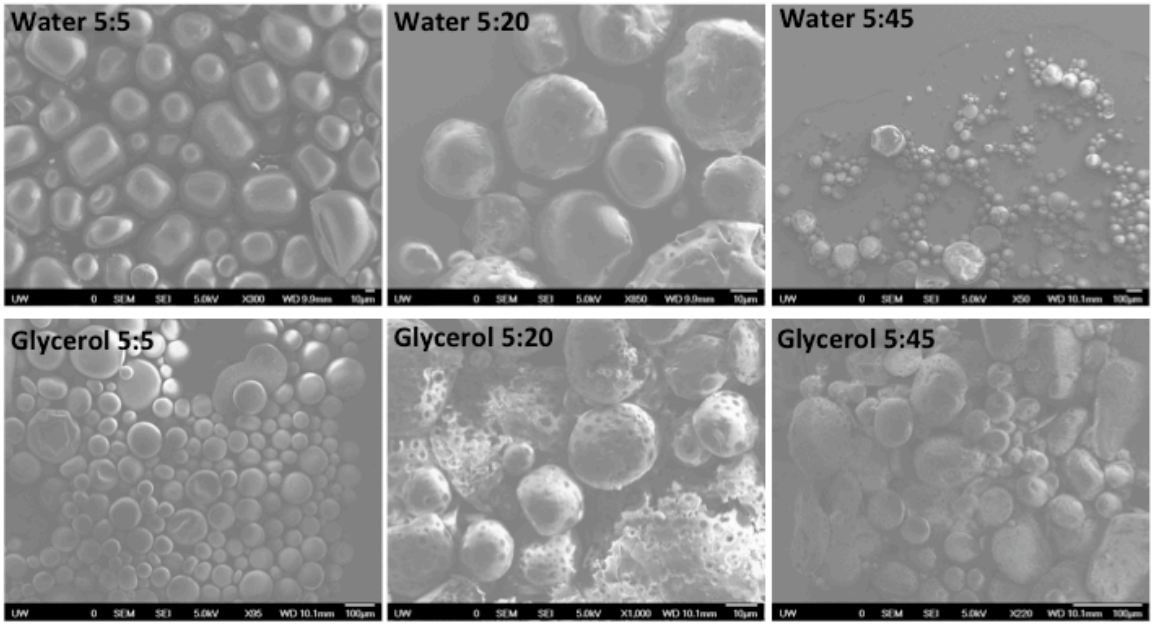

Figure 4.3. Scanning electron microscopy images of various system II particles *(ratios are DMSO : hydrophilic additive (v/v); top row = water as the hydrophilic additive; bottom row = glycerol as hydrophilic additive). Scale bar = 10um or 100um as indicated.*

4.4.1.3 System III: Core/Shell Particles

System III has two types of core/shell particles: 1) an amphiphilic terpolymer coating and 2) a hydrogel core with polymeric shell. In the first system we created PLGA/BMA-PAA-DMAEMA (PLGA/ter) particles, this amphiphilic polymer should add more hydrophilicity to the particle surface while acting as an additional barrier for drug release. For the second system, we created alginate particles encapsulating the drug, then coating with a PLGA shell (PLGA/Alg). The hydrogel inner core should facilitate containment of the drug during fabrication.

The size, size distribution, and zeta potential for system III particles were analyzed using DLS (Table 4.3). Following the table, the first four samples of PLGA/ter nanoparticles compares two things: 1) made via single emulsion (o/w, no water for internal phase) and double emulsion (w/o/w) and 2) nanometer versus micron-sized particles. The next samples are increasing combinations of DMSO:water for PLGA/ter double emulsion particles. The PLGA/Alg particles are denoted with an asterisk at the bottom of the table below the dividing line.

System III: Core/Shell particles

PLGA (mg/mL)	DMSO (uL)	water (uL)	RM-1-132 (ug drug/ mg polymer)	Peak 1 Mean (nm)	PDI	Zeta Potential (mV)	
50	1	none	5	450	0.3	12	
50	1	1	5	460	0.2	17	
50	1	none	5	1000	0.8	26	A
50	1	1	5	1160	0.8	29	B
50	5	5	10	780	0.6	27	
50	10	90	none	442	0.3	9	
50	10	90	10	540	0.4	23	
50*	0.12	50	5	5360	1	-5	C
50*	0.24	100	10	2090	1	-23	D

Table 4.3. Size and zeta potential data for various formulations of system III (core/shell particles). *PDI is the polydispersity index based on the width of the assumed Gaussian distribution, with 0 indicating a narrow monodisperse population.*

The PLGA/ter nanoparticles had an average size of approximately 450 - 460nm, with low PDI and zeta potential between 12 -17 mV. The positive zeta potential is due to the terpolymer presence at the surface of the particle. The microparticles displayed double the size at approximately 1 um and more positive

zeta potential at 26 – 29 mV indicating colloidal stability.[16] Polydispersity was also elevated. The varying DMSO:water ratios produced moderate-sized stable PLGA/ter particles, 450 – 800nm in diameter with zeta potentials between 9 - 27mV. The PLGA/Alg particles had diameters between 2 – 5 um, increasing as initial drug loading decreased. The zeta potentials were negative, in agreement with the negative charge on PLGA. The polydispersity was at the maximum, possibly due to the micron-sized particles. This high polydispersity makes the DLS size data not as reliable, suggesting that size should also be observed via microscopy and imaging (as described below).

SEM imaging reveals a smooth, spherical particle structure with some size distribution for the PLGA/ter particles regardless of single or double emulsion fabrication techniques (Figure 4.4). The PLGA/Alg particles displayed higher size variability with particles ranging from 300 nm to 5 um in diameter. Letters on SEM images correspond to samples on Table 4.3.

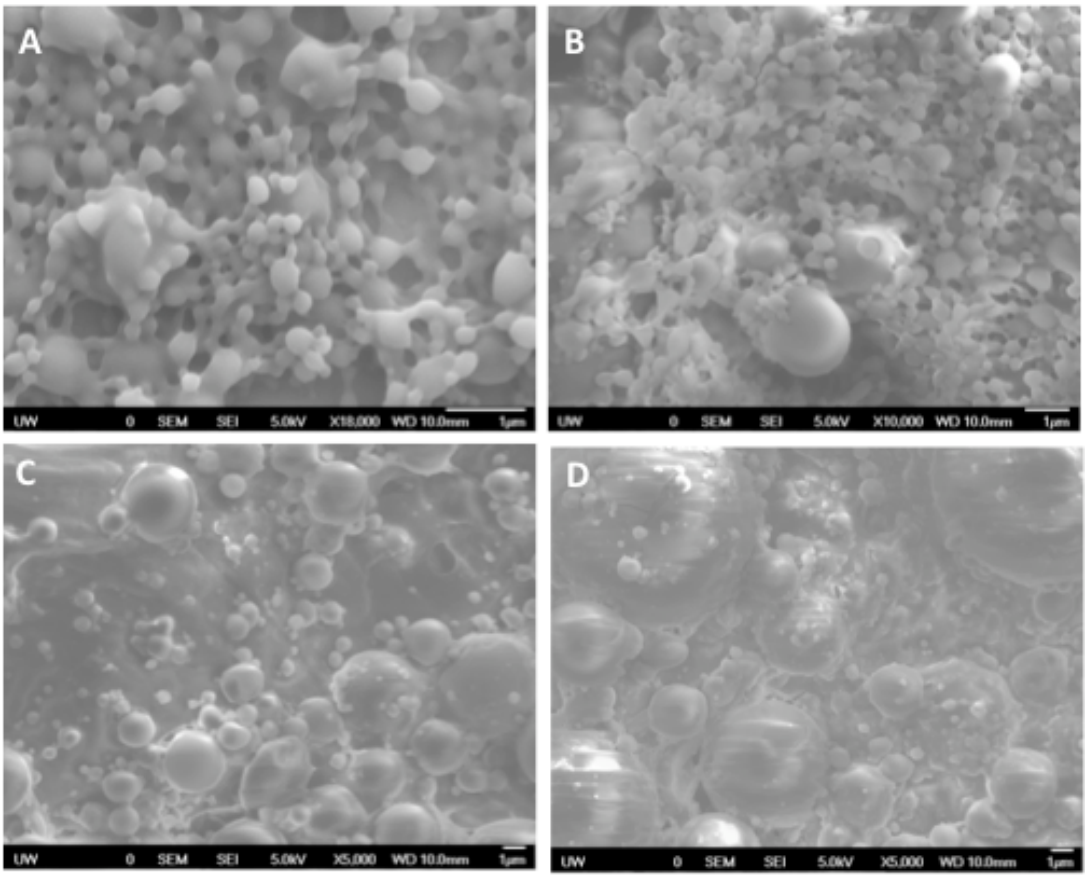

Figure 4.4. Scanning electron microscopy images of various system III (core/shell)particles *(A = single emulsion PLGA/ter microparticles, B = double emulsion PLGA/ter microparticles, C = PLGA/Alg with 5ug/mg drug loading, D = PLGA/Alg with 10ug/mg drug loading). Scalle bar = 1um.*

4.4.1.4 System I – III: BKI Incorporation

RM-1-132 incorporation into the particles was determined from half-maximal inhibition IC50 assays *(Plasmodium falciparum calcium-dependent protein kinase (PfCDPK) half-maximal inhibition (IC50) assays developed by K.K. Ojo and colleagues in the Van Voorhis group, Department of Medicine, University of Washington),* (examples of IC50 assay raw results in Appendix D-1). From that, efficiency was calculated as (final loading / initial loading) X 100%. For system I particles, decreasing the amount of DMSO and increasing the PLGA

concentration seemed to enhance loading efficiencies (Appendix D-2, Appendix D-3). For system II particles, an even ratio between DMSO : hydrophilic additive caused a slightly higher incorporation efficiency, especially for water where 5% efficiency was reached at a 1:1 DMSO : water ratio (v/v) (Figure 4.5). This corroborates with SEM imaging which shows higher porosity as more water was added, which can explain the decrease in loading efficiency seen here. The SEM imaging also displayed pores for all of the glycerol samples; this can explain why there is not a change in efficiency as the DMSO:glycerol ratio (v/v) is altered. Overall, inclusion of a hydrophilic additive produced a higher efficiency than fabricating particles without. On a side note, there is only one sample per data point due to needs to conserve the amount of drug that can be used for preliminary testing.

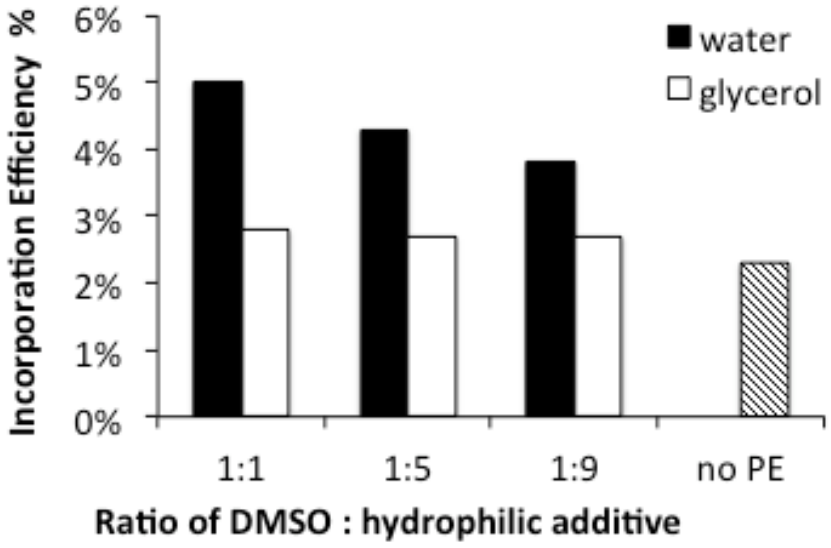

Figure 4.5. Incorporation efficiency of system II (hydrophilic additives) particles based on DMSO: hydrophilic additive ratio (v/v) *(no PE = control sample with no hydrophilic additive).*

The loading efficiencies were tabulated for all three systems (Table 4.4). The highest loading efficiencies were for system II particles, double emulsions with either water or glycerol as the hydrophilic additive. The lowest loading efficiencies were the PLGA/Alg particles, then the particles with higher amounts of DMSO or a lower concentration of PLGA. Overall, these efficiencies are low, so alternative systems were necessary for improvement of particle loading *(improved systems are described in the following sections)*. Additionally, since there is only one sample per data point due to requirements to conserve drug stock, samples may have to be repeated to ensure veracity.

Sample	Loading Efficiency
5:5 (W)	5.0%
5:20 (W)	4.3%
5:45 (W)	3.8%
1:1	3.8%
1:0	3.3%
5:5 (G)	2.8%
5:45 (G)	2.7%
5:20 (G)	2.7%
5:0	2.3%
10:90 (50mg/mL PLGA)	1.6%
PLGA/ter (1:1)	0.5%
PLGA/ter (1:0)	0.5%
150:0	0.39%
20:0	0.19%
10:90 (10mg/mL PLGA)	0.12%
PLGA/Alg (10ug/mg)	0.1%
PLGA/Alg (5ug/mg)	0.04%

Code: System I | System II | System III

Table 4.4. Loading efficiencies of RM-1-132/PLGA particles from all three systems. *(Ratios are DMSO:water (v/v), unless otherwise indicated by G = glycerol, systems are color-coded with key at bottom).*

To summarize, this system's major goal is sustained release of RM-1-132 from an easy-to-administer particulate carrier system. Eventually this delivery system can provide at least 1uM of drug each day for at least one month. Here, the size of the produced particles was consistent for the most part considering that emulsion fabrication methods typically generate a range of sizes and high polydispersities.[15] Surface charge of the particles correlated with the materials that make up the particle. Furthermore, it seems that higher drug incorporation occurs with increased PLGA concentration, lower DMSO amounts, and inclusion of a hydrophilic additive like water or glycerol. The low DMSO amounts can assist in RM-1-132 solubility in the organic solvent DCM, while being low enough to retain the drug during fabrication due to inadequate compatibility with the aqueous continuous phase. This could explain the high drug incorporation seen with the low DMSO samples. Hydrophilic additives are meant to pull hydrophilic drugs into internal pockets within the particle, which can increase incorporation. When an excessive amount of hydrophilic additive is reached, this could cause porosity due to internal pocket combination and release of the drug instead. This trend was seen with higher volumes increasing porosity of the particles and slightly reducing the loading efficiency.

Lower incorporation was seen with high DMSO samples, PLGA/ter samples, and PLGA/Alg particles. The high DMSO amounts increases the hydrophilicity of the system enabling faster solvent release during fabrication, but too high of an amount will facilitate the release of the drug during fabrication as seen here. The PLGA/ter samples may have also introduced too much

hydrophilicity into the system causing the release of drug during fabrication. PLGA/Alg particles could have either incorporated too much aqueous solution into the system also causing the low drug retention during fabrication or burst of the inner gel core of some particles may have occurred during the fabrication process causing the drug loss.

4.4.1.5 System I – III: BKI Release Kinetics

In vitro degradation of the particles and release of RM-1-132 over one week was tested. Plots of the non-cumulative amount of drug released per mg particles versus time were graphed based on inhibitor IC50 assay results of the time- released samples (Figure 4.6, Figure 4.7).

The top graph compares: 1) single versus double emulsions and 2) increasing amounts in the DMSO:water ratio (Figure 4.6). It seems all samples display an initial burst release except for the 0:0 (no water, no DMSO) sample, which also released the highest amount of RM-1-132. The middle graph is a comparison of hydrophilic additives water and glycerol. It seems like there is not a huge difference between type or amount of hydrophilic additive added. In addition, all samples with a hydrophilic additive displayed a higher release than the control sample with just DMSO added (5:0 on graph, 5uL of DMSO). The bottom graph displays samples that modify either: 1) the DMSO:water amounts or 2) the total DMSO:water volume added. It seems like a increasing the amount of water in the ratio (5:5 to 5:20 to 5:45) facilitated low release. In addition, a

total volume of 100uL of a DMSO:water mixture (highest total volume tested) displayed the best release trend and lack of initial burst.

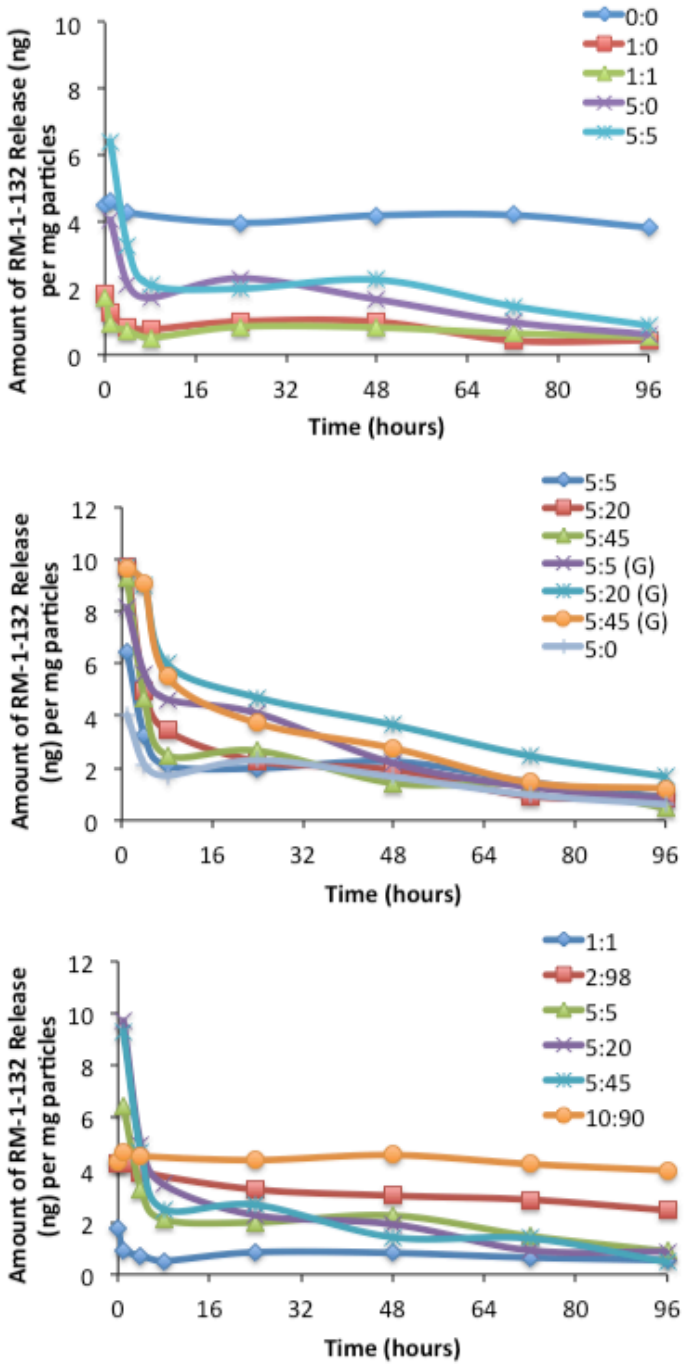

Figure 4.6. Release profiles of RM-1-132 from various systems per mg of particles. *(Ratios are amounts in uL of DMSO : water or DMSO : glycerol, if indicated by (G) in middle graph).*

System III (core/shell) particles were also analyzed for release over time (Figure 4.7). The top graph analyzes: 1) the effect of a terpolymer coating and 2) effect of single or double emulsion on release of RM-1-132. The addition of the terpolymer coating seemed to have diminished the initial burst for the microparticles, but the released amount was just slightly higher compared to particles without terpolymer coating. Furthermore, the nano-sized particles displayed a higher release initially, and then declined down to levels comparable to the other particles. This is most likely due to the shorter distance the drug has to diffuse through the particle to the surface to be released. There seemed to be no apparent differences between a single or double emulsion, possibly due to the low total volume. Therefore, the middle graph displayed the effects of altering the DMSO:water ratio for PLGA/ter particles at a higher total amount. It seems like increasing the total amount of DMSO:water displays a declining release profile, without any differences in the range 10 – 100uL for total amount. The bottom graph contains the two PLGA/Alg samples, which show a high initial burst release. The PLGA/Alg particles released most of their contents within the first couple hours, possibly due to internal swelling of the hydrogel.

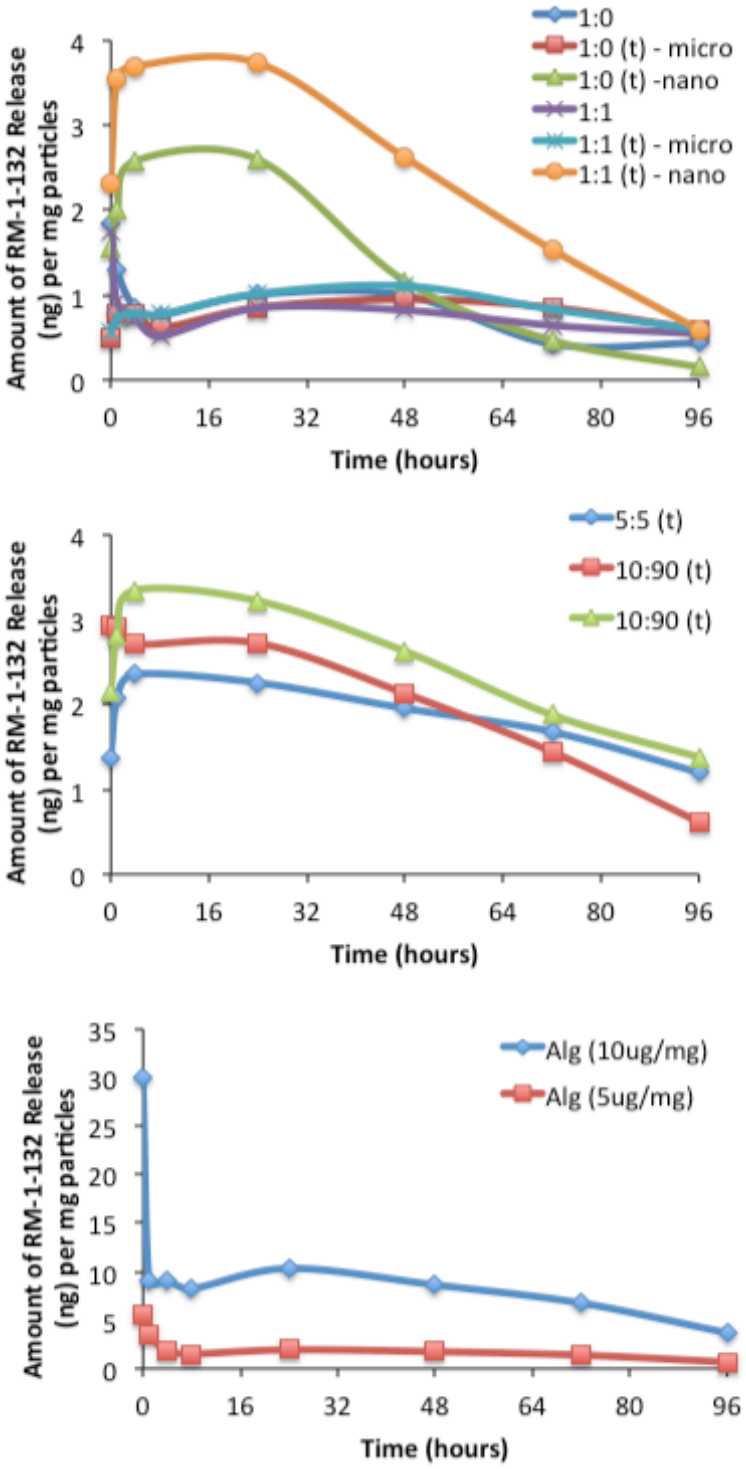

Figure 4.7. Release profiles of RM-1-132 from various systems per mg of particles. *(Ratios are amounts in uL of DMSO : water; t =terpolymer coating, Alg = alginate core; ug/mg are initial loadings of ug RM-1-132 / mg PLGA polymer).*

Furthermore, cumulative percent release of the total incorporated amount of RM-1-132 in these PLGA particles was evaluated to determine the kinetic order of drug disposition *(data not shown)*. The goal is a zero-order output to deliver a constant amount of drug over a set period of time. The low DMSO, PLGA/ter, and system II (hydrophilic additives) particles looked the most promising with the cumulative release increasing over time with a roughly linear slope. The total percent released over one week was tabulated for particles from all three systems (Table 4.5). These values followed an opposite trend to the loading efficiencies seen in Table 4.4, where system II (hydrophilic additives) particles with the smallest rate of release and PLGA/Alg particles with almost 100% release within 7 days. The higher percentages are due to a initial burst of the particles releasing drug content, and are not very good systems to administer when a sustained release over time is desired. The lower percentages might be suitable, but release does not occur rapid enough to sustain an effective amount above clearance rates. Additionally, the release is plateauing, so adaptations of the systems need to be investigated, as shown in the following sections, to improve release over time.

Sample	Total % released
5:5 (W)	0.36
5:1	0.39
5:0	0.47
5:20 (W)	0.58
5:45 (W)	0.60
5:0	0.62
5:5 (G)	1.00
5:45 (G)	1.28
5:20 (G)	1.45
PLGA/ter (1:0)	2.52
PLGA/ter (1:1)	2.60
20:0	6
10:90 (50mg/mL PLGA)	8
150:0	21
10:90 (10mg/mL PLGA)	21
PLGA/Alg (10ug/mg)	75.39
PLGA/Alg (5ug/mg)	100.90

Code: System I | System II | System III

Table 4.5. Percent of total release of RM-1-132 from all three systems particulate systems over 7 days. *(Ratios are DMSO:water, unless otherwise indicated by G = glycerol; mg/mL are PLGA concentrations; ug/mg are initial loadings of ug RM-1-132 / mg polymer)*.

For release over 7 days, the most steady release trends were samples without DMSO:water, 100uL volume of a DMSO:water mixture, and low DMSO:water PLGA/ter particles. The lack of water allowed a release based on diffusion of the drug and the rate of particle degradation. Increased water in the DMSO:water ratio permitted formation of internal compartments to retain RM-1-132. This allowed a consistent release once pockets are exposed to the surface

or drug is diffused out. The initial burst seen for samples with less water in the DMSO:water ratio was possibly due to not well-formed pockets or aggregation of the drug. The PLGA/ter displayed decent release profiles due to the terpolymer coating operating as a membrane for drug release. Although decrease in particle size or increase in volume of DMSO:water ratio facilitated more release within the first couple days, possibly due to pocket location closer to the surface. The highest release was for the PLGA/Alg particles which experienced complete burst release possibly due to swelling of the core as evidenced by the jump in release at the initial timepoints. Release rates for these systems can be found in the Appendix (Appendix D-4).

These preliminary studies show that we need to alter more than the particle type to improve release kinetics and increase the total drug incorporation beyond 5% (summarized results in Figure 4.8), as we demonstrate in the next section by altering the system parameters. Altering the system parameters, i.e. fabrication pH, generated the desired sustained drug delivery particulate system for the malarial inhibitor, RM-1-132, and for the more hydrophobic 1294 BKI. This system can then be further modulated for the inclusion of more types of drug molecules.

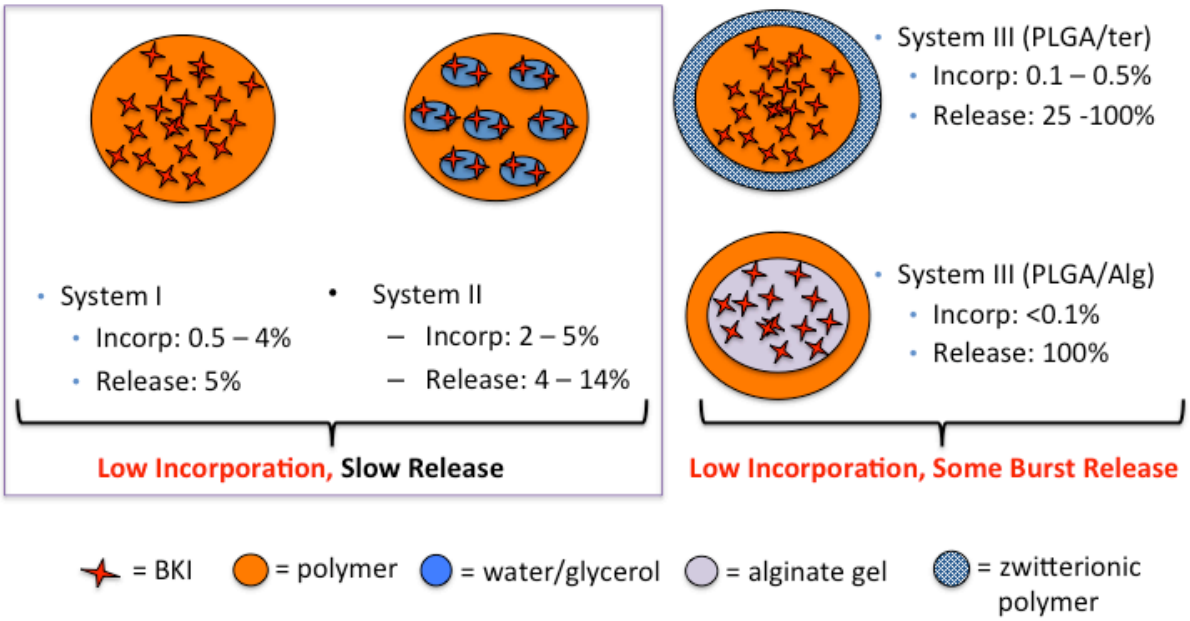

Figure 4.8. Schematic and summarized results of the three systems employed for RM-1-132 drug incorporation. *(System 1 = solid dispersion / emulsion, System 2 = hydrophilic additives, System 3 = core/shell).*

4.4.2 Altering System Parameters for Improved BKI Incorporation and Release

It was apparent that just altering the particle structure itself (i.e. single vs. double emulsion, core/shell) was not sufficient enough to provide maximal BKI incorporation and release. We decided to investigate altering system parameters during the fabrication process (i.e. fabrication pH, solvents used) to force an increase in BKI incorporation. Manipulation of the fabrication parameters has been shown to control physicochemical properties of particles, in turn altering drug yield and release.[17] Varying factors like the initial pH has been utilized in reaction-based and ionotropic particle formation where reactivity, affinity, and exposure of binding sites of two or more different molecules occur within a range

of pH.[18, 19] In this section we discuss the neutralization of the BKI molecule by increasing the pH beyond the pKa to assist in incorporation with the polymer in the hydrophobic phase. Changing the amount or type of solvent used has also been shown to play a major role in physical properties of the particles (i.e. size).[15, 20] We discuss the solvent changes in this section and further in Chapter 6 and Appendix A.

4.4.2.1 pH Effects

We created a small parameter design matrix to test the effects of increasing the pH past the RM-1-132 molecule pKa (pH = 9.71).[14] pH for the internal water phase in a double emulsion (water pH), the continuous aqueous phase (fabr. pH), and the water used for centrifugation and rinsing of the particles (rinse pH) was varied from the normal pH of MilliQ water used, pH = 6.4, to a very basic pH, pH = 12. From Figure 4.9, we can see that increasing the pH of only the fabrication phase increases incorporation by approximately 15%.

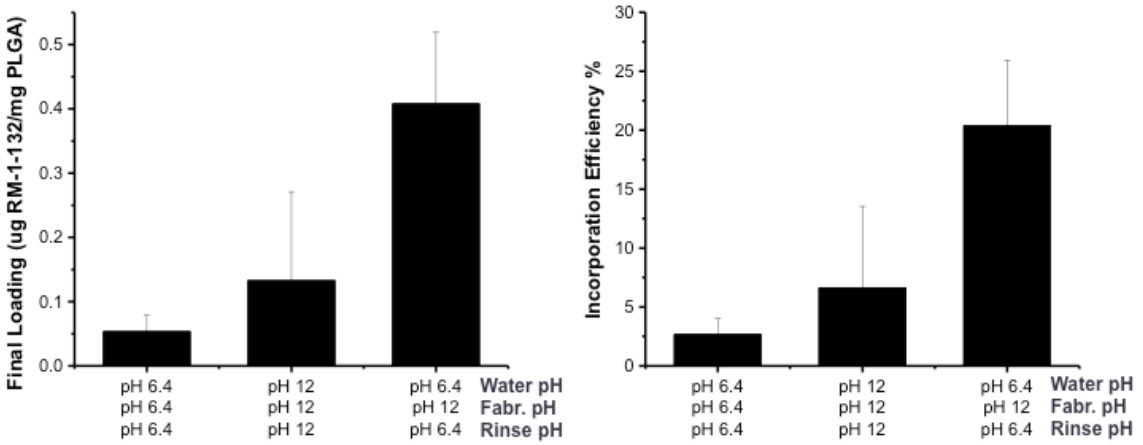

Figure 4.9. Final loading and incorporation efficiency of select parameters from a parameter design matrix for pH effects on three steps in the fabrication process. (*Initial loading was set at 2ug RM-1-132/mg PLGA, Water pH: pH of internal*

aqueous phase of double emulsion NPs, Fabr. pH: fabrication pH of emulsification or fNP system, Rinse pH: pH of water used to triple rinse particles after fabrication).

Here, the increase in pH above the pKa of the RM-1-132 forces the deprotonation of certain groups on the molecule (schematic in Chap 1, Fig. 1.1), allowing a preference for the non-polar hydrophobic phase with the PLGA polymer.[21] We tested the partition coefficient of the RM-1-132 molecule to confirm that this loss in affinity to the aqueous phase was occurring (Figure 4.10). In Figure 4.10 we tested increasing concentrations of RM-1-132 in a mixture of the organic dichloromethane (DCM) and water at various pH. Between pH 10 and pH 12 there is a transition from a negative Log P, usually indicative of a molecule with a hydrophilic tendency, to a positive Log P, indicative of a molecule with hydrophobic tendencies (Figure 4.10). There is also a noticeable increase in hydrophobicity at the highest concentration of RM-1-132. We speculate that this may be due to a variety of reasons, for example aggregation of the amphiphilic molecule due to oversaturation in both phases causing either neutralization and transport into the organic phase or dissolution out of solution to the more dense layer (organic phase in this case). Most literature determines log P at a concentration <75% of the solubility point, and not a range of concentrations beyond that (5mg/mL is approximately 200x higher then the estimated solubility at pH 7.4).[22]

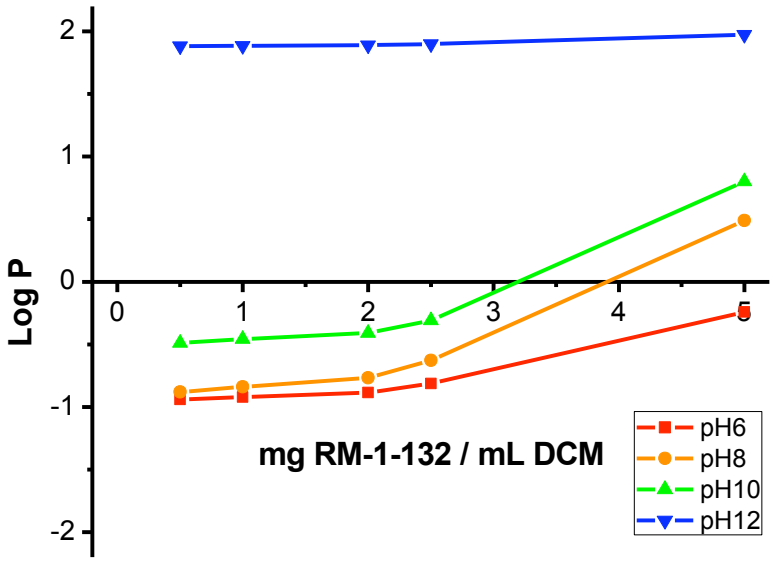

Figure 4.10. Partition coefficient for increasing concentrations of RM-1-132 at pH 6, 8, 10, and 12. *(A concentration of 1 ug/mL is equivalent to 20ug/mg initial loading during particle fabrication).*

Since the pH increase would cause the RM-1-132 molecule to have a preference for the organic phase, we revisited the idea of using a single versus double emulsion system (Figure 4.11). It seems that the single emulsion particles without an internal aqueous phase elicited slightly higher incorporation and less variability than the double emulsion particles, especially at 2ug/mg initial loading, where incorporation efficiency was approximately 100%. Full matrix of parameters tested along with additional parameters including fNP fabrication speed can be found in Appendix D-5 and D-6.

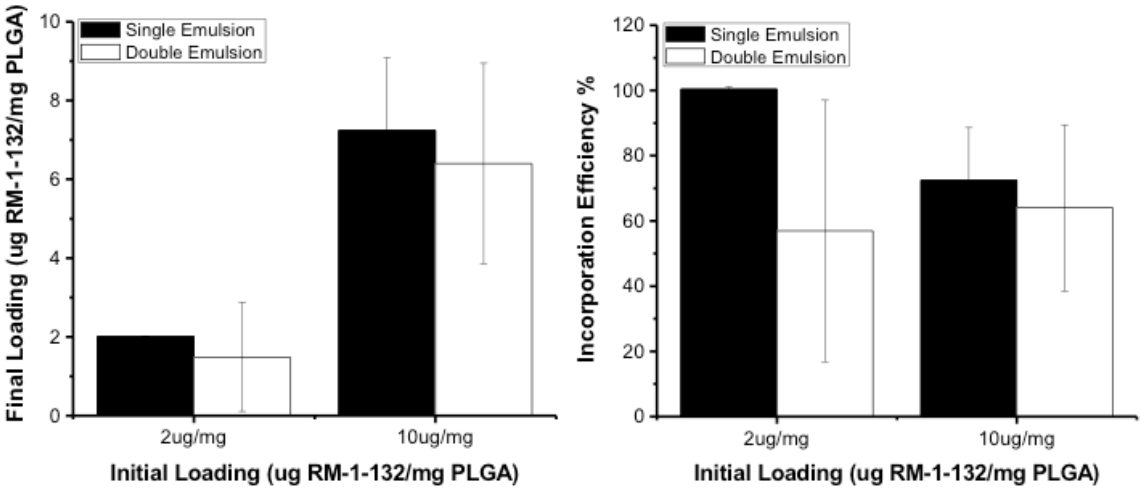

Figure 4.11. Final loading and incorporation efficiency of single and double emulsion RM-1-132-loaded PLGA particles at 2ug/mg and 10ug/mg initial loadings *(Fabrication pH = 12).*

4.4.2.2 RM-1-132 Size and Incorporation

We then tested a range of initial loadings of 2, 10, 20 and 50ug/mg incorporation of the RM-1-132 molecule into PLGA particles at a fabrication pH = 12 for both emulsion and fluidic nanoprecipitation (fNP) fabrication methods. The sizes were analyzed by DLS measurements and SEM images. For the emulsion fabrication method DLS revealed a 200 – 300nm sized particle, mostly monodisperse due to low PDI, with a surface charge of ~ –2mV, a typical surface charge for blank PLGA particles (Appendix D-7, D-8). For the fNP fabrication method DLS revealed sizes ranging from 500 nm to 2um with moderate to high PDI, and surface charge between –7 to –2mV (Appendix D-7, D-8). Based on SEM measurements, the particle diameter for the emulsion-fabricated particles was similar to the DLS measurements with most diameters below 1um (Figure 4.12). Although, for the highest loading of 50ug/mg there were some particles

with diameters of 2 – 8um. For the fNP-fabricated particles, most particles were around 200nm to 1um. As the initial loading increased there was more particles seen with diameters from 20 – 160um, especially for the 20 ug/mg and 50ug/mg initial loadings, where average particle diameter based on SEM measurements was approximately 10um. Comparisons and analysis between size and incorporation, as well as size and release will be described in Chapter 5. Additionally, we are further investigating the particle size and morphology to confirm trends via SEM and TEM for a related paper publication.

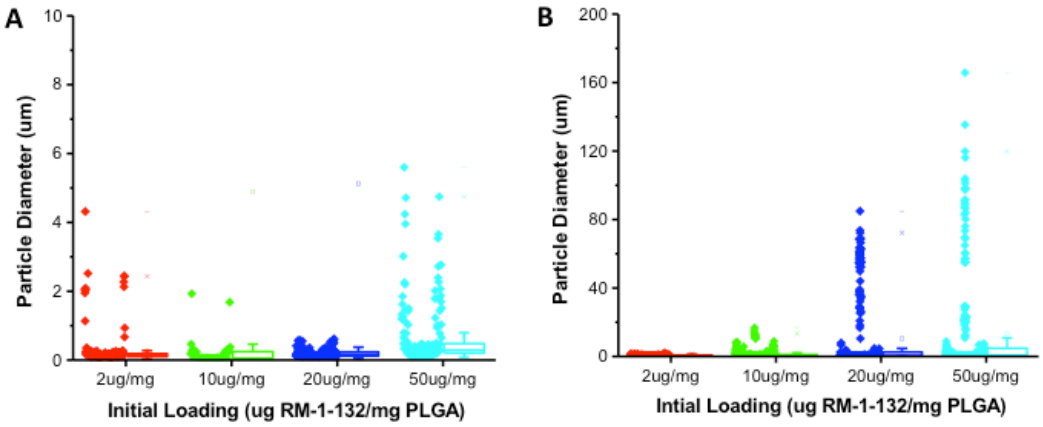

Figure 4.12. Particle diameter based on SEM size measurements for RM-1-132-loaded PLGA particles at various initial loadings *(A = emulsion fabricated particles, B = fNP fabricated particles).*

The final loading and the incorporation efficiency were tested for a range of initial loadings of the RM-1-132-loaded PLGA particles (Figure 4.13). For emulsion-fabricated particles the maximum incorporation occurred at 2ug/mg initial loading with a decrease in incorporation efficiency seen as initial loading

was pushed higher. For fNP-fabricated particles incorporation efficiency remained between 60 – 100% as initial loading increased from 2 to 50ug/mg.

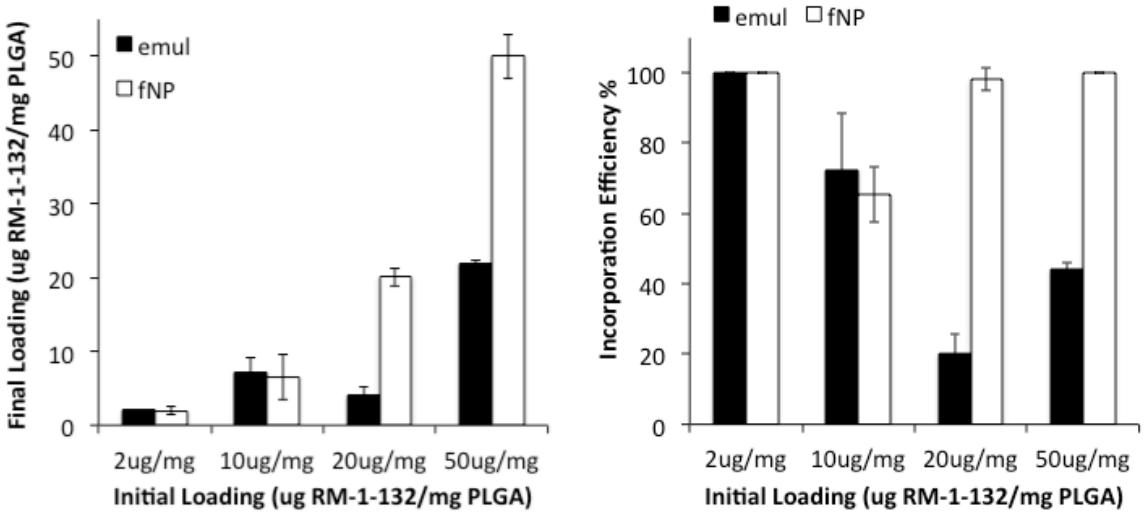

Figure 4.13. Final loading and incorporation efficiency of RM-1-132-loaded PLGA particles from 2ug/mg to 50ug/mg initial loading.

4.4.2.3 RM-1-132 Release Kinetics

The release was tested for up to four weeks for initial loadings of 2, 10, and 20ug/mg for both emulsion and fNP-fabricated particles by a method described early in the chapter (Section 4.3.3.3 and Figure 4.14). Cumulative percent release is the cumulative amount of RM-1-132 released from the particles at set times divided by the total amount of RM-1-132 incorporated into the particle. Cumulative amounts and release data are per mg of RM-1-132-loaded particles unless otherwise stated. For the RM-1-132-loaded PLGA particles, the highest percent release is for the emulsion-fabricated particles. At the end of Week 4 almost 100% is released from the 2ug/mg emulsion-fabricated particles followed by the 20ug/mg at ~80%. The final loading for the 20ug/mg

particles is approximately 5.3ug/mg, indicating that at the end of week 4 only 4.2ug is released per 1mg of particles. The 10ug/mg emulsion-fabricated particles released ~35% of its contents (~1.6ug per 1mg particles) by Week 4, followed by the fNP-fabricated particles at 10 – 20% released by Week 4.

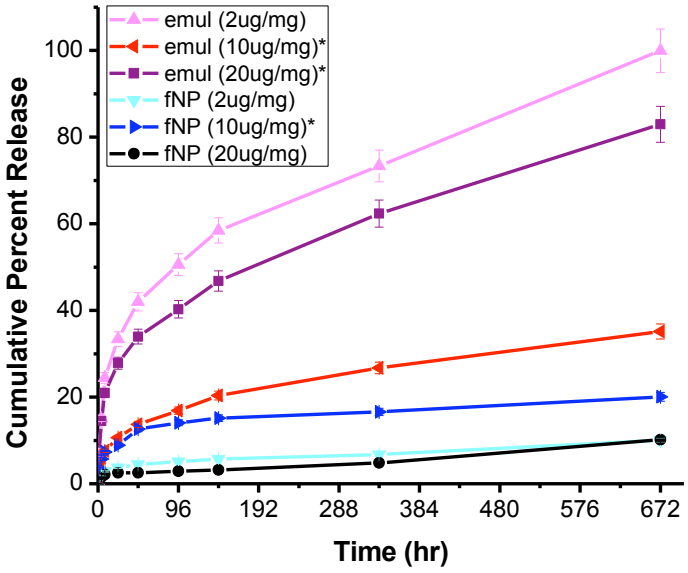

Figure 4.14. Cumulative percent release of RM-1-132 from particles for 4 weeks for various initial loadings for both emulsion and fNP-fabricated particles.

Release rates were calculated for both emulsion and fNP-fabricated RM-1-132-loaded PLGA particles on a per mg particle per hour basis (Figure 4.15). There seems to be an initial burst then leveling off around 2ng/hr per mg of particles after 4 days. For a 25 mg dosage of particles, release rates would be approximately 40ng/hr for the emulsion-based systems after 4 days. These release rates would require a higher amount of particles to be effective due to the release rate not surpassing the clearance rate at a <25mg does. Therefore, the next section utilizes the 1294 molecule, an adaptation of the RM-1-132 molecule

with a lower clearance rate and higher hydrophobicity, which will assist in incorporation.

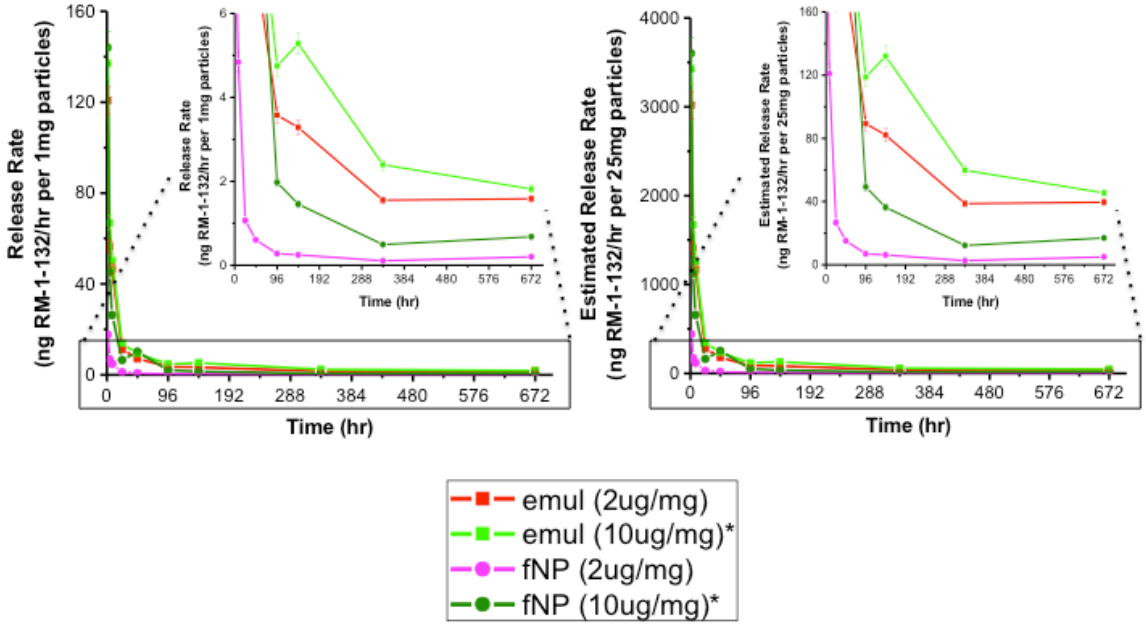

Figure 4.15. Release rates for various initial loadings of RM-1-132-loaded PLGA particles over 4 weeks. *(Left = release rates per 1mg of particles, Right = estimates release rates for 25mg of particles, inset is a zoomed in image to show release trends).*

4.4.3 Improving Drug Properties for Improved BKI Incorporation and Release

Although we had good incorporation and release for the RM-1-132-loaded PLGA particles, especially for the emulsion-based fabrication systems there was still an issue with overcoming the clearance rate during the release of the BKI in *in vivo* systems. The Van Voorhis group and Maly group, in the Department of Medicine and Department of Chemistry (University of Washington), respectively, have created a BKI library of molecules including the RM-1-132 molecule tested

earlier in this chapter. From the library, the 1294 molecule was the most similar to the RM-1-132 molecule in terms of molecular weight and size. In addition the 1294 BKI possessed properties which could assist in incorporation into particles and lowering the clearance rate of the molecule *in vivo.*

4.4.3.1 Drug Clearance: Advancing from RM-1-132 to 1294

Kasey Rivas, K.K. Ojo, and colleagues of the Van Voorhis group in the Department of Medicine along with members of the Maly group in the Department of Chemistry (University of Washington) developed and tested the 1294 BKI molecule.[14, 23] The 1294 molecule was designed with one extra methyl group added to the nitrogen in the bottom piperidine group of the structure. This enhanced the stabilization of the nitrogen in the piperidine group from hydrolytic attack as confirmed with *in vitro* liver microsome experiments.[23] Correspondingly the addition of the methyl group also allowed lower clearance rates *in vivo.* Lowering clearance rate, while keeping activity and size similar was a tremendous enhancement for the inhibitor. Furthermore, addition of the methyl group slightly increased the hydrophobicity of the molecule, which hypothetically can enhance incorporation into the particle (Table 4.6, Figure 1.1).

	RM-1-132	1294
MW (g/mol)	402.49	416.52
Log $P_{org/aq}$ (~50ug/mg, pH6)	-0.18	0.35
Log $P_{org/aq}$ (~50ug/mg, pH12)	1.54	1.99

Table 4.6. Properties for select BKIs RM-1-132 and 1294. *(Log P represents the partition coefficient between an organic phase and an aqueous phase, where a*

positive value indicates a hydrophobic tendency of the molecule and a negative value is the hydrophilic tendency of the molecule).

We also tested the partition coefficient of the 1294 molecule to confirm that a loss in affinity to the aqueous phase was occurring similar to the RM-1-132 molecule (Figure 4.16). pH 12, which is the fabrication pH for these experiments can provide a neutralized BKI molecule with a preference for the polymer and organic phase. But, instead of the transition between pH 10 and pH 12 from a negative to a positive Log P as seen with the RM-1-132 molecule, the transition occurred between pH 6 and pH 8. There is also a stronger trend with increase in hydrophobicity as concentration increases. We speculate that this may be due to the stronger hydrophobicity of the drug and perhaps aggregation of the amphiphilic molecule due to oversaturation in both phases causing either neutralization and transport into the organic phase or dissolution out of solution to the more dense layer (organic phase in this case).

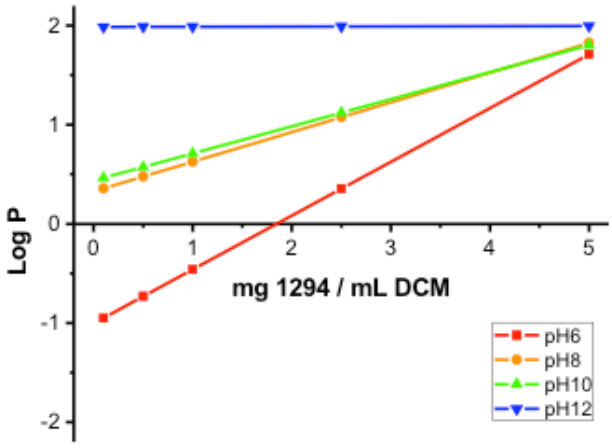

Figure 4.16. Partition coefficient for increasing concentrations of 1294 at pH 6, 8, 10, and 12. *(A concentration of 1 ug/mL is equivalent to 20ug/mg initial loading during particle fabrication).*

We determined the final loading and the incorporation efficiency of 1294-loaded PLGA particles for both the emulsion and fNP fabrication methods at a neutral and basic pH (Figure 4.17). Agreeing with the RM-1-132 loaded particles, the increase in pH of the fabrication conditions allowed a higher incorporation of the BKI. There was not much difference between the emulsion-fabricated and fNP-fabricated particles. Additional system parameters like fNP system speed were also examined (Appendix D-9).

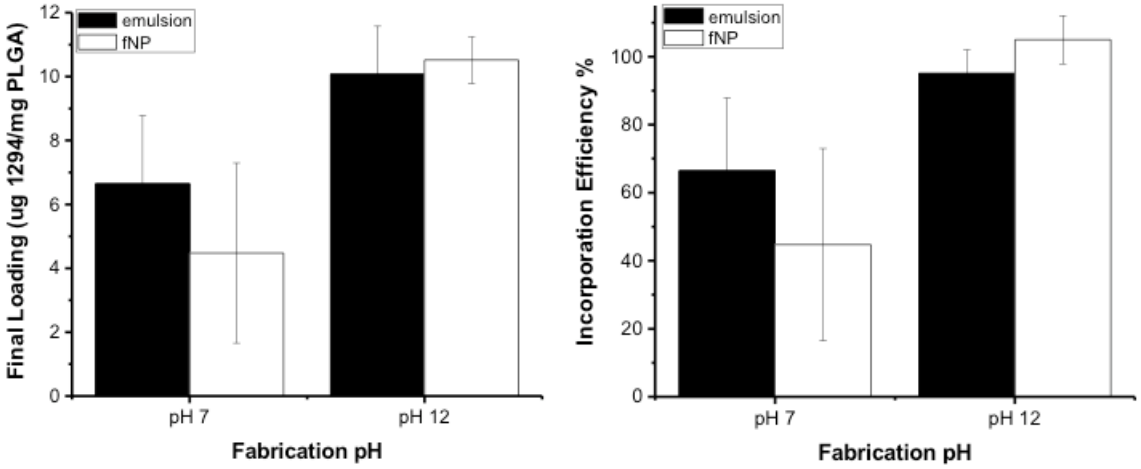

Figure 4.17. Final loading and incorporation efficiency for 10ug/mg 1294-loaded PLGA particles at pH 7 and pH 12.

4.4.3.2 Optimized 1294 Size and Incorporation

We then tested a range of initial loadings of 2, 10, 20, 50, and 100ug/mg incorporation of the 1294 molecule into PLGA particles at a fabrication pH = 12 for both emulsion and fluidic nanoprecipitation (fNP) fabrication methods. The sizes were analyzed by DLS measurements and SEM images. For the emulsion fabrication method DLS revealed a 200 – 300nm sized particle, mostly

monodispersed due to low PDI, with a surface charge of ~ –2mV for loadings up till 100ug/mg (Appendix D-10, D-11). At 100ug/mg initial loading particle size jumped to approximately 1.3um with a PDI = 0.7. For the fNP fabrication method DLS revealed sizes ranging from 500 nm to 3um with moderate to high PDI, and surface charge ~ –2mV (Appendix D-10, D-11). There was an increase in particle size and polydispersity at 100ug/mg initial loading, as well as lower concentrations of 2ug/mg. Based on SEM measurements, the particle diameter for the emulsion fabricated particles were similar to the DLS measurements with most diameters below 1um until the 100ug/mg initial loading was reached (Figure 4.18). For the highest loading of 100ug/mg there were particles ranging from <1 – 6um. For the fNP-fabricated particles, average particle diameter was under 1um, but particle sizes ranged from 200nm to 100um. Comparisons and analysis between size and incorporation as well as size and release will be described in Chapter 5. Additionally, we are further investigating the particle size and morphology to confirm trends via SEM and TEM for a related paper publication.

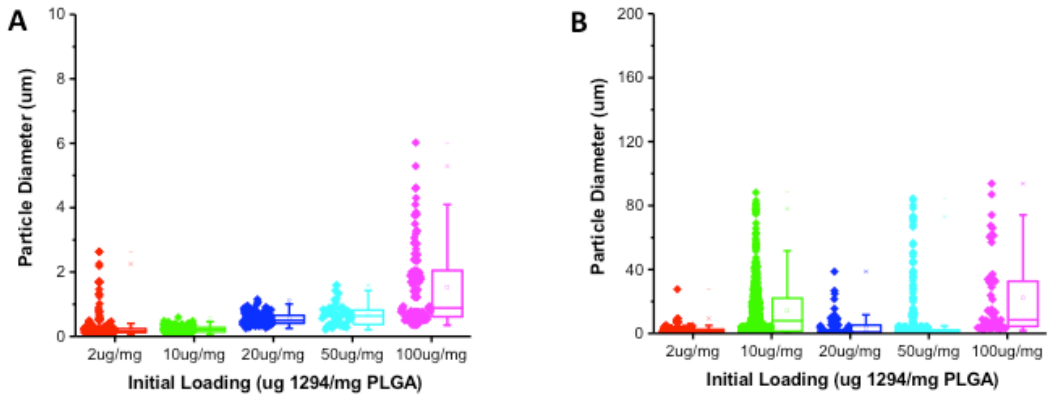

Figure 4.18. Particle diameter based on SEM size measurements for 1294-loaded PLGA particles at various initial loadings *(A = emulsion fabricated particles, B = fNP fabricated particles).*

The final loading and the incorporation efficiency were tested for a range of initial loadings of the 1294-loaded PLGA particles (Figure 4.19). For emulsion-fabricated particles full incorporation was seen between 10 to 50ug/mg initial loading with a decrease in incorporation efficiency as initial loading was pushed higher to 100ug/mg. For fNP-fabricated particles incorporation followed a similar trend, but with less of a decline at 100ug/mg.

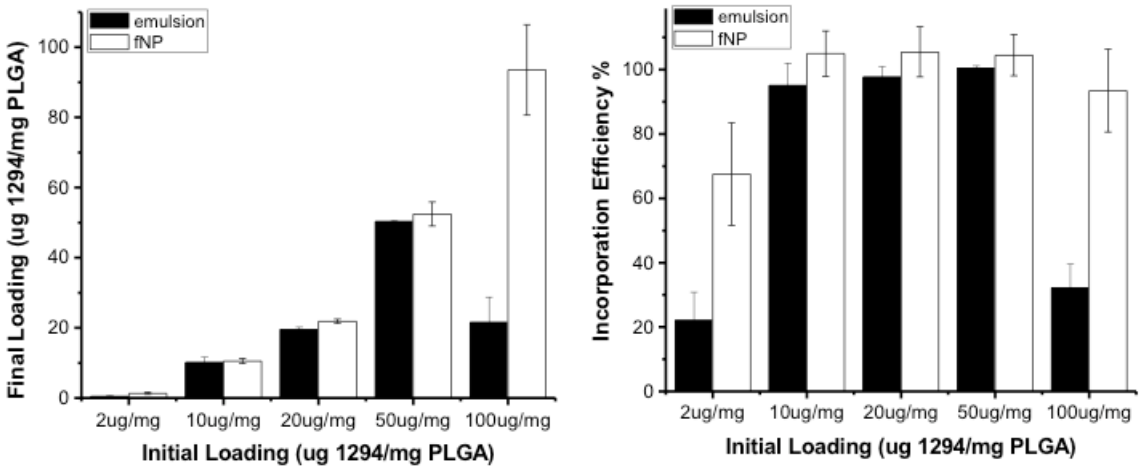

Figure 4.19. Final loading and incorporation efficiency for 1294-loaded PLGA particles fabricated at pH 12 for various loadings.

4.4.3.3 Optimized Release Kinetics

The release was tested for up to four weeks for initial loadings of 20, 50, and 100ug/mg for both emulsion and fNP-fabricated particles by a method described early in the chapter (Section 4.3.3.3, Section 4.4.2.3 and Figure 4.20). Cumulative amounts and release data are per mg of 1294-loaded particles unless otherwise stated. For the 1294-loaded PLGA particles, the highest percent release were for the 50ug/mg initial loading particles by the end of Week

4, regardless of fabrication method. The remaining loadings were all approximately 40% released by Week 4. The release may be the highest for the 50ug/mg particles because these displayed the maximal loading efficiency before declining when being pushed higher to the 100ug/mg initial loadings. The 50ug/mg particles also displayed an average particle diameter below 1um, unlike the 100ug/mg particles which displayed a increased average particle diameter, increased PDI, and a slightly larger range of surface charge.

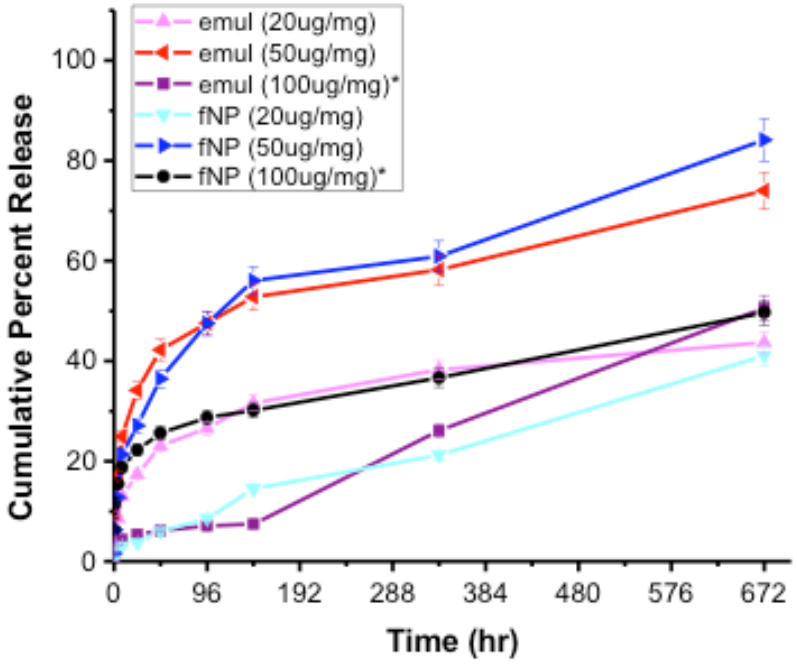

Figure 4.20. Cumulative percent release of 1294 from particles for 4 weeks for various initial loadings for both emulsion and fNP-fabricated particles.

Release rates were calculated for both emulsion and fNP-fabricated 1294-loaded PLGA particles on a per mg particle per hour basis (Figure 4.21). There seems to be an initial burst then leveling off around 2 to 6ng/hr per mg of particles after 4 days. For a 25 mg dosage of particles, release rates would be

approximately 50 to 200ng/hr for the emulsion-based systems after 4 days. The clearance rate for the 1294 molecule is estimated to be 100 – 200ng/hr in an *in vivo* animal model. It is important for the inhibitor to be released at a rate above the clearance rate to ensure that an effective amount of the component is in circulation for a prolonged time. In the graphs below, we look at the *in vitro* release rate per 1mg particles and the estimated release rate for a 25mg particle injection, a typical dose for an average mouse *in vivo* experiment.

All of the 1294-loaded particle systems were estimated to release the BKI above the clearance rate for at least 4 days, except for the 20ug/mg initial loading fNP-fabricated particles, which dropped to 50% clearance rate at the 4 hour timepoint. The 100ug/mg particles, both emulsion and fNP-fabricated remain around 150ng/hr per estimated 25mg particle dosage. The 50ug/mg particles decrease to approximately 50ng/hr for 25mg particles at the end of Week 2, but administering more particles (> 35mg particles) pushes the release rate above the clearance rate for that time.

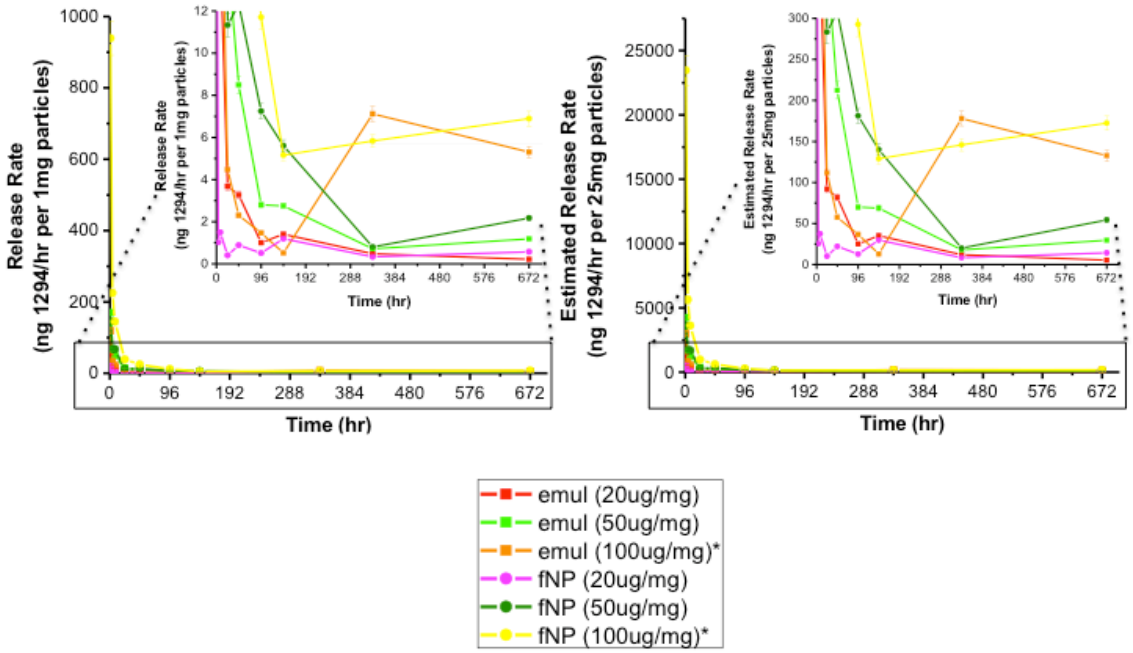

Figure 4.21. Release rates for various initial loadings of RM-1-132-loaded PLGA particles over 4 weeks. *(Left = release rates per 1mg of particles, Right = estimates release rates for 25mg of particles, inset is a zoomed in image to show release trends).*

4.5 Conclusions

This chapter discussed the fabrication of particulate delivery systems for the sustained release of bumped kinase inhibitors (BKIs) utilized in ceasing the transmission of malaria. Initially the type of particle (solid dispersions, single/double emulsions, and core/shell particles) was tested to increase the loading of the BKIs. We discovered that overall system parameters should be altered instead of the type of particle. Increasing the pH beyond the BKI's pKa neutralized the BKI charge and allowed the molecule to have an affinity for the

hydrophobic phase containing the polymer, permitting higher incorporation efficiency.

The particle size, incorporation of the BKI, and release kinetics were then examined for the RM-1-132 molecule for two fabrication methods, emulsification and fluidic nanoprecipitation (fNP). Particle size was in the nano range and incorporation was able to remain at ~100% for up to 50ug/mg initial loading for the fNP-fabricated particles. The release studies displayed that release of the RM-1-132 was decent, but may not be sufficiently above clearance rate for *in vivo* studies. The 1294 BKI molecule was then utilized for its low clearance rate and similarity to the RM-1-132 molecule to counter this dilemma. Particle size, incorporation, and release kinetics were examined. As compared to the emulsion-fabricated particles, the fNP-fabricated particles display a higher average particle diameter and a large range of particle diameters spanning the nano to micron size-range. The incorporation was approximately 100% for initial loadings from 10 – 50ug/mg, with fNP systems remaining close to 100% at 100ug/mg initial loading. Release studies suggested a level of 1294 could be provided above clearance rate for both emulsion and fNP-fabricated systems past Day 4 for a 25mg dosage of particles. Thus, this particle delivery system has promise in constant delivery of BKIs to achieve a therapeutic blood level for a prolonged period of time.

Overall, this chapter shows how a matrix of particle formulations, system parameter manipulation, and BKI molecule adaptation was tested to uncover the system with maximum BKI incorporation and optimal release profile. The next

chapter focuses on effects of fabrication method and type of BKI used on particle characteristics, incorporation, and *in vitro* release. There are also investigations into drug distribution within particles fabricated by different methods, retention at the site for particle injections, and BKI-loaded particles *in vivo* testing with a preliminary mouse model.

4.6 References

1. Solomon M, D'Souza GGM. Recent progress in the therapeutic applications of nanotechnology. *Current Opinion in Pediatrics* 2011, **23**(2)**:** 215-220.

2. Freese A, Sabel BA, Saltzman WM, During MJ, Langer R. CONTROLLED RELEASE OF DOPAMINE FROM A POLYMERIC BRAIN IMPLANT - INVITRO CHARACTERIZATION. *Experimental Neurology* 1989, **103**(3)**:** 234-238.

3. Rosenberg RT, Siegel SJ, Dan N. Release of highly hydrophilic drugs from poly(epsilon-caprolactone) matrices. *Journal of Applied Polymer Science* 2008, **107**(5)**:** 3149-3156.

4. Wen Y, Gallego MR, Nielsen LF, Jorgensen L, Everland H, Moller EH*, et al.* Biodegradable nanocomposite microparticles as drug delivering injectable cell scaffolds. *Journal of Controlled Release* 2011, **156:** 11-20.

5. Sullivan SP, Koutsonanos DG, Martin MD, Lee JW, Zarnitsyn V, Choi SO*, et al.* Dissolving polymer microneedle patches for influenza vaccination. *Nature Medicine* 2010, **16**(8)**:** 915-U116.

6. Doshi N, Zahr AS, Bhaskar S, Lahann J, Mitragotri S. Red blood cell-mimicking synthetic biomaterial particles. *Proceedings of the National Academy of Sciences of the United States of America* 2009, **106**(51)**:** 21495-21499.

7. Mohanraj V, Chen Y. Nanoparticles - a review. *Tropical Journal of Pharmaceutical Research* 2006, **5**(1)**:** 561-573.

8. De Temmerman M-L, Rejman J, Vandenbroucke RE, De Koker S, Libert C, Grooten J*, et al.* Polyelectrolyte LbL microcapsule versus PLGA microspheres for immunization with protein antigen. *Journal of Controlled Release* 2011**:** 8.

9. Anderson JM, Shive MS. Biodegradation and biocompatibility of PLA and PLGA microspheres. *Advanced Drug Delivery Reviews* 1997, **28**(1)**:** 5-24.

10. Crownover E, Duvall CL, Convertine A, Hoffman AS, Stayton PS. RAFT-synthesized graft copolymers that enhance pH-dependent membrane destabilization and protein circulation times. *Journal of Controlled Release* 2011, **155**(2)**:** 167-174.

11. Govender T, Stolnik S, Garnett MC, Illum L, Davis SS. PLGA nanoparticles prepared by nanoprecipitation: drug loading and release studies of a water soluble drug. *Journal of Controlled Release* 1999, **57**(2)**:** 171-185.

12. Yeo Y, Park KN. Control of encapsulation efficiency and initial burst in polymeric microparticle systems. *Archives of Pharmacal Research* 2004, **27**(1)**:** 1-12.

13. Augst AD, Kong HJ, Mooney DJ. Alginate hydrogels as biomaterials. *Macromolecular Bioscience* 2006, **6**(8)**:** 623-633.

14. Ojo KK, Pfander C, Mueller NR, Burstroem C, Larson ET, Bryan CM*, et al.* Transmission of malaria to mosquitoes blocked by bumped kinase inhibitors. *Journal of Clinical Investigation* 2012, **122**(6)**:** 2301-2305.

15. Xie H, Smith JW. Fabrication of PLGA nanoparticles with a fluidic nanoprecipitation system. *Journal of Nanobiotechnology* 2010, **8**(18)**:** 1-7.

16. Berg JC. **An introduction to interfaces & colloids : the bridge to nanoscience**. Hackensack, NJ: World Scientific; 2010. p. 785.

17. Gan Q, Wang T. Chitosan nanoparticle as protein delivery carrier - Systematic examination of fabrication conditions for efficient loading and release. *Colloids and Surfaces B: Biointerfaces* 2007, **59**(1)**:** 24 - 34.

18. Li Z, Gu L. Effects of Mass Ratio, pH, Temperature, and Reaction Time on Fabrication of Partially Purified Pomegranate Ellagitannin-Gelatin Nanoparticles. *Journal of Agricultural and Food Chemistry* 2011, **59:** 4225-4231.

19. Hu B, Pan C, Sun Y, Hou Z, Ye H, Hu B*, et al.* Optimization of Fabrication Parameters to Prodduce Chitosan-Tripolyphosphate Nanoparticles for Delivery of Tea Catechins. *Journal of Agricultural and Food Chemistry* 2008, **56:** 7451-7458.

20. Jahanshahi M, Sanati MH, Babaei Z. Optimization of parameters for the fabrication of gelatin nanoparticles by the Taguchi robust design method. *Journal of Applied Statistics* 2008, **35**(12)**:** 1345-1353.

21. Paik U, Hackley VA, Lee J, Lee S. Effect of poly(acrylic acid) and poly(vinyl alcohol) on the solubility of colloidal BaTioO3 in an aqueous medium. *Journal of Materials Research* 2003, **18**(5)**:** 1266-1274.

22. Pajouhesh H, Lenz GR. Medicinal Chemical Properties of Successful Central Nervous System Drugs. *NeuroRx* 2005, **2**(4)**:** 541-553.

23. Van Voorhis WC, Rivas KL, Bendale P, Nallan L, Horney C, Barrett LK*, et al.* Efficacy, pharmacokinetics, and metabolism of tetrahydroquinoline inhibitors of Plasmodium falciparum protein farnesyltransferase. *Antimicrobial Agents and Chemotherapy* 2007, **51**(10)**:** 3659-3671.

24. O.J.o.t.E. Communities, Annex V: Testing Methods, in: A.8. Partition Coefficient, 2002.

CHAPTER 5. COMPARISON OF NANO/MICROPARTICLE BKI-DELIVERY SYSTEMS

5.1 Introduction

The last chapter discussed the fabrication of particle systems in detail and the optimization steps for enhancing BKI incorporation and release including creating the optimal particle type, adjusting system parameters, and modifying the drug itself. The most enhancement of BKI incorporation was from increasing the continuous phase pH above the drug molecules' pKa to neutralize the charge of the molecule and allow the BKI to prefer the organic phase and polymer matrix. The most improvement in BKI release resulted from adapting the drug molecule to possess a lower clearance rate, which inadvertently increased the hydrophobicity of the molecule permitting higher incorporation into the particle and increasing of the release rate estimated to be at a level above the clearance rate (for an appropriate dose and system). Overall, these systems could allow slow delivery of BKI for therapeutic uses needing long exposure, such as prevention of the transmission of malaria.

This chapter emphasizes the effect we observed from slight variables added to the system, i.e. adding one methyl group to the drug molecule or altering the fabrication system. These changes are investigated here for their possible effect on the particle characteristics, drug incorporation, and drug release. Additionally a model drug system, utilizing quantum dots loaded into PLGA particles fabricated via emulsion or fluidic nanoprecipitation (fNP) methods, was used to elucidate the internal drug distribution within the particle.

5.2 Objectives

The objective of this chapter is to investigate into potential reasons why slight discrepancies were seen between different BKI molecules, RM-1-132 and 1294, and different fabrication systems, emulsification and fNP. We will examine the effects on particle characteristics, i.e. size and morphology, BKI incorporation, BKI release, and internal drug distribution within the particle (via a quantum dot/PLGA particle model system). The RM-1-132 molecule is a slightly hydrophilic malaria inhibitor and the 1294 molecule is a slightly hydrophobic malaria inhibitor, 1294 *(RM-1-132 and 1294 were provided by Dr. W. C. Van Voorhis from the Department of Medicine, University of Washington and Dr. D. J. Maly from the Department of Chemistry, University of Washington)*.[1] The nanoparticles size, size distribution, and zeta potential were characterized with dynamic light scattering (DLS) and scanning electron microscopy (SEM). Total drug incorporation and release kinetics were calculated from inhibition assays *(IC50 assays created by K.K. Ojo, Department of Medicine, University of Washington).*

5.3 Materials and Methods

5.3.1 Materials

Poly(DL-lactide-co-glycolide) (PLGA) resomer (50:50 ester-terminated with IV 0.55 – 0.75) was purchased from Lactel Absorbable Polymers (Cupertino, CA). RM-1-132 and 1294 BKIs were generously donated from Dr. W. Van Voorhis's group (Department of Medicine, University of Washington). Quantum

dots (CdSeS/ZnS, diameter = 6nm, emission = 525nm) and poly(vinyl alcohol) (PVA) was purchased from Sigma-Aldrich (St. Louis, MO). Dichloromethane (DCM), dimethyl sulfoxide (DMSO), and acetonitrile was purchased from EMD (EMD Chemicals, Inc., Gibbstown, NJ).

5.3.2 Particle Preparation

PLGA solutions were prepared by dissolving 50mg/mL PLGA in dichloromethane (DCM). Particles were created using either an emulsion method adapted from Dr. K. Tran (Chemical Engineering Department, University of Washington) which is described in more detail below, or a fluidic nanoprecipitation (fNP) method based on Xie, 2010.[2] PVA solutions were at pH=6.4 unless noted otherwise.

5.3.2.1 Emulsion System

RM-1-132 or 1294 was dissolved directly in 1mL of the 50mg/mL PLGA/DCM solution. Solutions were vortexed with the Vortex Genie 2 (Scientific Industries, Bohemia, NY) at a medium-high speed, then sonicated in a water bath approximately 5 times at 5 minutes each. For the emulsion system, this dispersion was sonicated for 10 seconds twice at output 7 with Model 3000 Ultrasonic Homogenizer (Biologics, Inc., Cary, NC). 2 mL of 5% PVA was added drop-wise while vortexing and sonicated. The solution was poured into 2 mL of 5% PVA while vortexing and lightly sonicated. Solution was then poured into 2mL of 1% PVA in a beaker and magnetically stirred for 3 – 4 hours. Solutions were collected and centrifuged twice at 12,000 rpm for 10 minutes using a

Sorvall Legend RT centrifuge (DJB Labcare Ltd. Buckinghamshire, England), and twice at 10,000rpm for 10 minutes using an Eppendorf Centrifuge 5415D (Eppendorf, San Diego, CA) with resuspensions in MilliQ water. Final resuspension was in 200 - 800uL MilliQ water depending on particle concentration. Samples were stored in 4C fridge if not used for testing immediately. For the total drug incorporated (burst) experiments samples were lyophilized overnight using a Freezone 4.5 Freeze Dry System (Labconco Corporation, Kansas City, MO), then used for testing.

5.3.2.2 Fluidic nanoprecipitation (fNP) System

RM-1-132 or 1294 was dissolved directly in the PLGA/DCM solution. Solutions were vortexed with the Vortex Genie 2 (Scientific Industries, Bohemia, NY) at a medium-high speed, then sonicated in a water bath approximately 5 times at 5 minutes each. For the fNP system, the initial solution of approximately 1mL of PLGA/BKI was injected into a flowing stream of dispersant, collected into a beaker immediately, and magnetically stirred for 3 – 4 hours. Specifically, a stainless steel needle (BD-305127 25 ½ G) was inserted approximately halfway into 12” length of Vincon tubing (ID 1/8”, OD 1/4”) that was used to flow the dispersant phase. The PLGA/BKI solution was fed through the needle using at 5mL/min using a 3 mL syringe controlled by a syringe pump (KD Scientific, Holliston, MA). The dispersant channel was 1% PVA adjusted to certain pH flowing at 60mL/min controlled by a Mini-pump with variable flow (Fisher Scientific). Solutions were collected and centrifuged twice at 12,000 rpm for 10 minutes using a Sorvall Legend RT centrifuge (DJB Labcare Ltd.

Buckinghamshire, England), and twice at 10,000rpm for 10 minutes using an Eppendorf Centrifuge 5415D (Eppendorf, San Diego, CA) with resuspensions in MilliQ water. Final resuspension was in 200 - 800uL MilliQ water depending on particle concentration. Samples were stored in 4C fridge if not used for testing immediately. For the total drug incorporated (burst) experiments samples were lyophilized overnight using a Freezone 4.5 Freeze Dry System (Labconco Corporation, Kansas City, MO), then used for testing.

5.3.2.3 Quantum Dot Loaded PLGA Particles

Approximately 7.5ug of CdSeS/ZnS quantum dots (QD, emission = 525) were added to 50mg of PLGA polymer dissolved in dichloromethane or acetonitrile. Solutions were vortexed with the Vortex Genie 2 (Scientific Industries, Bohemia, NY) at a medium-high speed, then sonicated for 10 seconds twice at output 7 with Model 3000 Ultrasonic Homogenizer (Biologics, Inc., Cary, NC). For emulsion-fabricated and fNP-fabricated particles the procedure stated above was followed (Sections 5.3.2.1 and 5.3.2.2), except that the QD-loaded PLGA particles were covered in foil and protected from light for some of the steps in the procedure to preserve the integrity of the fluorescence.

5.3.3 Particle Characterization

5.3.3.1 Size, Morphology, Zeta Potential, and Surface Area

10 uL of particles were resuspended into approximately 1 mL of 10mM KNO_3 solution. Particle size, polydispersity, and zeta potential were measured using a Zetasizer Nano-ZS (Malvern, Worcestershire, United Kingdom).

Scanning electron microscope (SEM) was used to examine the morphology of the particles. 1uL of previously stored particles were dried overnight on a silicon wafer, then sputter-coated with gold using a SPI Sputter Coater (Structure Probe, Inc., West Chester, PA). Images were taken with a JEOL7000F SEM with a beam voltage of 5 – 10 kV (Electron Microscopy Center, University of Washington, Seattle, WA). If size measurements from the DLS readings were out of the DLS range (>5um) then size was also measured from the SEM and TEM images taken (TEM for QD-loaded particles). Particle diameter was measured 2 – 3 times per particle and approximately 60 – 500 particles per sample. All particle sizes measured were reported on a box chart to allow representation of all populations of particle sizes. Surface area was calculated based on average diameter and mode of SEM measurements under the assumption that particles are spheres.

5.3.3.2 Total Drug Incorporated (IC50 Assay)

Lyophilized particles were completely dissolved in established amounts of DMSO to produce between 1 – 5 mM of estimated drug content. Samples were centrifuged to separate any remaining polymer out. Samples were tested for inhibition via a *Plasmodium falciparum* calcium-dependent protein kinase (Pfal-CDPK) specific kinase-Glo assay (IC50 inhibition assay) developed by Dr. K.K Ojo and colleagues of Dr. W Van Voorhis's Lab (Department of Medicine, University of Washington, Seattle, WA).

Both the total drug incorporated and the time-release samples were tested via the IC50 assay using. Data was analyzed using Prism software into a half maximal inhibitory concentration (IC50) graph with pure RM-1-132 or 1294 as a positive control. Values for total amount of BKI in particles were calculated using the following equation (*where I = amount of drug in particles (ug)*, C_s *= starting concentration (estimated, (mM)*, *D = dilution factor, usually 1000x*, $IC50_{RM1}$ *= soluble drug concentration for 50% inhibition (uM)*, $IC50_{NP}$ *= drug in nanoparticle concentration for 50% inhibition (uM)*, *V = volume used to dilute particles (L)*, *MW = molecular weight of drug (ug/umol)*):

$$I = C_s \times D \times \frac{IC50_{RM1}}{IC50_{NP}} \times V \times MW$$

5.3.3.3 Drug Release

Approximately 1 – 10mg of particles were resuspended in 100uL of sterile PBS (pH 7.4) and incubated in a 37C water bath. At each timepoint, samples were centrifuged for 10 minutes at 10,000 rpm. Entire supernatant was removed and particles were fully resuspended in 100 uL of fresh PBS. Samples were returned to the 37C water bath. Timepoints were between 0 – 12hrs on day 0, every day until day 7, and either weekly or bi-weekly after that. Amount of drug released, cumulative drug release, and percent release were calculated based on the IC50s of the time-released samples. Minimum reliability of inhibition, or the minimum effective concentration (MEC) was set at 20% or 0.2ng of RM-1-132 or 1294 for most samples. Values for total amount of BKI released from

particles were calculated using the following equation (*where R = amount of drug released from particles (ug),* I_{NP} *= percent inhibition of drug from nanoparticles,* I_{RM1} *= percent inhibition of drug from nanoparticles):*

$$R = I_{NP} \times \frac{IC50_{RM1}}{I_{RM1}} \times D \times V \times MW$$

Cumulative release, cumulative percent release, and release rates per mg of particles were calculated based on these IC50-based values.

5.4 Results and Discussion: Comparisons

5.4.1 Drug Hydrophobicity

5.4.1.1 Size and Morphology Based on Initial Loading

Particles loaded with RM-1-132, a slightly hydrophilic molecule, versus 1294, a slightly hydrophobic molecule produced somewhat different size and shape. The RM-1-132-loaded particles displayed a mostly small and spherical shape (Figure 5.1). The 1294-loaded particles displayed a spherical shape for some loadings and somewhat spherical shape for other loadings (Figure 5.2). Additional lower magnification SEM images are in the appendix (Appendix D-12).

For the emulsion-fabricated particles both RM-1-132 and 1294-loaded particles display changes at a 20ug/mg initial loading. For RM-1-132 the particles increased in size and for the 1294-loaded particles there was a change from spherical to less spherical in shape. For fNP-fabricated particles, both RM-1-132 and 1294-loaded particles displayed changes at 50ug/mg. RM-1-132-

loaded particles displayed a small, spherical size until 50ug/mg where the size slightly increased. 1294-loaded particles displayed a large spherical size (20ug/mg is at a lower magnification) until 50ug/mg, which showed an increase in size and 100ug/mg which showed a less spherical shape. Overall, for the RM-1-132 molecule there was an increase in size after increasing the initial loading to a certain level (20ug/mg for emulsion, 50ug/mg for fNP). The same trend was observed for 1294-loaded particles, except there was also an increase in non-spherical properties after a certain initial loading (20ug/mg for emulsion, 50ug/mg for fNP).

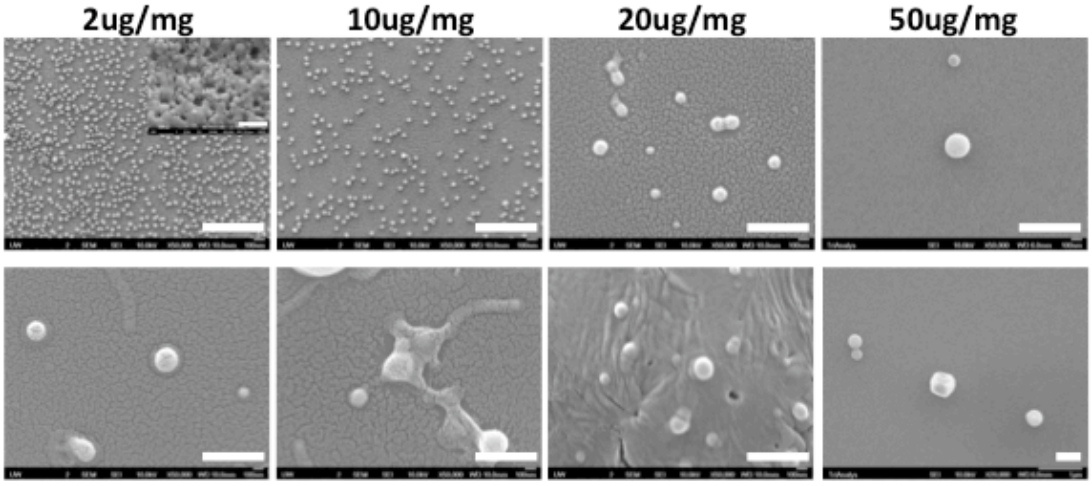

Figure 5.1. SEM images for RM-1-132-loaded PLGA particles fabricated via emulsion (top row) and via fNP (bottom row). *Scale bar = 500nm. Additionally, we are further investigating the particles to confirm trends due to low amounts of particles via SEM for a related paper publication. Particles were stored in fridge before SEM testing*.

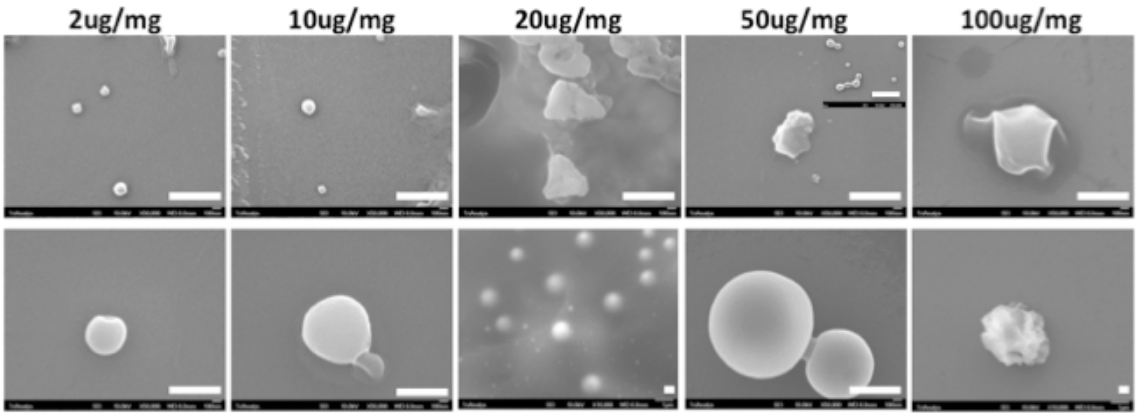

Figure 5.2. SEM images for 1294-loaded PLGA particles fabricated via emulsion (top row) and via fNP (bottom row). *Scale bar = 500nm. Additionally, we are further investigating the particles to confirm trends due to low amounts of particles via SEM for a related paper publication. Particles were stored in fridge before SEM testing*.

5.4.1.2 BKI versus Incorporation

For each fabrication method, we looked at the differences between incorporation based on the type of the BKI used (Figure 5.3). Corresponding incorporation efficiencies can be found in the appendix (Appendix D-13). For the emulsion method, the more hydrophobic molecule (1294) displayed a higher incorporation as the initial loading increased. This may be due to the fact that the higher hydrophobicity mixes better with the polymer in the organic phase. For the fNP-fabricated system, the two different BKIs were comparable in final loading, increasing as initial loading increased. Since fNP is considered crash precipitation with instantaneous particle formation, it may retain drug regardless of hydrophobicity due to the rapid rate of the solvent crash out.

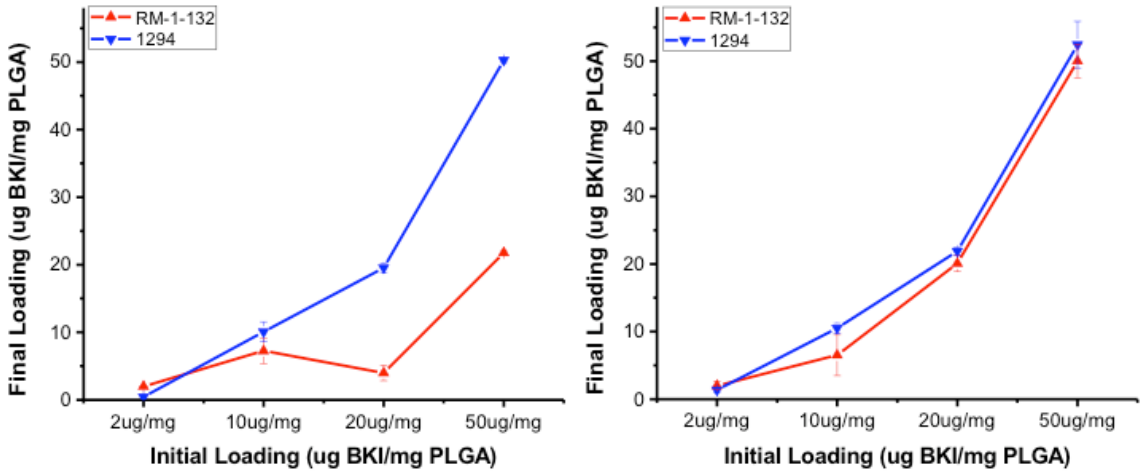

Figure 5.3. Final Loading for two types of BKIs (RM-1-132 and 1294) for emulsion (left) and fNP (right) fabricated particles at various initial loadings.

5.4.1.3 BKI versus Release

We also investigated the effect of different BKIs on release (Figure 5.4). The RM-1-132 loaded emulsion-fabricated particles had a lower final incorporation, which caused the highest cumulative percent release seen. Out of the other systems with similar final incorporation, and it looks like the 1294-loaded particles released a higher amount by week 4 than the RM-1-132-loaded particles. This agrees with the cumulative amounts released, highest for the 1294-loaded particles at 8ug, then the emulsion-fabricated RM-1-132 (5ug), and lastly fNP-fabricated RM-1-132 (2ug). This is an interesting trend because theoretically the more hydrophilic drug should release a higher amount from a hydrophobic polymer.

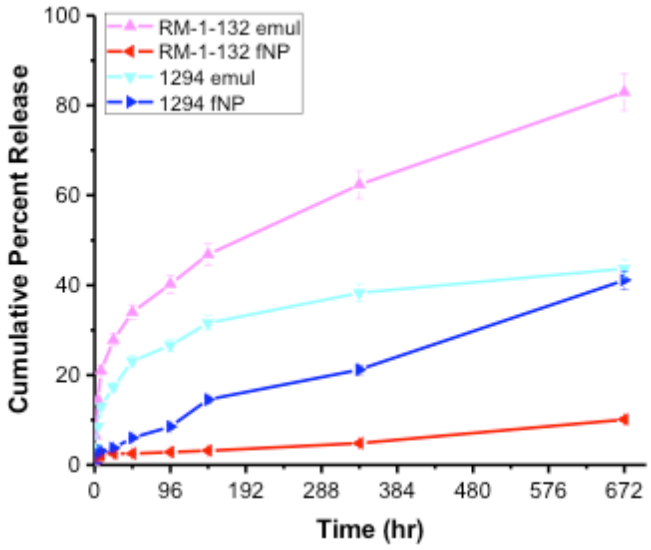

Figure 5.4. Cumulative percent release for two types of BKIs (RM-1-132 and 1294) for emulsion and fNP fabricated particles. *(All particles are fabricated at 20ug/mg initial loading).*

5.4.2 Fabrication Method

5.4.2.1 Size Based on Fabrication Method

The surface area was calculated based on SEM size measurements for both types of BKI molecules and both fabrication methods (Figure 5.5). Emulsion-fabricated particles exhibited a low particle surface area for both RM-1-132 and 1294-loaded particles as initial loading increased. The more hydrophobic 1294-loaded particles displayed a slightly smaller surface area for the emulsion system. This makes sense because the 1294 and polymer are closer in hydrophobicity than the RM-1-132 and polymer. For the fNP-fabricated particles there was a small trend of increasing surface area with increasing initial loading, but the 10ug/mg initial loading (1294) seemed unusually high possibly due to some larger particles raising the average.

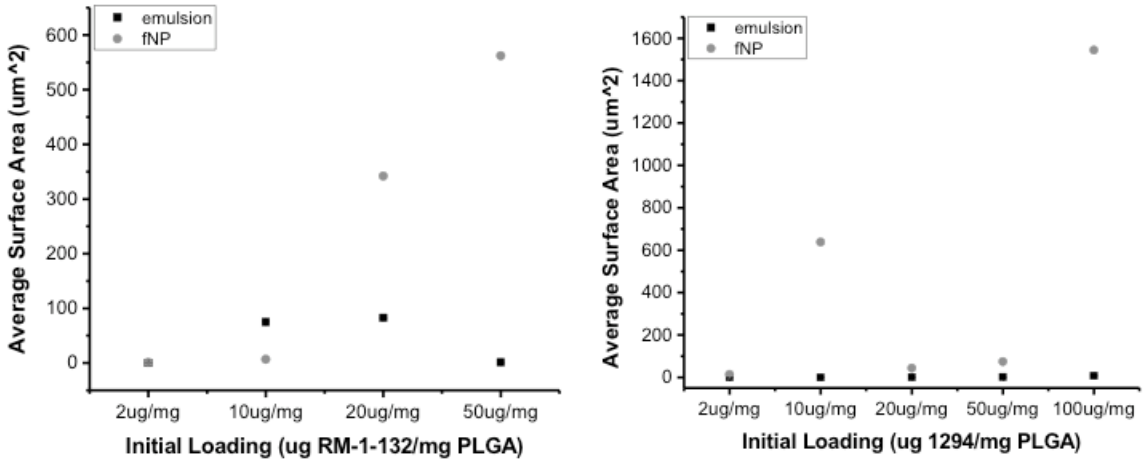

Figure 5.5. Average particle surface area of RM-1-132 (left) and 1294 (right) loaded-PLGA particles for emulsion and fNP fabricated particles at various initial loadings.

5.4.2.2 Method versus incorporation

Surface area versus incorporation was investigated for the emulsion-fabricated and fNP-fabricated particles. For RM-1-132-loaded particles, the emulsion-fabricated particles had increasing, but low surface area and declining incorporation efficiency as the initial loading increases (Figure 5.6). At 50ug/mg initial loading there was a slight decrease in surface area and an increase in incorporation efficiency. For emulsion-fabricated 1294-loaded particles the surface area increased at 100ug/mg as the incorporation efficiency % dropped to approximately 30% (Figure 5.7). For the emulsion-based system it seems that an increase in surface area depressed the incorporation efficiency.

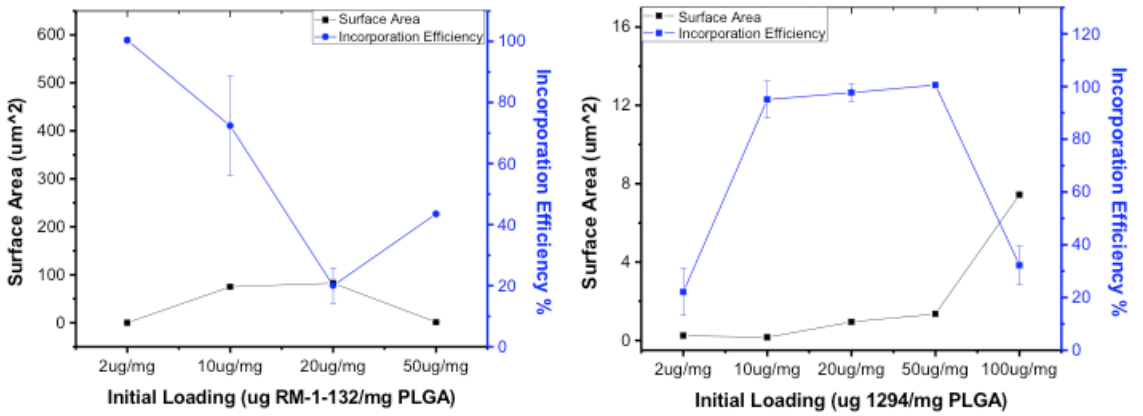

Figure 5.6. Average particle surface area versus incorporation efficiency of emulsion-fabricated RM-1-132 (left) and 1294 (right) loaded PLGA particles at various initial loadings.

For fNP-fabricated RM-1-132-loaded particles the surface area increased and the incorporation efficiency remained relatively high as initial loading increased. For the fNP-fabricated 1294-loaded particles the surface area was fluctuating but the incorporation efficiency remained between 90 – 100%. However, there was a large increase in surface area at 100ug/mg with a slight drop in incorporation efficiency, but it was not as drastic as seen with the emulsion-fabricated particles. For the fNP-fabricated particles it seemed that an increase in surface area did not affect incorporation efficiency like the emulsion-fabricated particles.

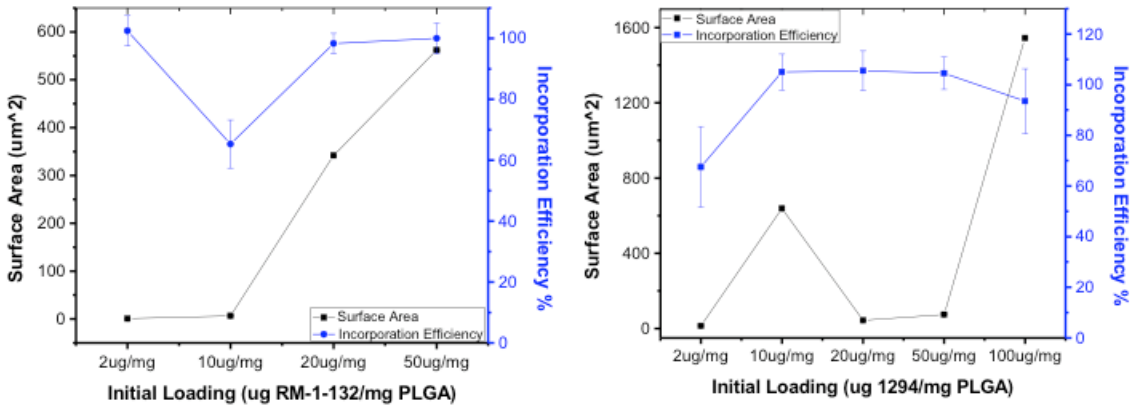

Figure 5.7. Average particle surface area versus incorporation efficiency of fNP-fabricated RM-1-132 (left) and 1294 (right) loaded PLGA particles at various initial loadings.

5.4.2.3 Method versus Release

We also investigated the surface area versus the total cumulative amount released by week 4. The range of initial loadings is different for each type of BKI used because the *in vitro* release experiments were performed on select optimal samples. Both emulsion-fabricated and fNP-fabricated particles showed increases with amount of BKI released by the end of week 4 (Figure 5.8 and Figure 5.9). The one exception is the emulsion-fabricated 1294-loaded particles with 100ug/mg initial loading. This sample displayed a decrease due to the drastic decline in incorporation efficiency and the hydrophobicity of drug allowing a stronger incorporation into the particle. A drop in incorporation efficiency was also seen for the emulsion-fabricated RM-1-132-loaded particles with a 20ug/mg initial loading, but no drop in amount release was seen perhaps due to the

hydrophilicity of the RM-1-132 molecule weakening the connection with the polymer particle.

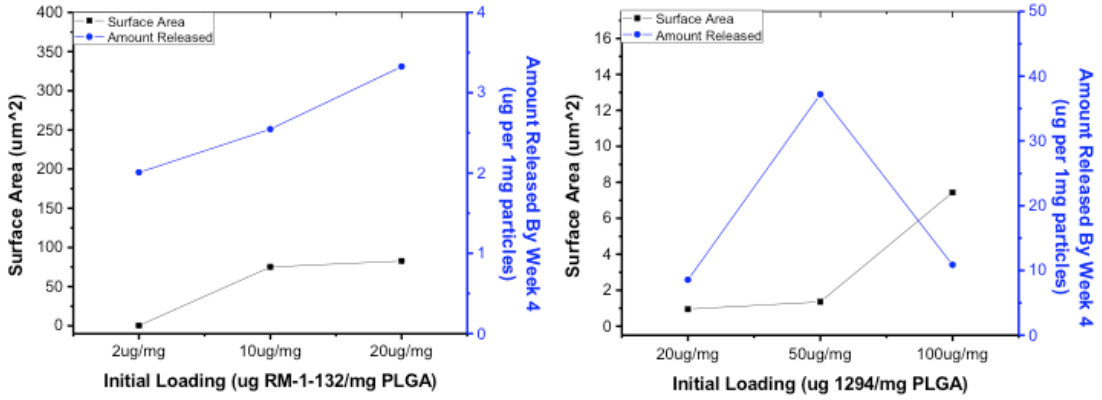

Figure 5.8. Average particle surface area versus total cumulative amount released by Week 4 for emulsion-fabricated RM-1-132 (left) and 1294 (right) loaded-PLGA particles at various initial loadings.

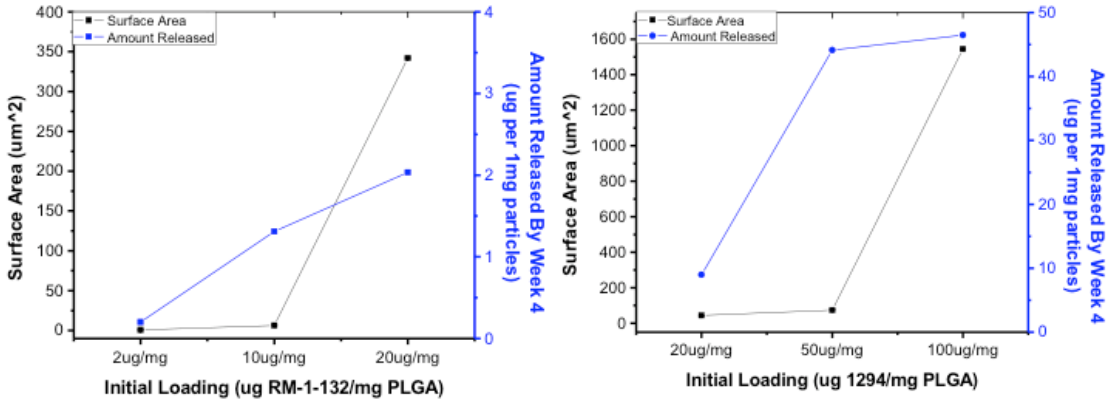

Figure 5.9. Average particle surface area versus total cumulative amount released by Week 4 for fNP-fabricated RM-1-132 (left) and 1294 (right) loaded-PLGA particles at various initial loadings.

5.4.2.4 Drug Distribution within a Particle

5.4.2.4.1 Emulsion versus fNP-fabricated QD-loaded particles

To investigate the effects of fabrication method even further, we used a model system to examine the internal drug distribution within a particle fabricated using either emulsion or fNP methods. Quantum dots (QDs) were mixed in with the PLGA/organic solution and utilized to make either single emulsion or fNP-fabricated particles. Based on size analysis by DLS particles were approximately 300nm in diameter, but the fNP-fabricated particles displayed signs of aggregation with presence of a peak 2 and a moderate PDI level *(data not shown).* Therefore, size measurements based on SEM and TEM images were measured and correlated with the DLS results (Figure 5.10). Measured diameters of the emulsion-fabricated particles were 100 – 400nm while fNP-fabricated particles displayed sizes from 200nm to 1um. For our further experiments we examined the particles on or close to the nano-scale.

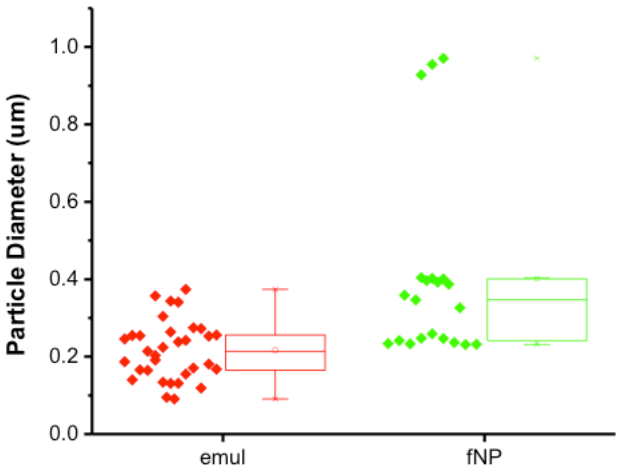

Figure 5.10. Average particle diameter for QD-loaded PLGA particles based on SEM and TEM measurements.

TEM images were taken to investigate the internal distribution of quantum dots from both emulsion and fNP-fabricated PLGA particles (Figure 5.11). The emulsion-fabricated particles displayed a good distribution of quantum dots for most particles. Few particles exhibited an internal pocket at the center of the particle that seems to not contain any quantum dots (QDs, Figure 5.11, top row, fourth image). For the fNP-fabricated particles, most particles displayed clusters of the quantum dots. Few particles exhibited an even distribution of QDs throughout most of the particle. The fNP-fabricated particles also looked slightly darker in color, perhaps due to the clustering of the QDs.

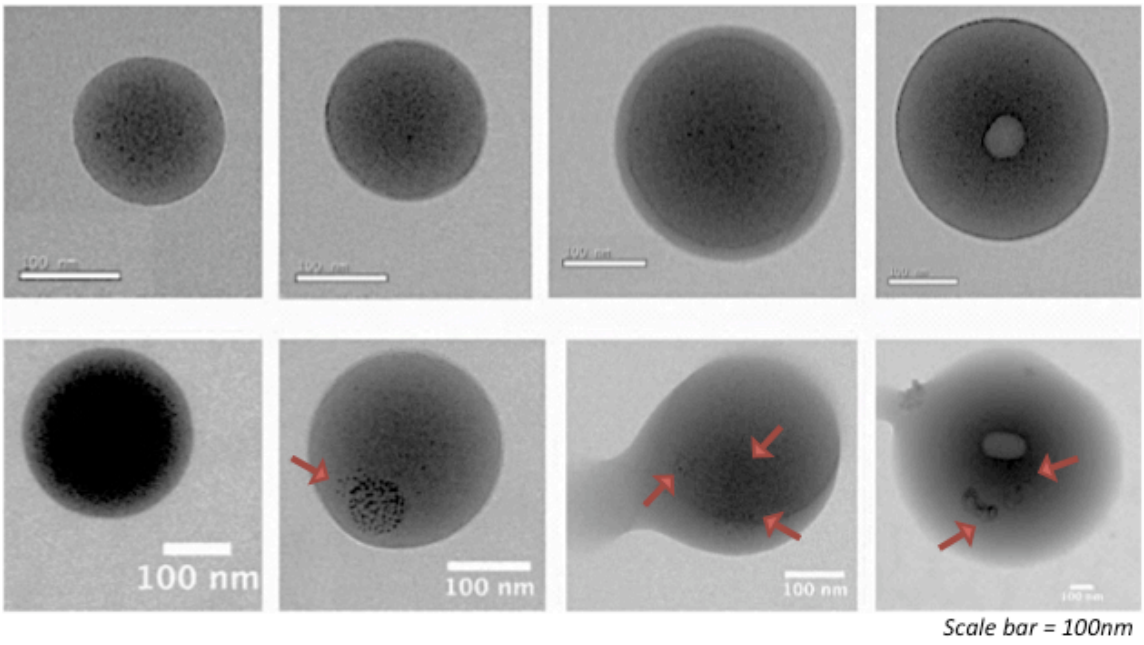

Figure 5.11. Internal distribution of QDs via TEM imaging for both emulsion (top row) and fNP-fabricated (bottom row), *scale bar = 100nm*.

Additionally, we examined the internal distribution of the QDs via fluorescence imaging (Appendix D-14). The fNP-fabricated QD-loaded PLGA particles seemed to have displayed a similar trend displaying clustering of the quantum dots exhibited by fluorescence clustering. The emulsion-fabricated QD-loaded particles were also imaged via fluorescence imaging, but since most particles were on the nano-scale it was difficult to see distribution within the particle (Appendix D-15).

5.5 Conclusions

In comparing two types of BKIs, hydrophilic RM-1-132 and hydrophobic 1294, and two types of fabrication methods, emulsion and fNP-based, we discovered some trends. The incorporation of 1294 was higher than RM-1-132 for emulsion-fabricated systems. When looking at release the major difference in BKIs was that 1294-loaded particles released higher amounts than their RM-1-132 counterparts, perhaps due to this increased incorporation.

For fabrication methods, the fNP-fabricated particles displayed variability in the surface area, while emulsion-based particles maintained a low surface area. For the emulsion-based system, an increase in surface area correlated with lower incorporation efficiency. The fNP-fabricated particles did not follow the same trend. For incorporation, the fNP-fabricated particles yielded higher incorporation efficiencies than their emulsion counterparts, allowing both hydrophilic and hydrophobic BKIs to load in the particles to a similar extent. There was minimal difference between emulsion-fabricated and fNP-fabricated

particles for the amount of BKI released by the end of week 4. Additionally, the QD-loaded PLGA particles displayed that the fNP-fabricated particles promoted clustering of the QDs, while the emulsion-fabricated particles seemed to have a more even distribution of the loaded QDs. The QD clustering may explain the variability in size and the higher final loadings observed for the fNP system.

To summarize, the hydrophobic 1294 molecule can be more efficiently incorporated and effectively released than its hydrophilic counterpart, RM-1-132. Perhaps because the hydrophobic drug mixes more efficiently with the polymer during fabrication, and this higher incorporation yields a better release when removed from the pH=12 environment. For fabrication methods, the emulsion-fabricated particles have a very low size range, diameter, and surface area. But, their properties like incorporation seemed to be more affected by size then their fNP-fabricated counterparts. The QD internal distribution study corroborated these observations showing that the fNP-fabricated particles may have higher incorporation because the system can incorporate drug clusters and vary its size to maintain 100% incorporation efficiency. But, size is a factor for injection-based systems where particle size needs to be small to pass through a needle with ease. In that case, the emulsion system has a more reliable size for injection and will be chosen for our systems even though there are incorporation limitations. Although, for applications where size is not a major issue, the fNP-fabricated system can provide higher incorporation regardless of factors such as molecule hydrophobicity.

5.6 References

1. Ojo KK, Pfander C, Mueller NR, Burstroem C, Larson ET, Bryan CM*, et al.* Transmission of malaria to mosquitoes blocked by bumped kinase inhibitors. *Journal of Clinical Investigation* 2012, **122**(6)**:** 2301-2305.

2. Xie H, Smith JW. Fabrication of PLGA nanoparticles with a fluidic nanoprecipitation system. *Journal of Nanobiotechnology* 2010, **8**(18)**:** 1-7.

CHAPTER 6. *IN VIVO* RELEASE SYSTEMS

6.1 Introduction

Previously in this report we discussed the fabrication of particle systems in detail and the optimization steps for enhancing BKI incorporation and release including creation of the optimal particle type, adjusting system parameters, and modifying the drug itself. The last chapter emphasized the effects we observed from slight variables added to the system, i.e. adding one methyl group to the drug molecule or altering the fabrication system. Additionally we investigated the internally distribution of a drug using a model systems with quantum dots based on fabrication method. Overall, we determined the hydrophobic BKI 1294 over the hydrophilic RM-1-132 yielded higher incorporation and improved release. We also determined that although the fNP-fabricated particles can allow higher incorporation due to adaptability of particle size, there is an issue with the high particle size seen.

In this chapter we hoped to elucidate and improve *in vivo* outcomes of injection of a BKI-loaded particle system for sustained release. We tested a model system using a traceable drug and detectable polymer system and prepared for an *in vivo* experiment of the BKI-loaded emulsion-fabricated particles. We also investigated ways to decrease the size range observed from the fNP-produced particles to allow the fNP fabrication method to become a viable option for BKI delivery again.

6.2 Objectives

The first objective of this chapter is to predict the outcome of an injection of BKI-loaded PLGA particles. We utilized a rhodamine-loaded PLGA particles retention and release *in vivo* study as well as set-up of a preliminary BKI-loaded PLGA particles *in vivo* experiment to assess the possible outcome. The second objective is to reduce the size range of the fNP system to make it a viable and comparable option for injection.

6.3 Materials and Methods

6.3.1 Materials

Poly(DL-lactide-co-glycolide) (PLGA) resomer (50:50 ester-terminated with IV 0.55 – 0.75) was purchased from Lactel Absorbable Polymers (Cupertino, CA). RM-1-132 and 1294 BKIs were provided by Dr. W. C. Van Voorhis's group (Department of Medicine, University of Washington). Quantum dots (CdSeS/ZnS, diameter = 6nm, emission = 525nm) and poly(vinyl alcohol) (PVA) was purchased from Sigma-Aldrich (St. Louis, MO). Dichloromethane (DCM), dimethyl sulfoxide (DMSO), and acetonitrile was purchased from EMD (EMD Chemicals, Inc., Gibbstown, NJ)

6.3.2 Particle Fabrication

PLGA solutions were prepared by dissolving 50mg/mL PLGA in dichloromethane (DCM), then mixing with either the RM-1-132 or 1294 BKI molecule. Particles were created using either an emulsion method adapted from Dr. K. Tran (Chemical Engineering Department, University of Washington) which

is described in more detail in previous chapters, or a fluidic nanoprecipitation (fNP) method based on Xie, 2010.[1]

6.3.2.1 Rhodamine-BSA-loaded PLGA Particles

PLGA and 5% (w/w) Alexa647 was dissolved in DCM at 50mg/mL. Either pure DPBS (control blank particles) or 2mg of rhodamine-BSA (rhod-BSA) at 100uL was added dropwise directly in the PLGA/DCM solution, while being vortexed with the Vortex Genie 2 (Scientific Industries, Bohemia, NY) at a medium-high speed, then sonicated for 10 seconds twice at output 7 with Model 3000 Ultrasonic Homogenizer (Biologics, Inc., Cary, NC). 2 mL of 5% PVA was added drop-wise while vortexing and then sonicated. The solution was poured into 2 mL of 5% PVA while vortexing and lightly sonicated. Solution was then poured into 2mL of 1% PVA in a beaker and magnetically stirred for 3 – 4 hours under foil. Solutions were collected and centrifuged twice at 12,000 rpm for 10 minutes using a Sorvall Legend RT centrifuge (DJB Labcare Ltd. Buckinghamshire, England), and twice at 10,000rpm for 10 minutes using an Eppendorf Centrifuge 5415D (Eppendorf, San Diego, CA) with resuspensions in MilliQ water. Final resuspension was in 200 - 800uL MilliQ water depending on particle concentration. Samples were stored in 4C fridge if not used for testing immediately. For the particle yield samples were lyophilized overnight using a Freezone 4.5 Freeze Dry System (Labconco Corporation, Kansas City, MO), then used for testing.

6.3.3 Particle Characterization

6.3.3.1 Size and Zeta Potential

10 uL of particles were resuspended into approximately 1 mL of 10mM KNO_3 solution. Particle size, polydispersity, and zeta potential were measured using a Zetasizer Nano-ZS (Malvern, Worcestershire, United Kingdom).

6.3.3.2 Total Incorporation

Total incorporation of the rhod-BSA-loaded particles was measured using two methods. First the particle's rhodamine-fluorescence was measured using a UV-Vis spectrophotometer (SpectarMax M5, Molecular Devices) at 575nm. Second a BCA protein assay was performed and measured using a UV-Vis spectrophotometer (SpectarMax M5, Molecular Devices) at OD 562nm and calculated to a final concentration from a standard curve.

For BKI-loaded particles, lyophilized particles were completely dissolved in established amounts of DMSO to produce between 1 – 5 mM of estimated drug content. Samples were centrifuged to separate any remaining polymer out. Samples were tested for inhibition via a *Plasmodium falciparum* calcium-dependent protein kinase (Pfal-CDPK) specific kinase-Glo assay (IC50 inhibition assay) developed by Dr. K.K Ojo and colleagues of Dr. W Van Voorhis's Lab (Department of Medicine, University of Washington, Seattle, WA).

Both the total drug incorporated and the time-release samples were tested via the IC50 assay using. Data was analyzed using Prism software into a half maximal inhibitory concentration (IC50) graph with pure RM-1-132 or 1294 as a

positive control. Values for total amount of BKI in particles were calculated using the following equation (*where I = amount of drug in particles (ug)*, C_s *= starting concentration (estimated, (mM)*, *D = dilution factor, usually 1000x*, $IC50_{RM1}$ *= soluble drug concentration for 50% inhibition (uM)*, $IC50_{NP}$ *= drug in nanoparticle concentration for 50% inhibition (uM)*, *V = volume used to dilute particles (L)*, *MW = molecular weight of drug (ug/umol)*):

$$I = C_s \times D \times \frac{IC50_{RM1}}{IC50_{NP}} \times V \times MW$$

6.3.3.3 Drug Release

In vitro release: Approximately 3mg of particles were resuspended in 100uL of sterile PBS (pH 7.4) and incubated in a 37C water bath. At each timepoint, samples were centrifuged for 10 minutes at 10,000 rpm. Entire supernatant was removed and particles were resuspended with 100 uL of fresh PBS. Samples were returned to the 37C water bath. Timepoints were at 0, 1, 4, 8hours and every day after that. Amount of drug released were calculated based on the fluorescence of the rhod-BSA of the time-released samples.

In vivo release: Approximately 3mg of particles were resuspended in 100uL sterile PBS for injection, 2 injections per mouse. Mice were injected in a reverse time-scheme at Day 7, Day 3, Day1, and 4hr. Mice were sacrificed and samples were collected from surrounding the injection site, the lymph nodes, and the spleens. Both injections and sacrifice were performed by Dr. Kenny Tran of the H. Shen group. Samples were grinded and dissolved in chloroform, then

fluorescence was measured for both the AlexaFluor-647 labeled polymer and the rhodamine-BSA molecule loaded inside of the particles.

6.4 Results

6.4.1 Release Models

6.4.1.1 Retention and Release from Injection Site

Rhodamine-labeled bovine serum albumin (rhod-BSA) was loaded into PLGA particles via double emulsion (due to the strong hydrophilicity of the rhod-BSA). The procedure is described in the methods section above. Particles were loaded at a 40ug rhod-BSA/mg PLGA polymer initial concentration. Control double-emulsion particles containing PBS were also fabricated. Particle characterization via DLS revealed that particle diameter was approximately 300nm in size, with a low polydispersity (0.2), and a zeta potential of approximately -1mV *(data not shown).* Loading of rhod-BSA was characterized using a protein assay. Blank PLGA particles were empty, while rhod-BSA-loaded PLGA particles displayed 31ug/mg final loading. This calculates to a 77% loading efficiency.

The *in vitro* release profile was examined for two weeks (Figure 6.1). The release profile was steady for 2 weeks, releasing approximately 2 to 4 ug of rhod-BSA at each timepoint for a 3mg sample. The cumulative percent release was also calculated and displayed a almost zero order release trend reaching approximately 60% by the end of week 2 (Figure 6.2, *note: timepoints are not spread evenly on the x-axis*).

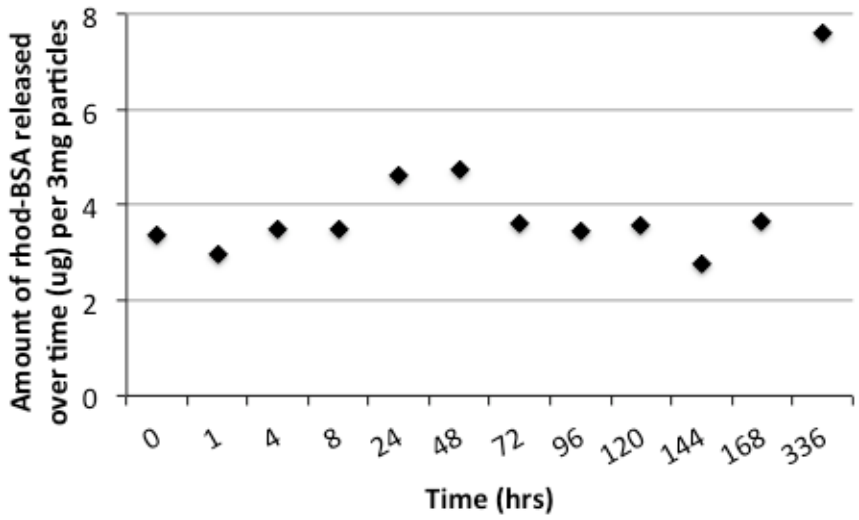

Figure 6.1. Amount of rhod-BSA released from loaded PLGA particles over two weeks for a 3mg *in vitro* sample.

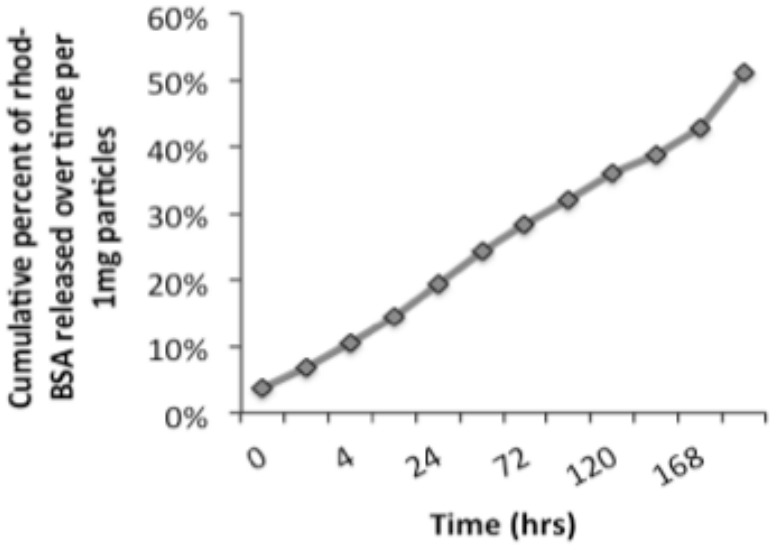

Figure 6.2. Cumulative percent release of rhod-BSA released from loaded PLGA particles over two weeks for a 3mg *in vitro* sample.

Next, we investigated the release kinetics of an *in vivo* injection of the particles. We investigated both the retention of the particles at the injection site and the release of rhod-BSA from the loaded PLGA particles. The mass of the remaining particles from a 3mg injection was measured (Figure 6.3). By the end of week 1 a low amount of particles remained at the site of injection. The amount of rhod-BSA released from the particles remaining at the injection site was calculated (Figure 6.4, *left figure*). This follows the same trend as the amount of particles remaining indicating that the particles retained at the injection site are still releasing rhod-BSA in approximately a zero-order release profile. Only about 10% of the rhod-BSA remained at the site 4 hours after injection (Figure 6.4, *right figure*). This suggests that most of the rhod-BSA had traversed from the particles or with the particles from the injection site.

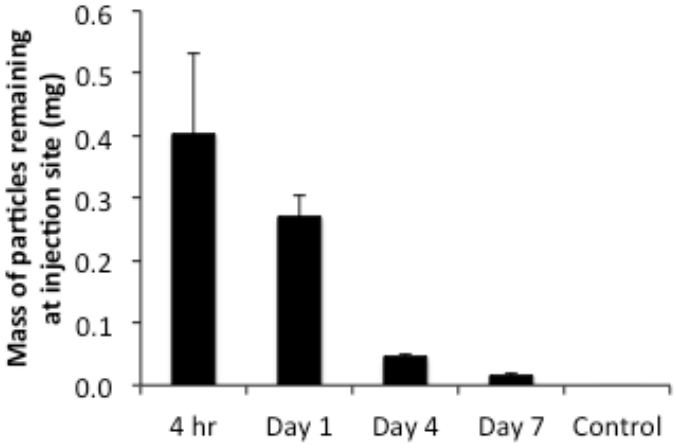

Figure 6.3. Mass of particles remaining at the injection site for rhod-BSA loaded PLGA particles.

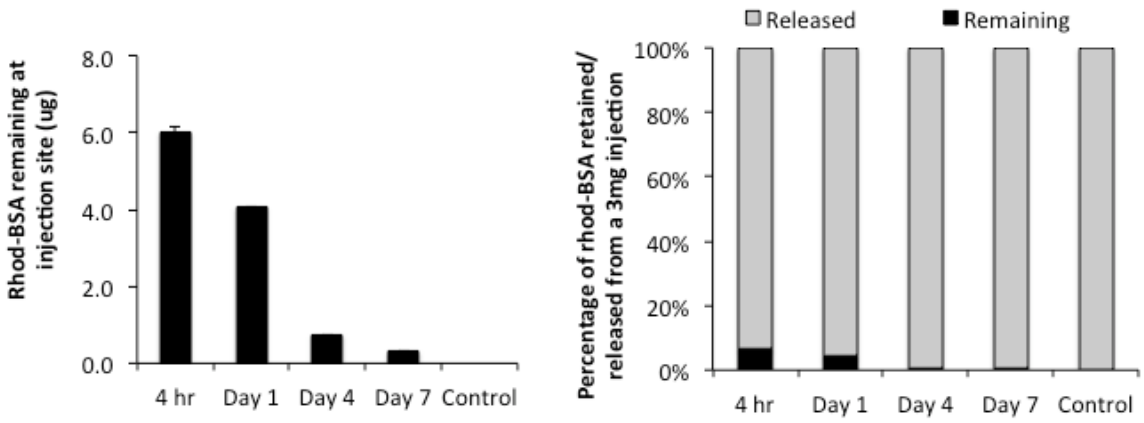

Figure 6.4. Rhod-BSA fluorescence measured at injection site (left) compared to the amount of unreleased or diffused away rhod-BSA (right) from rhod-BSA loaded PLGA particles.

In regards to this retention and release study, it seems a low amount of particles are remaining at the injection site. Only the injection site was sampled and not the nearby tissues, so there is a chance that the particles might have a formed a clump of particles from where they were injected *(collected area)* and also spread throughout a wider region surrounding the site that was not completely captured when the sample was pulled. Additionally, samples from the spleen and lymph node were taken but did not account for the particle amount released from the injection site, indicating that particles could be spreading a greater distance from the injection site.

6.4.1.2 *In vivo* BKI blood levels

50ug/mg 1294-loaded PLGA particles were created via the emulsion fabrication method. DLS size analysis displayed an approximately 250nm diameter, with very low PDI (0.08), no presence of a peak 2, and a zeta potential

of -1.3mV. SEM images showed small particle size and no signs of aggregation, matching the DLS results (Figure 6.5). Final loading was tested via an IC50 inhibition assay and calculated to be 42ug/mg, approximately 83% incorporation efficiency. Approximately 40mg of particles were resuspended in 100uL of sterile DPBS. Particles were injected into mice and blood samples pulled at predetermined times for mass spectrometry analysis of the BKI content. Blood sample pulls were performed by K.K. Ojo (Van Voorhis Lab, Department of Medicine, University of Washington) and mass spectrometry analysis of blood was performed by Kasey Rivas (Van Voorhis Lab, Department of Medicine, University of Washington). Analysis of these samples exhibit presence of BKI in blood up to 24hrs, the last timepoint tested. A longer *in vivo* experiment is needed to confirm longer timepoints past 24hrs.

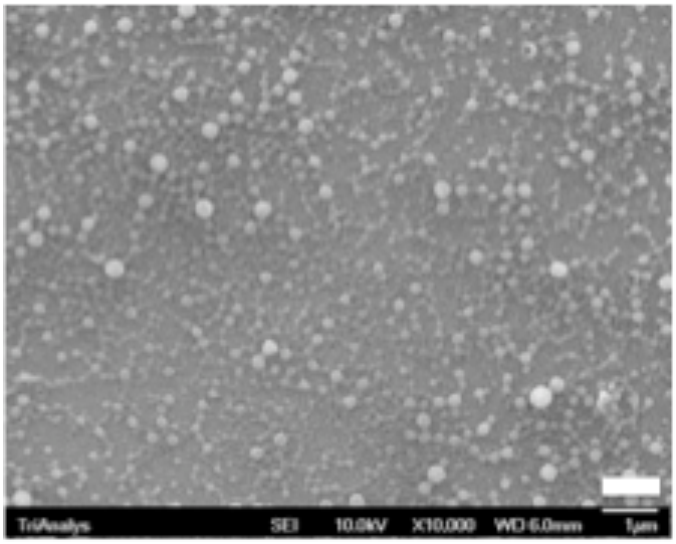

Figure 6.5. SEM images of 50ug/mg 1294-loaded PLGA particles. *Scale bar = 1 um.*

6.4.2 Particle Fabrication Models

6.4.2.1 Size Control on the fNP system

The fNP fabrication method displayed better results for incorporation and release than the emulsion fabrication method, but the one downfall was the larger particle size range. Working with two undergraduate students, Jinwoo Lee (B.S. Chemical Engineering from UW, 2012) and Tyler Gjersee (BS, Chemical Engineering from UW, *expected 2013*) we optimized the fNP system to create a smaller size range of particles and a more controllable fabrication system.

Some factors were investigated previously in the literature, i.e. altering flow rate, increasing PLGA concentrations, and adding a hydrophilic additive to the continuous phase.[1] We rechecked those parameters during optimization of the fNP system and adjusted additional parameters to find an ideal system. First we checked the effects of particle size versus PLGA concentration, dispersant flow rate, and inlet polymer flow rate. The particle size slightly increased as PLGA concentration was increased (Figure 6.6). This makes theoretical sense because addition of polymer would add to the overall particle size. We also examined a range of dispersant channel speeds (Figure 6.7). Increasing the speed to 60mL/min decreased the particle size. All these flows are in the laminar regime of fluid flow. This makes theoretical sense because a faster flow rate would break the polymer input into smaller droplets. Additionally, we investigated the effects of increasing the polymer inlet flow rate (Figure 6.8). At a certain speed, between 10 to 25mL/min we saw a large increase in particle size from 200 to almost 800nm. At such a high polymer speed, the particles might not be

able to have such a controlled, small particle size as seen with flow rates below 10mL/min.

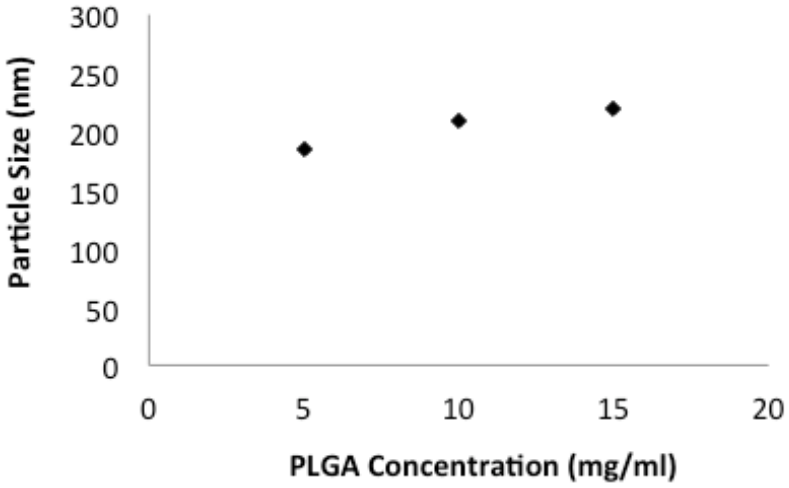

Figure 6.6. Particle diameter of blank PLGA particles fabricated via fNP as PLGA concentration increases.

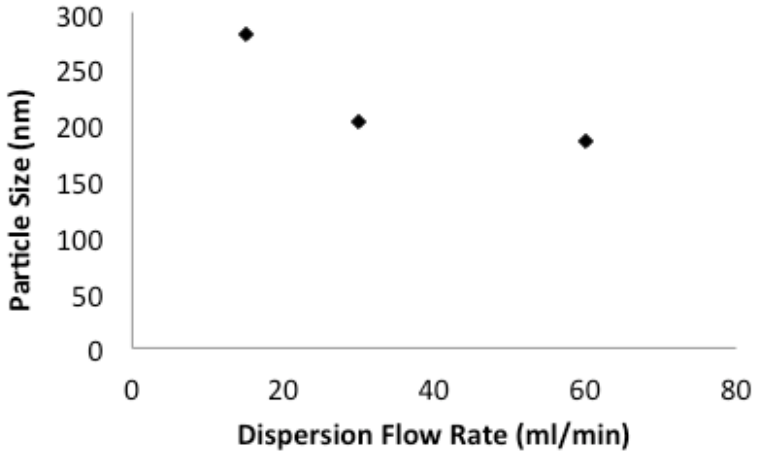

Figure 6.7. Particle diameter of blank PLGA particles fabricated via fNP as dispersion flow rate increases.

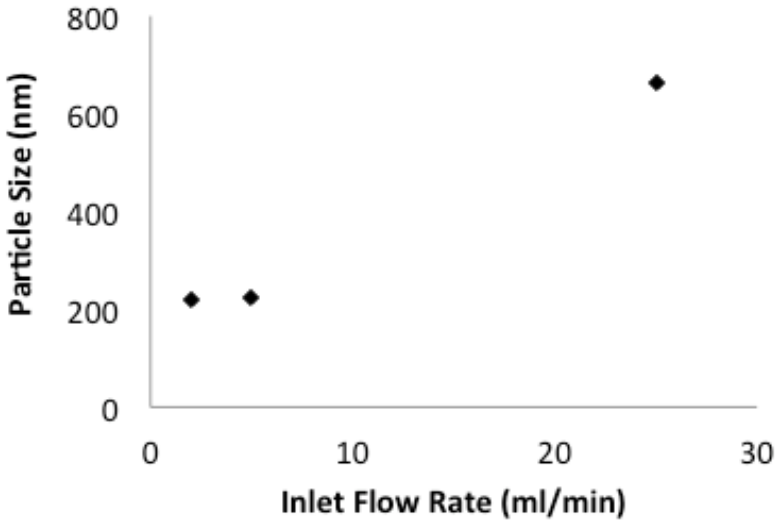

Figure 6.8. Particle diameter of blank PLGA particles fabricated via fNP as inlet flow rate increases.

We also adjusted the needle tip position, direction, and solvent used in the continuous phase. For the needle tip position, we looked at top, middle, and the bottom of the locations in respect to the tube used for the continuous flow. Not much of a size difference was seen for the different positions, although the bottom location did produce a slightly smaller particle *(data not shown).* The needle direction in respect to the flow of the continuous phase was also investigated. The needle opening was either with the flow (+x direction), against the flow (-x direction), sideways to the flow (y direction), or the needle precision-cut at the tip to have a flat surface against the flow (Figure 6.9). The flat needlepoint displays the highest particle diameter by far, followed by the sideways flow (y direction), then the x direction flow (x, -x directions). The "against the flow" direction (-x direction) also displayed the smallest PDI, making it the optimal choice for our system.

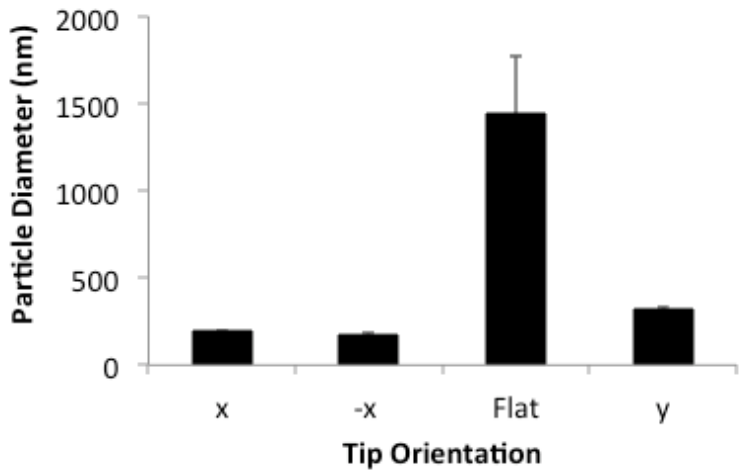

Figure 6.9. Particle diameter of blank PLGA particles fabricated via fNP as needle direction with respect to the continuous phase flow changes.

Lastly, we investigated the effects of using pure DCM versus mixtures of DCM and a more water-miscible solvent, acetonitrile, to fabricate particles via the fNP fabrication method with a smaller size range. We tested several ratios of solvents 0:100, 10:90, 30:70, and 50:50 DCM:acetonitrile and discovered that the lowest ratio of 0:100 provided the smallest particle size with the lowest PDI (Figure 6.10). Overall, the lowest sized particles were achieved while utilizing acetonitrile as a solvent instead of the less water-miscible DCM. This system can be adapted to the BKI-loaded particles to create particles that have a lower size range and low PDI, while still using the fNP fabrication method. Some factors will still need to be assessed, but this could potential be utilized to fabricate the 1294-loaded particles with a controllable small size and push the final loading even further then the emulsion-fabricated particles allowed. These

studies along with additional studies will be compiled into a paper for publication (Appendix A).

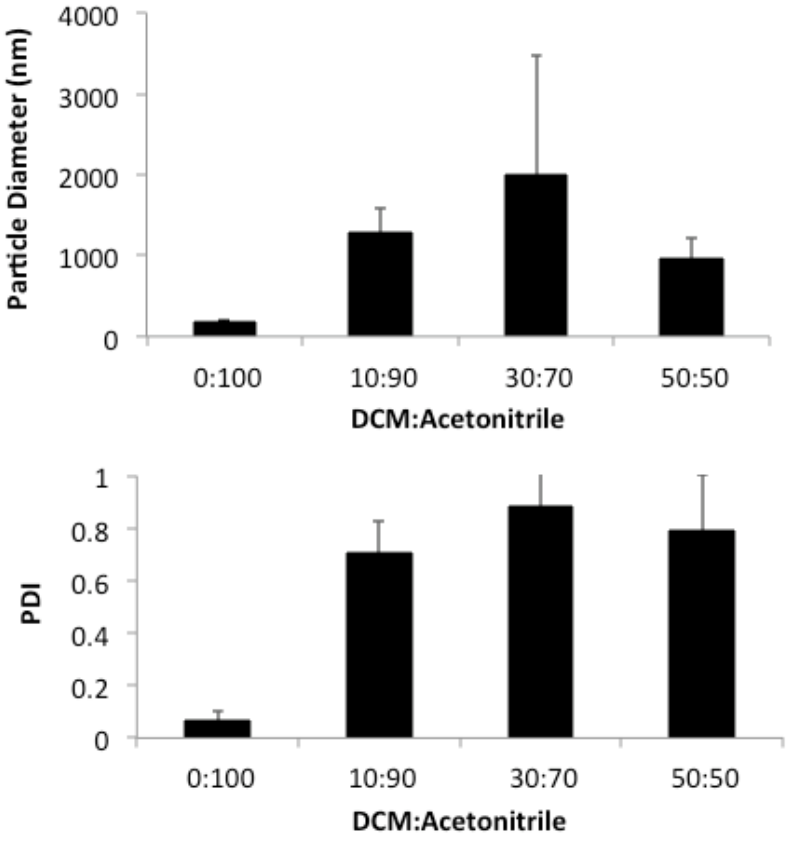

Figure 6.10. Particle diameter of blank PLGA particles fabricated via fNP at various ratios of DCM:acetonitirile for the polymer input.

6.5 Conclusions

This chapter used a rhod-BSA loaded PLGA (AF647) particle model to investigate the retention of particles and release of drug *in vivo.* The model displays low particle retention nearest to the injection site, but the area of particle dispersion around the injection site may be larger than chosen for analysis.

Release *in vivo* follows a similar trend to the *in vitro* release tested. Steps are being made toward a preliminary *in vivo* experiment for 50ug/mg 1294-loaded emulsion-fabricated PLGA particles to detect the 1294 blood content after injection. Additionally, we uncovered ways to lower the size range of the fNP-fabricated particles via a change in solvent used to dissolve the polymer. This improved system can potentially be utilized for BKI-loaded particles to further increase the maximum incorporation (seen with fNP fabricated particles, over emulsion-fabricated particles) while keeping the particle size and range low.

6.6 References

1. Xie H, Smith JW. Fabrication of PLGA nanoparticles with a fluidic nanoprecipitation system. *Journal of Nanobiotechnology* 2010, **8**(18)**:** 1-7.

CHAPTER 7. CONCLUSIONS

Bumped kinase inhibitors (BKIs) can block transmission of malaria, but do not remain in the circulation for longer than 8 hours.[1, 2] Therefore, in this thesis we investigate the creation of sustained delivery systems for BKIs to extend their delivery. Various particle systems, fabrication parameters, and BKIs were altered to design the optimized BKI delivery system. The greatest effects were seen from increasing the pH of the continuous phase during fabrication to a pH above the pKa of the BKI being incorporated. This neutralized the BKI and forced higher loading into the particle, especially for the solid dispersion particles.

We performed an extensive analysis on the effects of two types of amphiphilic BKIs (the more hydrophilic RM-1-132 and slightly hydrophobic 1294) and two types of fabrication methods (emulsion and fluidic nanoprecipitation (fNP)). Out of the two BKIs, the 1294 molecule was more advantageous due to its higher incorporation and release probably due to its slightly higher hydrophobicity. The 1294 molecule was also engineered to have a reduced clearance rate compared to the other BKIs.[2] Out of the two fabrication systems, the fNP provides higher incorporation efficiencies as the initial loading is increased, but the emulsion-fabricated particles were selected due to lower particle size and polydispersity. The 50ug/mg 1294-loaded emulsion-fabricated particles are currently being used for an *in vivo* experiment as our optimal system.

Additionally, we utilized model systems to investigate drug distributions within a particle based on fabrication method (emulsion versus fNP) and particle

retention/release at the injection site. QD-loaded particles displayed clustering inside of the fNP-fabricated particles, while the emulsion-fabricated particles displayed an even distribution of QDs. The rhod-BSA loaded particles injected into a mouse exhibited low retention of particles at the injection site, but particles may have been more spread out than the sample collected. We also developed the fNP fabrication method to create smaller, more monodisperse particles by changing the solvent. Future directions can include using the improved fNP system for fabrication of the BKI-loaded particles to help push the incorporation higher while keeping the particle size low.

Overall, we were able to successfully prepare a delivery system for the sustained release of the BKI 1294. We were able to have approximately 100% incorporation and *in vitro* release of >100ng/hr release (per 25mg particles) up to 4 days (~50ng/hr per 25mg particles up to 4 weeks). Additionally the comparisons made between particle size, fabrication methods, and drug hydrophobicity elucidated fundamentals of amphiphilic drug incorporation and optimized the delivery system even further.

1. Ojo KK, Larson ET, Keyloun KR, Castaneda LJ, DeRocher AE, Inampudi KK*, et al.* Toxoplasma gondii calcium-dependent protein kinase 1 is a target for selective kinase inhibitors. *Nature Structural & Molecular Biology* 2010, **17**(5)**:** 602-U102.

2. Ojo KK, Pfander C, Mueller NR, Burstroem C, Larson ET, Bryan CM*, et al.* Transmission of malaria to mosquitoes blocked by bumped kinase inhibitors. *Journal of Clinical Investigation* 2012, **122**(6)**:** 2301-2305.

CHAPTER 8. ACKNOWLEDGEMENTS

Committee members:

Advisor/Chair: Dr. Hong Shen, Dr. Charlie Campbell, Dr. David Castner, Dr. Dustin J. Maly, and Dr. Wesley C. Van Voorhis

For sustained drug delivery experiments: K.K. Ojo, Dr. Van Voorhis, and Dr. Maly for providing RM-1-132 and 1294 molecules and guidance on experiments. Also, K.K. Ojo, Kasey Rivas, Molly Reid, and Katelyn Keyloun for assistance with the IC50 inhibition assays and the mice experiments.

For fluidic nanoprecipitation experiments (throughout thesis and Appendix A): Jinwoo Lee, Candace Yang, and Tyler Gjersee for assistance with preliminary fNP experiments. Megan Goude for assistance with preliminary alginate nanoparticle experiments. Xi Zhan and Tyler Gjersee for assistance with transmission electron microscopy (TEM) imaging. Dr. P Stayton for generously donating the BMA-PAA-DMAEMA.

For surface chemistry experiments (Appendix B): Jung Park and Min Chang for assistance with preliminary surface chemistry experiments. Dr. Bingbing Sun for his assistance with atomic force microscopy (AFM) and surface-enhanced Raman spectroscopy (SERS) imaging.

For mechano-regulation and T cell experiment (Appendix C): Thanapon Sangvanich for establishing preliminary T cell experiments, Erika Hayes for assistance with PA gel fabrication, and Dr. Kenny Tran for assistance with flow cytometry.

Additionally, I would like to acknowledge the following people for their support: my family (especially Mom, Dad, my sister Rosemary, Grandma (RIP), & Tim), my friends, my colleagues (the Shen Lab, K.K. Ojo from Van Voorhis Lab, the Van Voorhis Lab, the Maly Lab, fellow ChemEs), and the Chemical Engineering Department at the University of Washington (students, faculty, & staff).

APPENDIX A

Molecule distribution within particles via alterations in an optimized fluidic nanoprecipitation system

Christina Yacoob, Tyler Gjersee, Jinwoo Lee, Hong Shen

Department of Chemical Engineering, University of Washington, Seattle, WA 98195, USA

ABSTRACT

Nanoparticles are essential for a variety of applications including pharmaceutics, advanced targeting techniques, drug delivery, and gene therapy.[1] Therefore, formulation of nanoparticles with the appropriate size, consistent composition, and predictable drug distribution is a challenge in order to have both an effective and reliable treatment.[2] Nanoprecipitation, a particle fabrication technique, has recently been adapted to a fluidic system where the polymer mixture is added to a flowing stream of stabilizer/water (fluidic nanoprecipitation: fNP).[3] This method allows facile control over particle properties by manipulation of certain fabrication parameters including polymer concentration and velocity of dispersant.[3 4] This paper will focus on the optimization of the fNP system followed by manipulation of certain fabrication parameters for control of properties such as internal drug distribution. Drug distribution will be characterized by quantum dot loaded PLGA particles (QD-PLGA). PLGA was chosen because it is a biodegradable and biocompatible polymer.[5 6] For this system, the needle location/direction, geometry of channel, and solvent were altered to see effects on the internal distribution of the QDs. We expect that the needle in the -x direction (against flow) at the bottom of the channel would provide the best distribution

of the QDs because it provides the most control over its particle size and other properties. Good control over drug distribution within the particle can help provide a sustained, zero-order release.

References

1. Mohamed F, van der Walle CF. Engineering biodegradable polyester particles with specific drug targeting and drug release properties. *Journal of Pharmaceutical Sciences* 2008, **97**(1)**:** 71-87.

2. Li XA, Anton N, Arpagaus C, Belleteix F, Vandanune TF. Nanoparticles by spray drying using innovative new technology: The Buchi Nano Spray Dryer B-90. *Journal of Controlled Release* 2010, **147**(2)**:** 304-310.

3. Xie H, Smith JW. Fabrication of PLGA nanoparticles with a fluidic nanoprecipitation system. *Journal of Nanobiotechnology* 2010, **8**(18)**:** 1-7.

4. Schubert S, Delaney JT, Schubert US. Nanoprecipitation and nanoformulation of polymers: from history to powerful possibilities beyond poly(lactic acid). *Soft Matter* 2011, **7**(5)**:** 1581-1588.

5. De Temmerman M-L, Rejman J, Vandenbroucke RE, De Koker S, Libert C, Grooten J, *et al.* Polyelectrolyte LbL microcapsule versus PLGA microspheres for immunization with protein antigen. *Journal of Controlled Release* 2011**:** 8.

6. Anderson JM, Shive MS. Biodegradation and biocompatibility of PLA and PLGA microspheres. *Advanced Drug Delivery Reviews* 1997, **28**(1)**:** 5-24.

APPENDIX B

DESIGNING SELF-ASSEMBLED MONOLAYERS AT THE NANOSCALE FOR CONTROL OVER DENDRITIC CELL MATURATION, FUNCTION, AND IMMUNE RESPONSE.

CHRISTINA YACOOB[*], JUNG PARK[†], BINGBING SUN[*], HONG SHEN[*,§]
[*]*Department of Chemical Engineering, University of Washington*
Box 351750, Seattle, WA 98195, USA
[§]*hs24@uw.edu*

[†]*Department of Neuroscience and Behavioral Biology, Emory University*
201 Dowman Dr., Atlanta, GA 30322, USA

Dendritic cells (DCs) are the most potent antigen presenting cells (APCs) in the immune system. They are the primary target for inducing effective immune responses or instigating tolerance. Self-assembled monolayers (SAMs) have been utilized in a variety of biomaterial applications to direct cell growth and activation, but with few studies on its effect on APCs. In this study, we investigated the control of the immune response of dendritic cells by manipulating the nanoscale properties of the SAMs. Immature DCs (iDCs) were exposed to various lengths of poly(ethylene glycol) (PEG)-terminated self-assembled monolayers (PEG SAMs) from 0 to 6 units, terminating in either a negatively charged carboxyl (COOH) or neutral hydroxyl (OH) end group (at physiological pH 7). PEG SAMs were characterized via contact angle, atomic force microscopy (AFM), and surface enhanced Raman spectroscopy (SERS). These frequently overlooked, small nanoscale alterations instigated significant differences on the level and activation of the DCs plated on the SAMs. OH-terminated PEG SAMs induced a significant level of matured DCs (mDCs) as compared to their COOH-terminated PEG SAMs counterparts. Among all the OH-terminated PEG SAMs, the length of PEG units correlated with the level of mDCs; the longer the PEG unit, the more iDCs advanced to mDCs. Interestingly, none of SAMs induced secretions of cytokines characteristic of either inflammatory or tolerogenic DCs, suggesting that an alternative maturation pathway was triggered. We demonstrated that our strongest maturation inducer, C_{11}-PEG_6-OH SAMs, activated DCs mainly through the sarcoma (Src) family kinase (SFK)-dependent pathway. Overall, these PEG SAMs can be employed to activate or to induce tolerance from DCs and potentially other immune cell types (with SFK-dependent pathways) via nanoscale alterations of length and functionality. This control over the immune response via biomaterial design can be harnessed for applications such as disease treatment and immunomodulation.

Keywords: biocompatibility, surface modification, complement, immunotherapy, immunology

APPENDIX C

Mechano-regulation of the T cell activation

Christina Yacoob, Erika T. Hayes, Thanapon Sangvanich, Kenny K. Tran and Hong Shen*

Department of Chemical Engineering, University of Washington, Box 351750, Seattle, WA 98195

ABSTRACT

Surface mechanical properties have been shown to affect cells' functions in several aspects such as adhesion, movement, and morphologies. In this paper, we demonstrated that the surface stiffness regulated the T cell activation process by utilizing polyacrylamide (PA) gels as synthetic surfaces with variable stiffness. PA gels' Young's Moduli were measured to be 5 to 82 kPa with a constant amount of acrylamide and increasing amounts (0.05 - 0.85%) of bis-acrylamide. The $CD8^+$ T cell activation is much more sensitive to substrate elasticity than the $CD4^+$ T cells, with an optimum $CD8^+$ T cell activation occurring on the substrates with 30 - 55 kPa Young's Moduli. $CD8^+$ T cells also exhibited higher proliferation rates and calcium signaling within the first 16 hours of contact for the intermediate stiffness (30 – 55kPa). Furthermore, we examined gel stiffness effects on purified naïve mouse $CD4^+$ and $CD8^+$ T cells. Activation was sensitive to surface stiffness especially for $CD8^+$ T cells. The optimum $CD4^+$/$CD8^+$ T cell proliferation, activation, and release of cytokines IL-2 (for $CD4^+$ T cells) and IFN-γ (for $CD8^+$ T cells) occurred on the intermediate substrates. Overall this research demonstrates how T cell proliferation and activation can be mechano-regulated via substrate contact.

APPENDIX D

Additional RM-1-132 and 1294-loaded PLGA particle data.

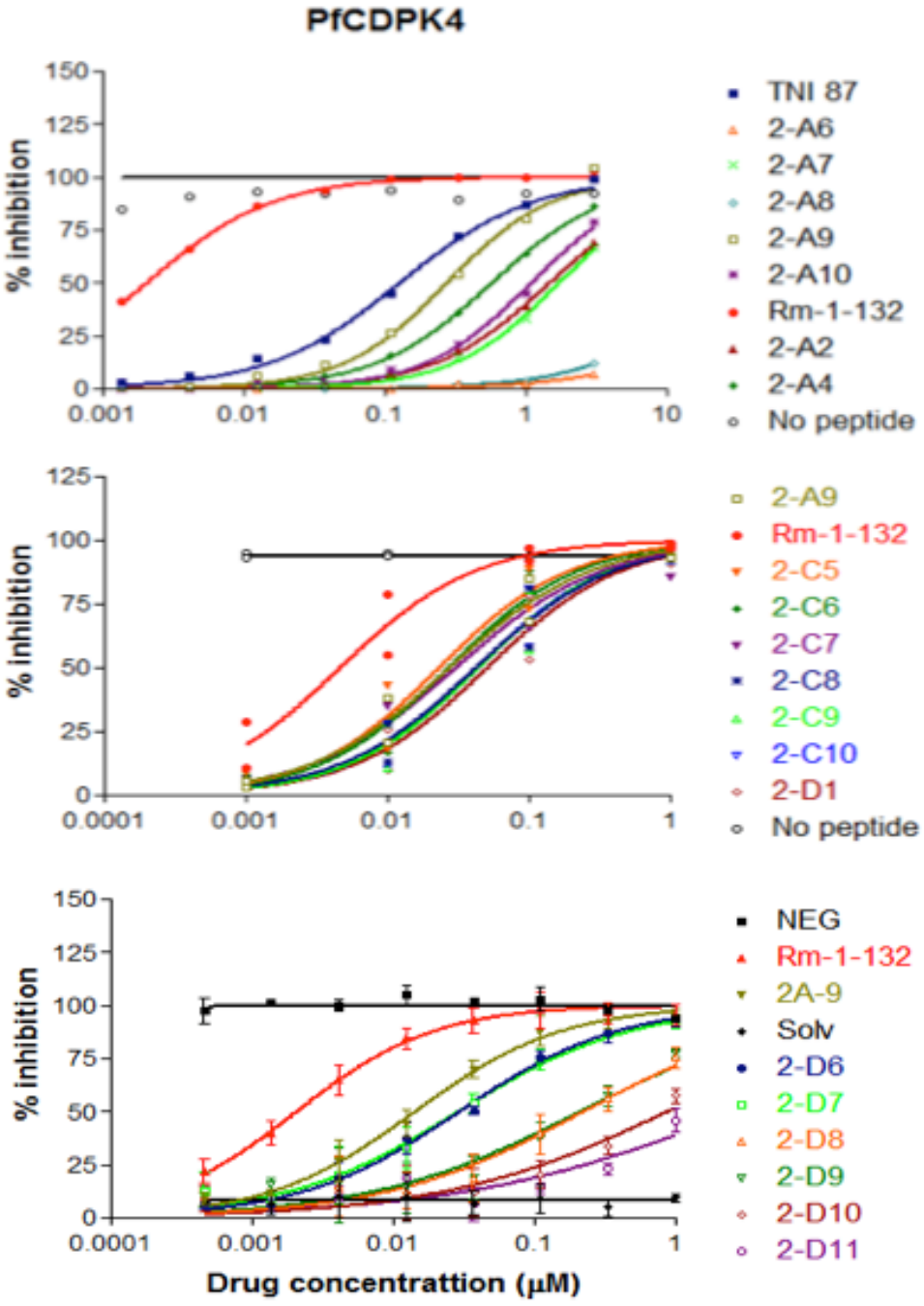

D-1: Plasmodium falciparum calcium-dependent protein kinase (PfCDPK) half-maximal inhibition (IC50) assay for RM-1-132-loaded PLGA particles

APPENDIX D

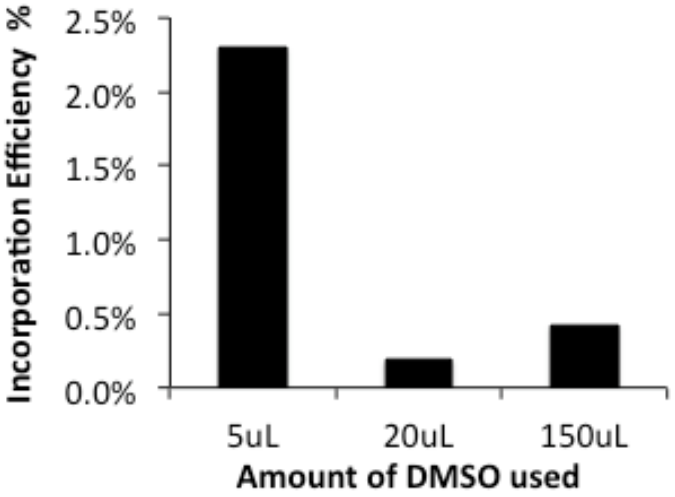

D-2: Incorporation efficiency of RM-1-132 into system I (solid dispersion and emulsion) PLGA particles based on DMSO amount *(5uL point has 50mg/mL PLGA concentration, other samples have 10mg/mL PLGA concentration).*

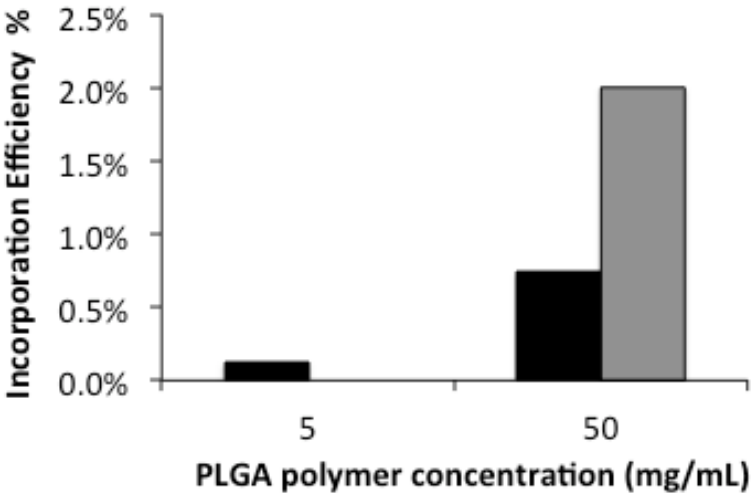

D-3: Incorporation efficiency of RM-1-132 into system I (solid dispersion and emulsion) PLGA particles based on PLGA concentration *(grey bar indicates a repeated sample).*

APPENDIX D

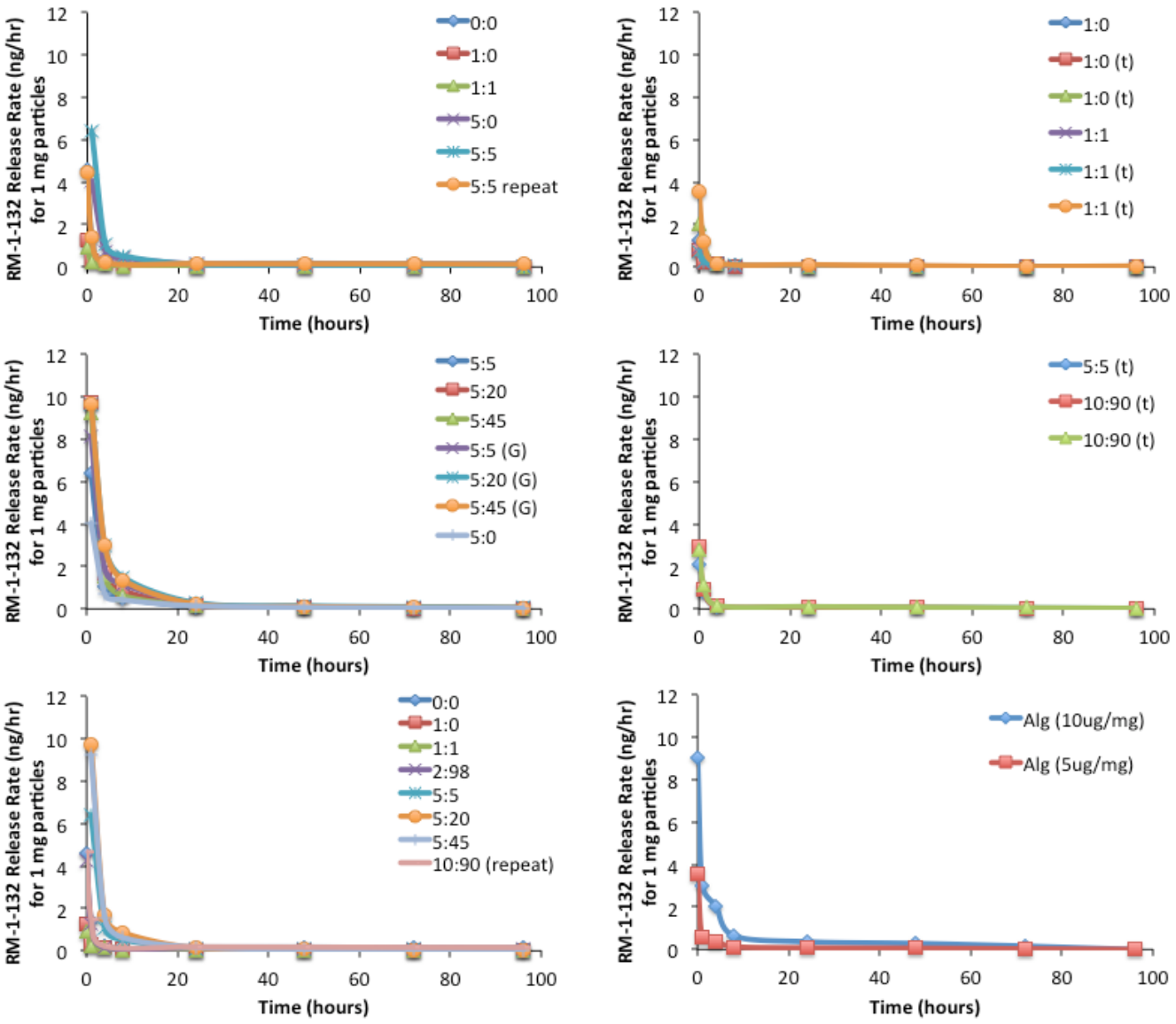

D-4: Release rates for various RM-1-132 loaded particulate systems. *(ratios are DMSO:water, unless indicated by a G = glycerol; t = terpolymer, Alg = alginate, ug/mg = initial ug RM-1-132 to mg PLGA loading).*

APPENDIX D

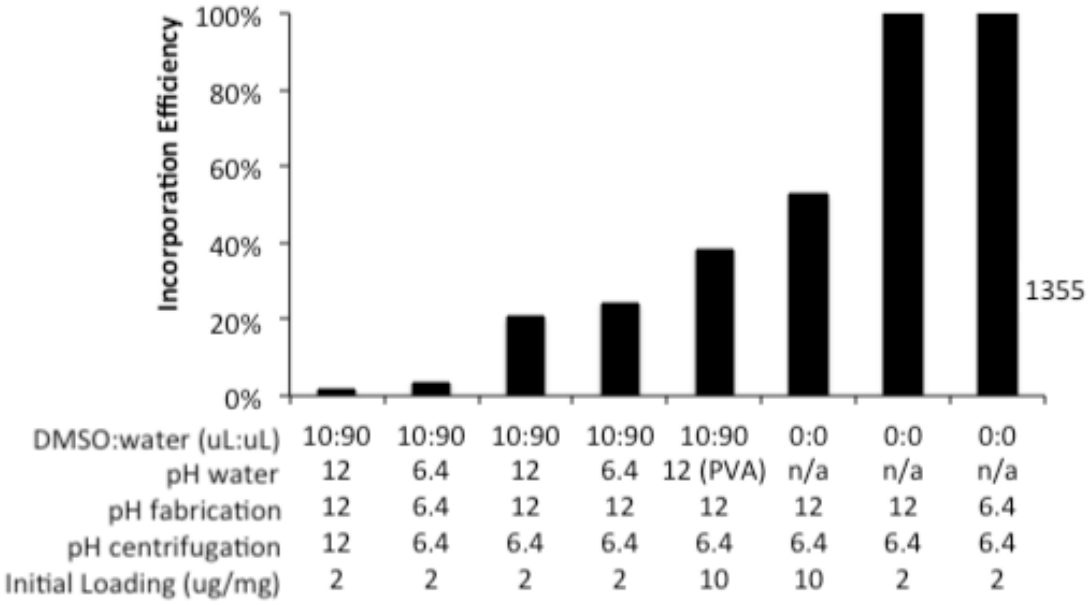

D-5: Incorporation efficiency from a parameter design matrix for pH effects on three steps in the fabrication process of RM-1-132-loaded PLGA particles. (*Initial loading varies from 2 to 10ug/mg, pH water: pH of internal aqueous phase of double emulsion NPs, pH fabrication: fabrication pH of emulsification or fNP system, pH centrifugation: pH of water used to triple rinse particles after fabrication, 1355 indicates a slightly different BKI).*

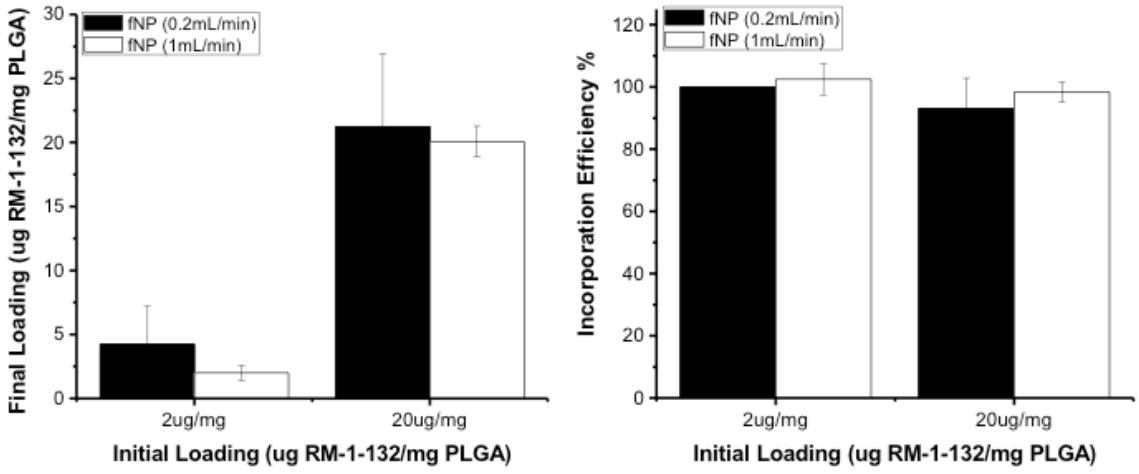

D-6: Final Loading and incorporation efficiency for RM-1-132-loaded particles at various fNP fabrication speeds. *(Fabricated at pH = 12).*

APPENDIX D

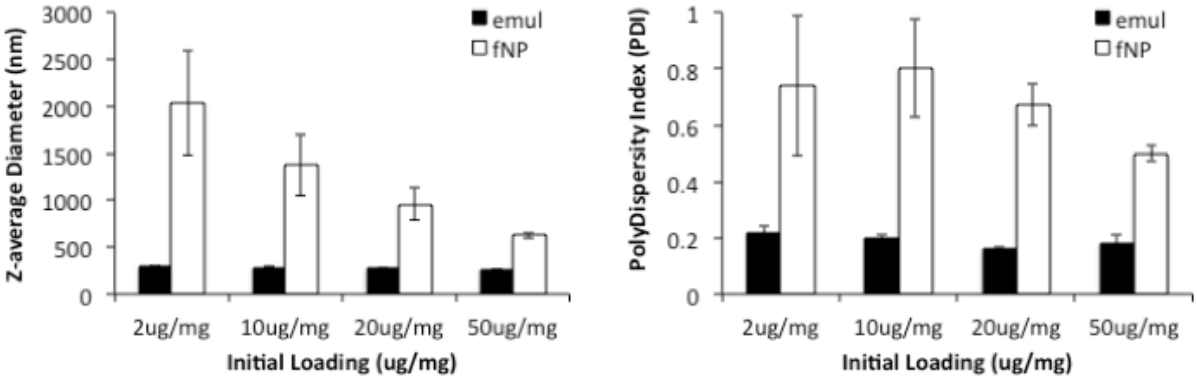

D-7: DLS size data for RM-1-132-loaded particles at various initial loadings. *(Fabricated at pH = 12).*

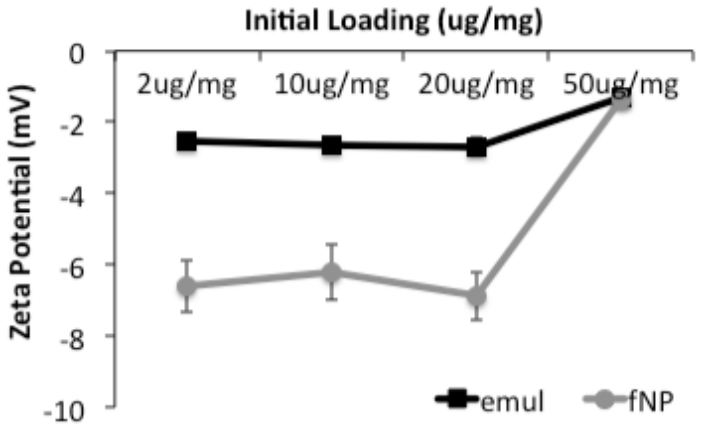

D-8: Surface Charge data for RM-1-132-loaded particles at various initial loadings. *(Fabricated at pH = 12).*

APPENDIX D

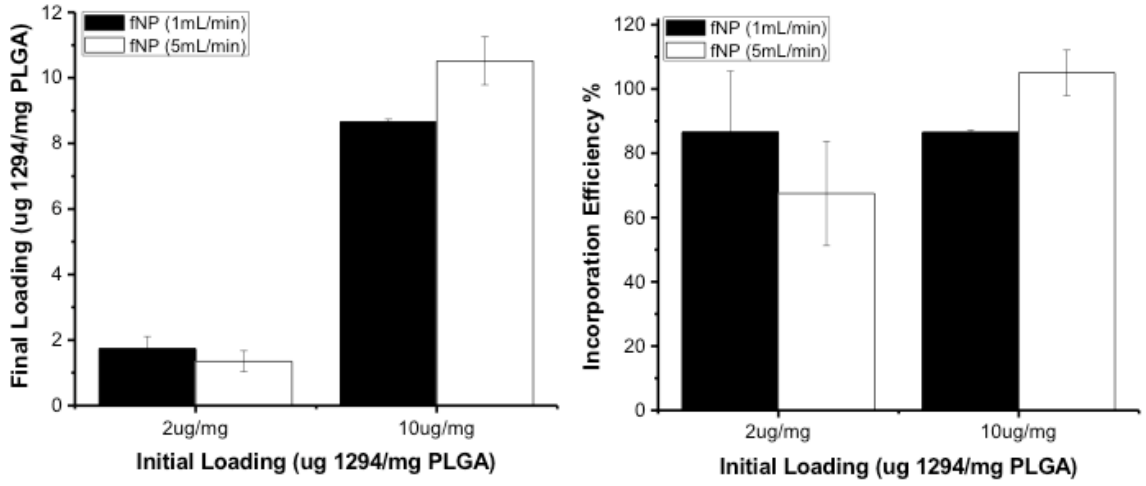

D-9: Final Loading and incorporation efficiency for 1294-loaded particles at various fNP fabrication speeds. *(Fabricated at pH = 12).*

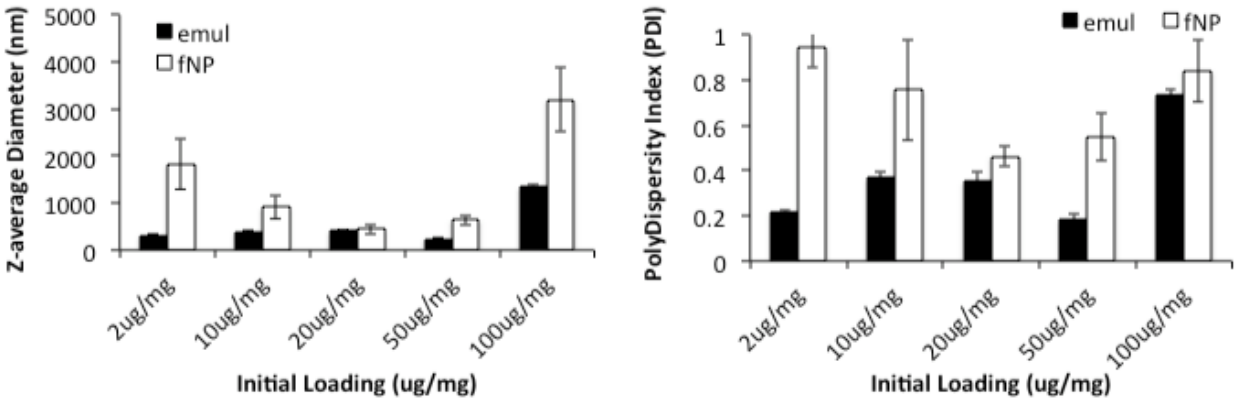

D-10: DLS size data for 1294-loaded particles at various initial loadings. *(Fabricated at pH = 12).*

APPENDIX D

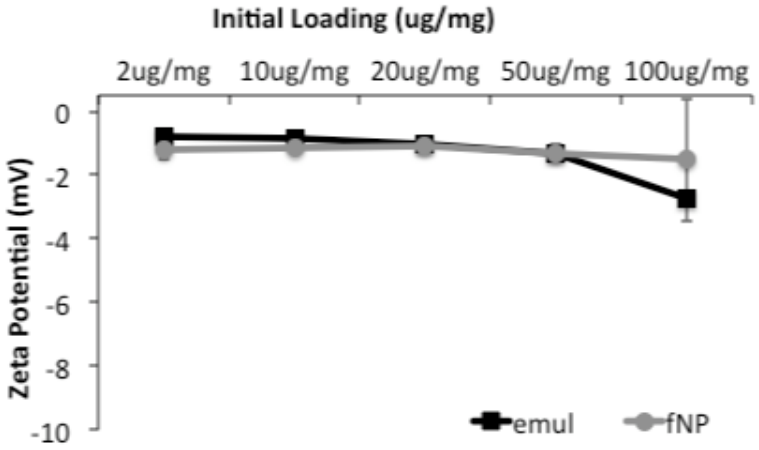

D-11: Surface Charge data for 1294-loaded particles at various initial loadings. *(Fabricated at pH = 12).*

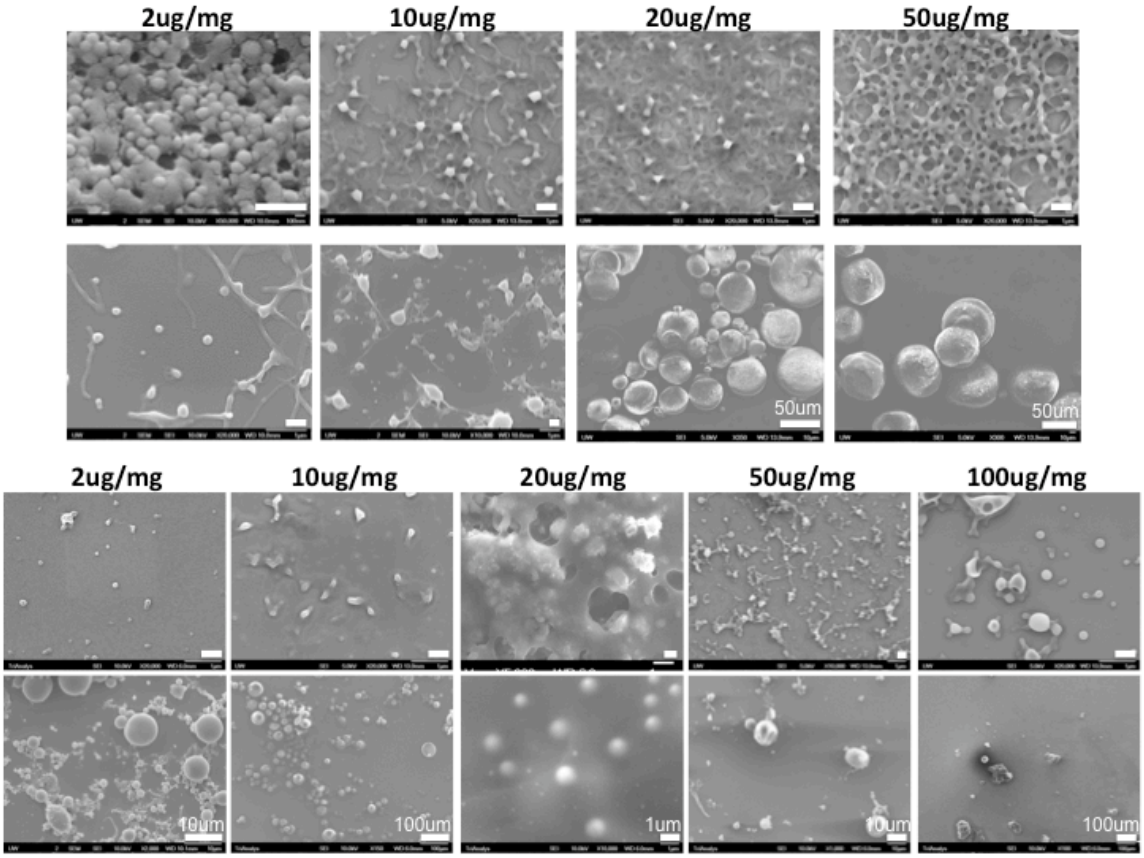

D-12: Additional SEM images for RM-1-132 (emulsion = first row, fNP = second row) and 1294 (emulsion = third row, fNP = fourth row) loaded PLGA particles at various initial loadings. *Scale bar = 500nm unless otherwise noted. Additionally, we are further investigating the particles to confirm trends due to low amounts of particles via SEM for a related paper publication. Particles were stored in fridge before SEM testing*.

APPENDIX D

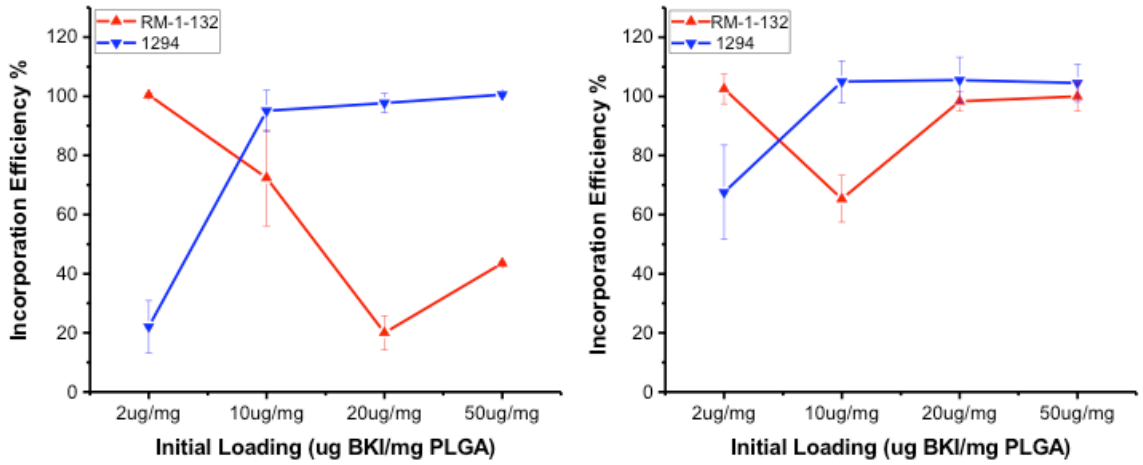

D-13: Incorporation efficiency for two types of BKIs (RM-1-132 and 1294) for emulsion (left) and fNP (right) fabricated particles.

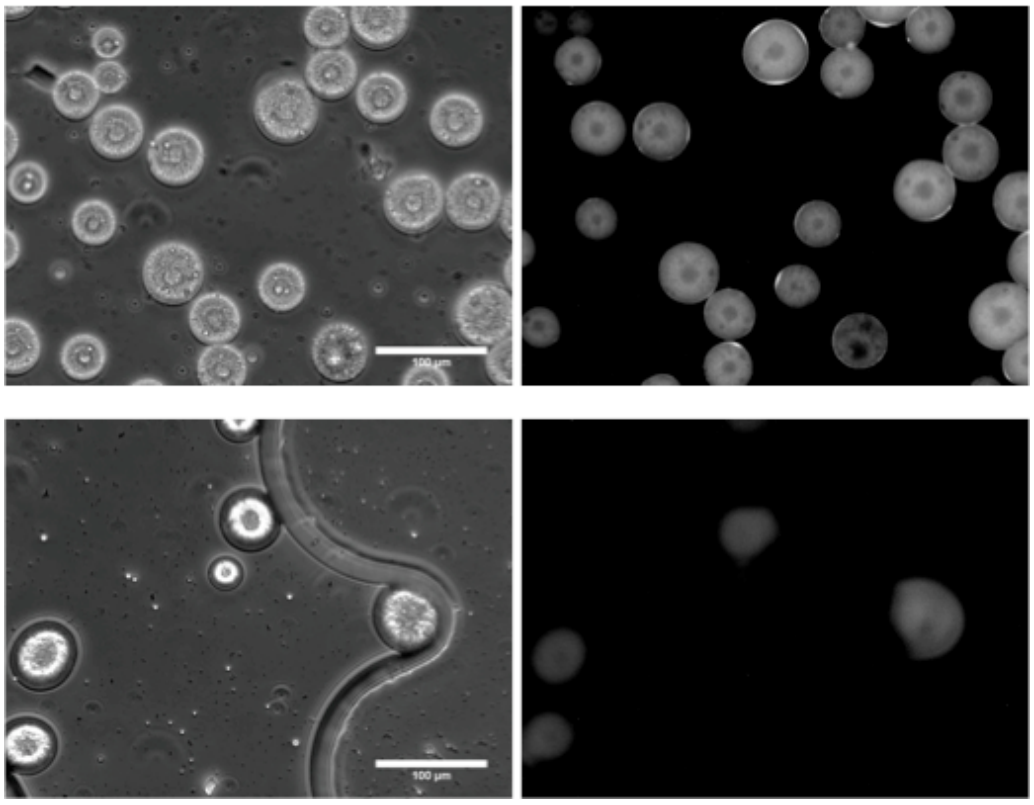

D-14: Internal distribution of quantum dots via fluorescence imaging for micro-scale fNP-fabricated QD-loaded PLGA particles. Real imaging on left column, fluorescence imaging on right column. *Scale bar = 100um.*

APPENDIX D

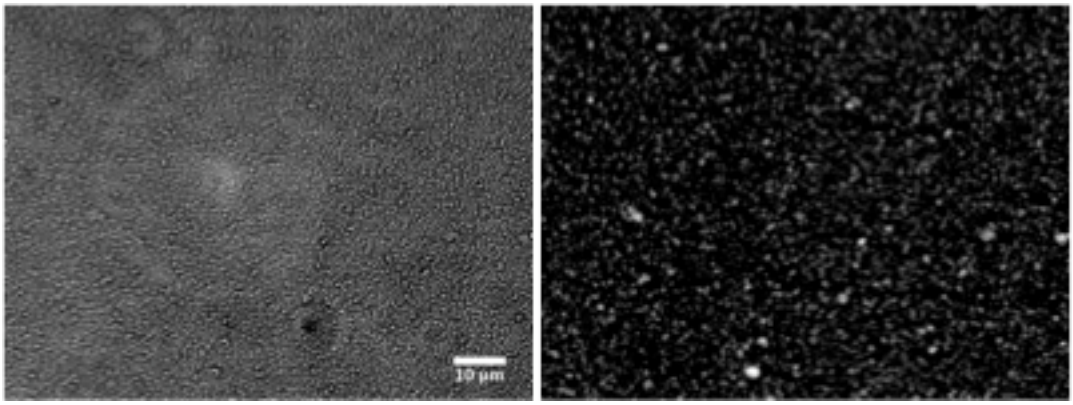

D-15: Fluorescence imaging for emulsion-fabricated QD-loaded PLGA particles. Real imaging on left column, fluorescence imaging on right column. *Scale bar = 10um.*